Adhesion of micropatterned adhesives to rough substrates and at elevated temperatures

Dissertation
zur Erlangung des Grades
des Doktors der Naturwissenschaften
der Naturwissenschaftlich-Technischen Fakultät
der Universität des Saarlandes

von

Viktoriia Barreau

Angefertigt am INM – Leibniz-Institut für Neue Materialien
Programmbereich Funktionelle Mikrostrukturen

Saarbrücken
2017

Tag des Kolloquiums:	27.10.2017
Dekan:	Prof. Dr. G. Kickelbick
Berichterstatter:	Prof. Dr. E. Arzt
	Prof. Dr.-Ing. F. Mücklich
Vorsitzender:	Prof. Dr.-Ing. D. Bähre
Akad. Mitarbeiter:	Dr.-Ing. F. Aubertin

Contents

Danksagung

An erster Stelle möchte ich *Prof. Dr. Eduard Arzt* für die freundliche Überlassung dieses hochinteressanten Themas und die Bereitstellung des Arbeitsplatzes herzlich danken. Ich verdanke ihm darüber hinaus hilfreiche Unterstützung und viele anregende Diskussionen.

Prof. Dr. Frank Mücklich gilt mein Dank für die freundliche Übernahme des Zweitberichterstatters.

Des Weiteren danke ich *Prof. Dr. Wulff Possart* für seine Unterstützung als wissenschaftlicher Bergleiter.

Ich danke *Dr. Elmar Kroner* für die zahlreichen Ideen und konstruktiven Gespräche zu Beginn meiner Doktorarbeit.

Herzlich bedanken möchte ich mich ebenfalls bei *Frau Dr. Natalie Guimard*, die mir bei der Planung und Durchführung der vorliegenden Arbeit außerordentlich sachkundige, erfahrene und wertvolle Unterstützung gewährte.

Mein besonderer Dank gilt *Dr. René Hensel* für seine ständige Diskussions- und Hilfsbereitschaft. Ohne seine Hilfe wäre die Anfertigung dieser Doktorarbeit in diesem Umfang nicht möglich gewesen.

Für die unermüdliche und professionelle Einführung in sämtliche Verfahren, danke ich *Jessica Kaiser*, *Susanne Selzer*, *Marlon Jochum* und *Oscar Torrents Abad* ganz herzlich.

Ich bedanke mich ebenfalls bei der gesamten Arbeitsgruppe Funktionelle Mikrostrukturen für die freundschaftliche Arbeitsatmosphäre, die vielen wertvollen Anregungen und stete Hilfsbereitschaft. Es hat mir viel Freude bereitet ein Teil der Gruppe zu sein.

Meinen Bürokollegen danke ich für die freundliche Atmosphäre in unserem Büro.

Bei meiner Familie möchte ich mich ganz besonders herzlich bedanken für die uneingeschränkte, liebevolle und vielseitige Unterstützung während meiner Doktorarbeit.

Ich danke auch meinen Freunden, die mir stets zur Seite standen und mich immer wieder aufgemuntert haben.

Abbreviations and symbols

AFM	Atomic Force Microscopy
AR	Aspect Ratio
DMT	Derjaguin Muller Toporov Theory
DMTA	Dynamic Mechanical Thermal Analysis
DSC	Differential Scanning Calorimetry
GS	Glass Substrate
JKR	Johnson Kendall Roberts Theory
MAD	Macroscopic Adhesion Measurement Device
SEM	Scanning Electron Microscopy
SP	Sandpaper
XRD	X-Ray Diffraction Analysis
WLI	White Light Interferometry
δ	indentation depth, (m)
E	Young´s modulus, (N/m²)
E^*	reduced Young´s modulus, (N/m²)
K	reduced stiffness, (N/m)
R_a	arithmetic average roughness, (m)
R_q	standard deviation of the distribution of the surface heights, (m)
R_z	the mean peak-to-valley profile roughness, (m)
S_m	the mean spacing between the profile peaks at mean line, (m)

S	the average distance between adjacent local peaks, (m)
D	pillar diameter, (m)
H	pillar height, (m)
U_{Debye}	Debye interaction potential, J
U_{el}	elastic strain energy, (Nm)
U_{Keesom}	Keesom interaction potential, J
U_{London}	London dispersion potential, J
$U_{V\,dW}$	Van der Waals potential, (Nm)
v	Poisson's ratio, (–)
P	load, (N)
T_g	glass transition temperature, (°C)
R	the effective radius of the spheres, (m)
a	the contact radius, (m)
P_p	preload, (N)
P_c	pull-off force, (N)
s	splitting efficiency, (-)
θ	tilt angle, (°)
w	the work of adhesion, (Nm^{-1})
γ_1, γ_2	the respective surface energies, (Nm^{-1})
γ_{12}	the interfacial energy for the two materials in contact, (Nm^{-1})
K_I	the stress intensity factor in mode I displacement, [$N/m^{3/2}$]
tan δ	viscoelastic loss factor, (-)

Abstract

The gecko is of high interest for scientists due to its ability to attach and to move on different surfaces with various roughnesses. To date, research groups worldwide aim to study adhesion mechanisms of gecko-like structures and to mimic gecko adhesion. However, most investigations have been performed in controlled environments and under near to ideal conditions, which present a significant constraint for transferring the results to applications. Therefore, two important parameters have been the subject of investigations in the present work, the surface roughness and elevated temperatures. For the first time, the impact of roughness on the adhesion of gecko-like, micropatterned structures was systematically studied. Two adhesive regimes, which are dependent on the pillar geometry and the roughness parameters, were discovered: an adhesive and a non –adhesive regime. The influence of the temperature on adhesion was studied on micropatterned samples fabricated out of three materials, which are interesting candidates for industrial applications. Promising correlations were determined between the temperature dependent mechanical properties and the adhesion values: the glass transition temperature was identified as the temperature of maximum adhesion. These results can support the improvement of bioinspired adhesives for industrial applications.

Zusammenfassung

Der Gecko ist für Wissenschaftler aufgrund seiner herausragenden Fähigkeit, sich an verschiedenen Oberflächen zu befestigen und fortzubewegen, ein besonderes Vorbild für temporäre Adhäsionssysteme. Bislang bezieht sich das Ziel vieler Forschungsgruppen darauf Geckostrukturen nachzuahmen und grundlegende Mechanismen zu studieren. Diese Untersuchungen finden jedoch bisher unter nahezu idealen Bedingungen und in einer kontrollierten Umgebung statt, was eine starke Einschränkung bei der Übertragung der Ergebnisse auf industrielle Anwendungen darstellt. Zwei wichtige Parameter waren Gegenstand der Untersuchungen in dieser Arbeit, die Rauigkeit und die Temperatur. Zum ersten Mal wurde der Einfluss der Rauigkeit auf das Adhäsionsverhalten einer großen Anzahl von mikrostrukturierten Strukturen systematisch untersucht. Hierbei wurden zwei Adhäsionsregime, die von der Pillargeometrie und den Rauigkeitsparametern abhängen, festgestellt: das adhäsive und das nicht-adhäsive Regime. Der Einfluss der Temperatur auf die Adhäsion wurde auf mikrostrukturierten Proben aus drei für industrielle Anwendungen sehr interessante Materialien erforscht. Hierbei wurden wichtige Korrelationen zwischen den temperaturabhängigen mechanischen Eigenschaften und den ermittelten Rauigkeitswerten festgestellt. So wurde die Glasübergangstemperatur als die Temperatur der maximalen Adhäsion identifiziert. Diese Ergebnisse können dazu beitragen, bioinspirierte Strukturen für industrielle Anwendungen zu optimieren.

1 Introduction

In nature, the physiology of a large number of animals enables them to attach on various surfaces with different characteristics. Mussels, for instance, irreversibly attach on rocks or ship hulls through a sophisticated adhesion system which withstands the tides and to survives in a harsh environment. Slugs, on the other hand use secretion as an adhesive solution. Different species of insects, spiders or lizards, use so-called “fibrillar adhesion” mechanisms. Hereby, the adhesion results from hairy structures on their attachment pads. The gecko has attracted the interest of many scientists who seek to understand the interaction of the physical factors behind this particular adhesion mechanism on smooth and rough surfaces and to reproduce it in a laboratory and subsequently on industrial scale. This animal exhibits a large number of hierarchical structures composed of micro- and nanosized hairs with characteristic geometries and mechanical properties on their toe pads, which enable it to firmly attach to and easily detach from a multitude of surfaces. Several investigations analyzed the adhesion of geckos on rough surfaces. Other works have been conducted with the objective to imitate the structure of gecko toe pads and to analyze their adhesion on artificial substrates. However, no systematical investigation of adhesion of gecko inspired structures to rough substrates has been performed yet.

The first part of the present thesis presents such a systematic exploration of micropatterned structures composed of pillars with different diameters and heights and their adhesive behavior on various substrates with defined roughnesses.

Another aim of many research projects is adhesion under certain conditions or in a specific environment. In particular, for the development of adhesive systems dedicated to a wide range of industrial applications, a profound understanding of the adhesion performance under varying or specific conditions is of outmost importance. In the second part of the present thesis, the impact of temperature on the adhesive behavior of different polymer materials, which are very interesting candidates for industrial applications of bioinspired adhesives, has been explored.

The thesis is outlined as follows: In Chapter 2, fundamental phenomena in adhesion science will be discussed. The chapter includes an overview of contact mechanics and introduces the contact splitting principle. Then the state of understanding of adhesion in biology, on rough and heated substrate will be discussed, and roughness parameters will be presented. At the end of this chapter, the state of the art will be critically commented and the

goal of this thesis will be clarified. Chapter 3 presents an overview of the materials, instruments and methods which have been used. In Chapter 4 the adhesion of micropatterned PDMS samples to rough glass substrates is investigated and discussed. Chapter 5 presents results of the adhesion tests to sandpaper.

In Chapter 6 the results of adhesion measurements of micropatterned PDMS, PFPEdma and PU-ht samples at elevated temperatures are presented and discussed. Chapter 7 concludes this thesis with a short summary and provides an outlook.

Chapter 4 was published as a full paper:

Barreau V, Hensel R, Guimard NK, Ghatak A, McMeeking RM, Arzt E. Fibrillar Elastomeric Micropatterns Create Tunable Adhesion Even to Rough Surfaces. Adv Funct Mater. 2016; 26(26):4687-4694.doi:10.1002/adfm.201600652.

Chapter 6 was published as a full paper:

Barreau V, Yu D, Hensel R, Arzt E. Elevated temperature adhesion of bioinspired polymeric micropatterns to glass. Journal of the Mechanical Behavior of Biomedical Materials. 2017; doi: 10.1016/j.jmbbm.2017.04.007.

2 Theoretical background

This chapter is organized in two parts. In the first part, adhesion will be introduced and the state of the art of adhesion in biology will be reviewed. Then, an overview of adhesion to rough substrates will be presented, followed by a discussion of roughness parameters. Further, the focus will be put on adhesion at elevated temperatures and the behavior of polymers under such conditions. In the second part an overview of contact mechanics principles will be presented before the contact splitting principle will be discussed. At the end of this chapter, the state of the art will be critically commented and the goal of this thesis will be clarified.

2.1 Adhesion

The contact between two surfaces causes the generation of interatomic and intermolecular interactions across their interface [1], which is called adhesion. The term adhesion implies that attractive forces outweigh repulsive forces.

Van der Waals attractive forces are short-range dipole interactions between electrical dipoles that can be divided into the following categories [2]:

- Keesom interaction: Interaction between permanent dipoles. If permanent dipoles are present, the Keesom potential, U_{Keesom}, as a function of the distance, r, between the dipoles can be described as follow:

$$\boldsymbol{U_{Keesom} = -\frac{\mu_d^4}{k_b T r^6}}, \qquad \textbf{(2.1)}$$

  where μ_d is the dipole moment, k_b is Boltzmann's constant, T the absolute temperature. Hence, the potential is temperature-dependent.

- Debye interaction: Interaction between a permanent dipole and an induced dipole. A permanent dipole induces a dipole moment in an adjacent atom or molecule. The Debye potential can be calculated as follow:

$$\boldsymbol{U_{Debye} = -\frac{\eta \mu_d^2}{r^6}}, \qquad \textbf{(2.2)}$$

where η is the polarizability and is approximately proportional to the volume of a molecule.

- London dispersion: Interaction between induced dipoles. The mutual attraction is based on spontaneous fluctuations of the electron density in an atom or molecule. This displacement creates an electric field, which in turn also induces a discharge displacement (dipol moment) in another atom. These temporary dipoles attract each other for a short time.

$$\boldsymbol{U_{London} = -\frac{3}{4}\eta^2 h^* \frac{f}{r^6}}, \qquad \textbf{(2.3)}$$

where h^* is Planck's constant and f is the dispersion energy.

The Van der Waals potential is the sum of all three possible interactions and can be calculated as follows : [2]

$$\boldsymbol{U_{VdW} = U_{Kessom} + U_{Debye} + U_{London}} \qquad \textbf{(2.4)}$$

It has to be noted that all terms are strongly dependent on the distance between the two bodies. As a result, this kind of interaction is significant for short distances, but can be neglected when considering long distances. It has to be noticed that the Van der Waals interaction between two molecules is very week. However, in a solid, the sum of the Van der Waals interactions of all pairs of atoms can amount to a large value.

Electrostatic repulsion is a common example of a repulsive force, which is, on an atomic scale, caused by the overlap of electron orbitals. The model proposed by Lennard – Jones can be used to combine the attractive and repulsive forces.

2.2 Contact mechanics

Decreasing the stored elastic energy generates a restoring force and leads to high adhesion. The elastic potential energy is converted into kinetic energy and is therefore lost for the adhesion process. In order to achieve a high adhesion the repulsive forces should be decreased. This can be performed by reducing the stored elastic energy. One of the possibilities for such energy decreasing is the surface structuring. The dimensions of the structures, especially the aspect ratio (height/diameter) of the pillars are a major factor that strongly impacts adhesion.

2.2.1 Spherical contact

There exist three fundamental theories to describe spherical contact on the continuum level: the Hertz theory [3], the Johnson-Kendall-Roberts theory [4] and the Derjaguin-Muller-Toporov[5] theory. Each of these theories is based on different assumptions.

The Hertz theory is the oldest and considers two elastic solid spheres in frictionless and adhesionless contact under compression with a preload P [3]. The contact radius, the penetration depth and the stress distribution can be calculated. The contact radius a can be calculated as follows:

$$a^3 = \frac{PR}{E^*}, \qquad (2.9)$$

where R represents the effective radius of the spheres and E^* the reduced stiffness, which are defined as:

$$\frac{1}{R} = \frac{1}{R_1} + \frac{1}{R_2}, \qquad (2.10)$$

$$\frac{1}{E^*} = \frac{3}{4}\left(\frac{1-\nu_1^2}{E_1} + \frac{1-\nu_2^2}{E_2}\right), \qquad (2.11)$$

E_1, E_2 are the Young's moduli and ν_1 and ν_1 are the Poisson's ratios of the spheres with radii R_1 and R_2. There exist no attractive forces between the spheres and the contact radius *a* has to be sufficiently small in comparison to the spheres radii.

The theory of Johnson-Kendall-Roberts, called JKR, on the other hand takes into account attractive forces, such as Van der Waals interactions [4]. Hereby, the elastic, potential and surface energy are in balance, which results in an equilibrium contact area at zero load. The contact radius a_{JKR}, which is generally larger than in the Hertzian case, can be calculated as:

$$\boldsymbol{a_{JKR}^3 = \frac{PR}{K} + \frac{PR}{K}\left[\frac{3\pi wR}{P} + \sqrt{2\frac{3\pi wR}{P} + \left(\frac{3\pi wR}{P}\right)^2}\right].} \quad \textbf{(2.12)}$$

Here *K* corresponds to the reduced stiffness and *w* to the work of adhesion and is calculated as:

$$\boldsymbol{w = \gamma_1 + \gamma_2 - \gamma_{12},} \quad \textbf{(2.13)}$$

were γ_1 and γ_2 describe the respective surface energies and γ_{12} is the interfacial energy for the two materials in contact.

The Derjaguin-Muller-Toporov theory (DMT) describes spherical contacts for hard materials and lower attractive interactions outside the contact area. The contact radius a_{DMT} can be calculated as follows:

$$\boldsymbol{a_{DMT}^3 = \frac{PR}{K} + \frac{2\pi\gamma R^2}{K}.} \quad \textbf{(2.14)}$$

A comparison can be performed between the Hertz, DMT and JKR theories. The Hertz theory results in repulsive forces throughout the contact area. For the JKR theory the contact area is increased due to attractive forces within the contact area. The DMT theory assumes Hertzian behavior within the contact area and additional attractive forces outside the contact area.

2.2.2 Flat punch contact

The characterization of adhesion between a rigid flat punch and an elastic half-space has been provided by Kendall [6]. Hereby he presents an equation to calculate the pull-off force F_c by using strain energy release rate calculations:

$$\boldsymbol{F_c = \sqrt{6\pi a^3 K w},} \qquad \textbf{(2.15)}$$

Now adhesion depends on the work of adhesion and on the probe geometry. Subsequently, Kendall derived an equation to describe the adhesion in the case of a flat punch and flat half space and calculated the pull-off force F_c:

$$\boldsymbol{F_c = K_I 2a\sqrt{\pi a}} \qquad \textbf{(2.16)}$$

where K_I is the stress intensity factor in mode I displacement.

2.2.3 Adhesion in biology

The gecko is considered to be one of the most fascinating animals. It is capable to locomote on vertical walls and ceilings and moves on various rough surfaces in nature such as trees, rocks and walls. Experimental evidence [7] has been found that the adhesion ability of geckos relies indeed on Van der Waals [8] combined with capillary forces [9] [10] [11]. Geckos use a special mechanism to actuate and disengage high adhesion. Their feet contain hundreds of thousands of keratinous hairs called setae (**Figure 2.1(a) and 2.1(b)).** Each seta is about 100 µm long and branches into hundreds of about 20 nm thick and 200 nm long spatulae (**Figure 2.1(c)**) [12] . In such a way the gecko's attachment system is a hierarchical system composed of micro- and nano-sized hairy structures. These structures can fit and adhere to micro- and nanoasperities of rough surfaces and help to achieve a large area of contact.

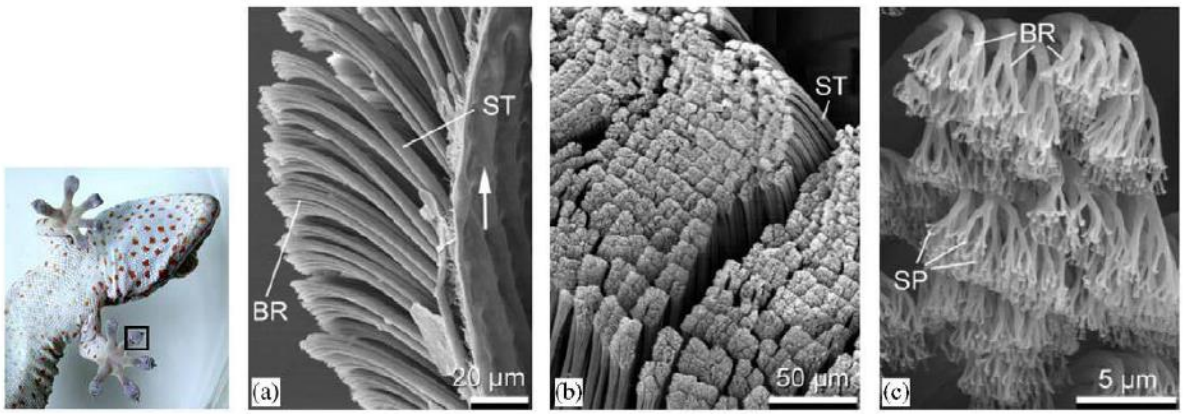

Figure 2.1 *The hierarchical adhesion structures of a gecko. A gecko toe contains hundreds of thousands of setae and each seta branches near its tip region into hundreds of spatulae. (a) and (b) scanning electron micrographs of setae at different magnifications, (c) spatulae, the finest terminal branches of seta. ST: seta; SP: spatula* [12].

2.2.4 Contact splitting principle

Interesting correlations between number and size of the attachment hairs and the animal weight have been discovered: with greater weight of the animal, the areal density of the hairs increases, and their size decreases [13] (**Figure 2.6**). As a consequence, the adhesion is increased at smaller diameters. Such dependencies have also been evidenced experimentally in artificial attachment systems: adhesion increases with decreasing radii [14] [15].

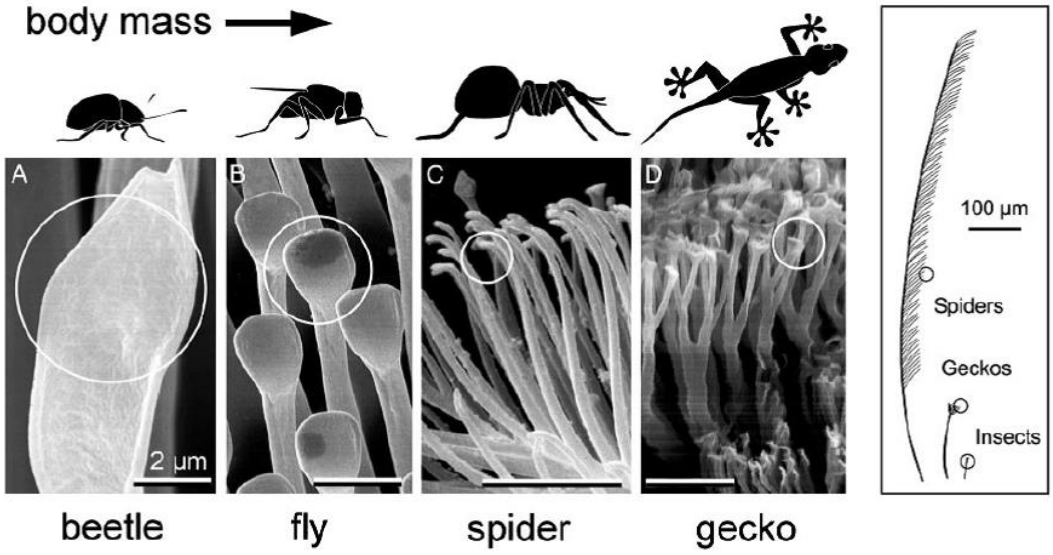

Figure 2.2 *Correlation between animal body weight and terminal element dimensions* [16].

Such observations can also be explained by the JKR theory and have been introduced as the principle of contact splitting by Arzt et al. [16] It was also shown that the shape of the pillars strongly influences their behavior. If the pull-off strength is plotted against the pillar radius (in log-log scale), absolute value of the slope of the curve is defined as "contact splitting efficiency" [14] (**Figure 2.7**).

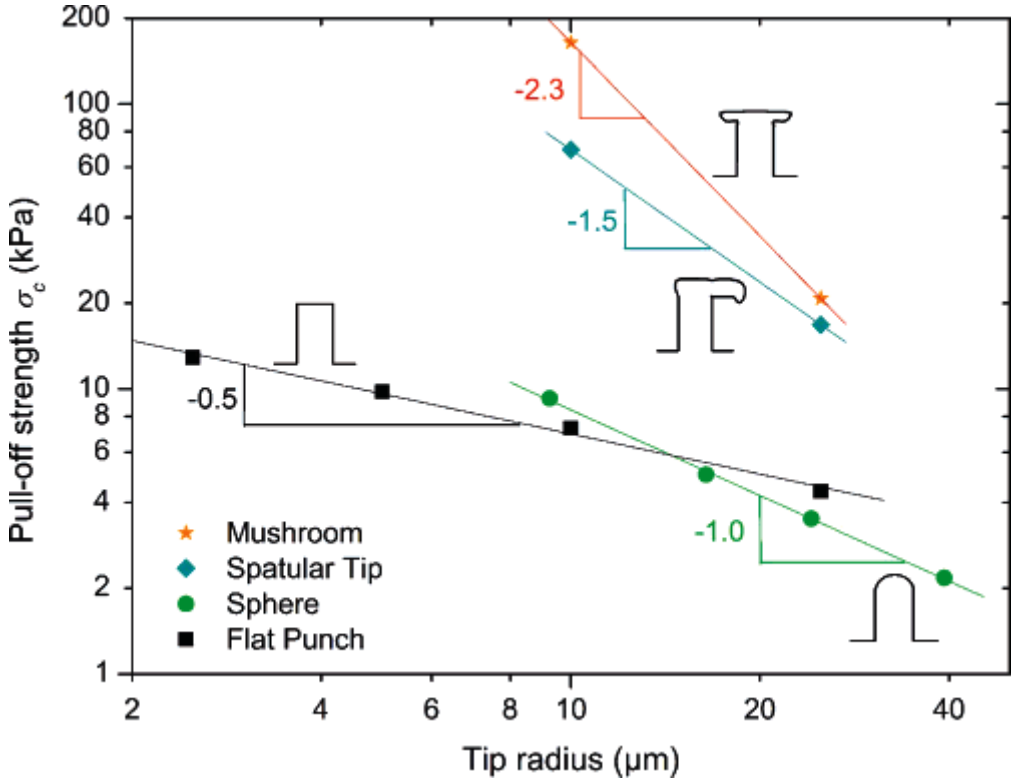

Figure 2.3 *"Contact splitting efficiency" for different tip radii (flat, spherical, spatula and mushroom tip)*[14].

Larger values of the slopes mean higher gains in adhesion stresses with progressive miniaturization. It has been demonstrated experimentally that the slope values are dependent on the geometry of the pillar tips [14]. Hereby, values for flat tips of 0.4 have been determined theoretically[17] and evidenced experimentally [14] for measurements on smooth glass substrates. For rough substrates, these values have not been determined yet. But with this concept the number of contact points on the rough substrate can definitively increase the ability to adapt to such surfaces and hence to provide high adhesion.

2.3 Adhesion to rough substrates

Over the last decade, biomimetic gecko structures have been fabricated in several laboratories. Hereby a lot of effort was put on the fabrication of gecko like structures and their adhesion to a smooth surface [18] [19] [20]. However, given that all natural and almost all artificial surfaces have a finite roughness on one or more different length scales, little research has been conducted to comprehend and optimize the adhesion of gecko-mimicking surfaces to such surfaces. Tests on geckos have shown that such parameters as roughness can influence adhesion [16] [21] [22] [23] [24]. Furthermore, Irshick et al.[25] have shown that in order to adhere to a surface the foot of a gecko needs to sustain a force of approximately 10 N (corresponding to a weight of 1 kg) and only 1 % of this force is needed to support its whole body weight (40 g). The reason for this large "safety factor" may result from a decrease of adhesion against rough surfaces [26]. Huber et al.[23] investigated the gecko's ability to cling to substrates with different roughness and measured the adhesion of a single setae hair of a gecko by atomic force microscopy (AFM). According to the assumption that the spatula contact area could be approximated as a circle of 100 nm radius, they found a critical value of surface roughness and discussed the interaction between the spatulae and the rough surfaces. The spatula apparently adapted well to the surface for low RMS roughness (<200 nm) and could also adhere strongly to substrates with RMS roughness >200 nm. A distinct minimum in adhesion was found at RMS roughness of 100 nm, which is typical of the spatula dimension. A similar drop of shear resistance for geckos on wavy substrates was observed by Gillies[27].

Using continuum theory and molecular simulations, it was found that an increase of roughness can decrease the adhesion between two surfaces [28] [29] [30] . Surface roughness is the main reason why solids usually do not adhere to each other with significant strength [31]. From a theoretical perspective, surface roughness will have a strong influence on the adhesion of flat tips [32]. On the other hand fibrillar structures should adapt to the surface and exhibit high adhesion, where a minimum elastic adaptability of the fiber structure is required [33] . First studies on the relationship between structures architecture and surface roughness were presented by Persson [26] [34]. Guduru [35] points out that full contact can be made between a very rough surface and a soft gel. Soft materials generally adhere well on hard,

rough surfaces, as they can deform without much energy storage. However, the stored energy is small compared to the energy produced by forming the contact, resulting in high adhesion. Another recent study [36] showed the influence of technologically rough surfaces on biomimetic adhesives. Fuller and Tabor [34] correlated the decrease of adhesion with an 'adhesion parameter', which is dependent on roughness. Measurements of attachment forces of micropillars against smooth glass and rough surfaces were conducted. The results showed a decrease in adhesion for rough surfaces.

There have been many attempts to investigate the influence of surface roughness on adhesive force of biomimetic fibrillar adhesive pads [37] [38] [39]. It has been discovered that biomimetic pillar arrays increase the adhesive force on various rough surfaces over that of unpatterned samples. Yu et al. demonstrated that the surface roughness can decrease or increase adhesion of gecko mimetic structures [40], dependent on roughness profile.

A major problem in the investigation of adhesion on rough substrates is the characterization of roughness.

2.3.1 Roughness parameters

Surface roughness description and characterization is very important for many problems including adhesion. However, roughness exists on different scales[41]. Two established methods for measuring roughness are profilometry and atomic force microscopy (AFM). In both techniques a sharp stylus is used to scan the surface and to record the surface profile. Then the roughness parameters can be determined in 2D or 3D.

The most universal amplitude parameter is the average roughness R_a. R_a is an arithmetic mean of the absolute values of the profile deviations within the reference roughness track l. This parameter corresponds to the height of a rectangle with the reference distance as the side length, which is also defined as the sum of the area enclosed by the profile and the center surface line (**Figure 2.4**)

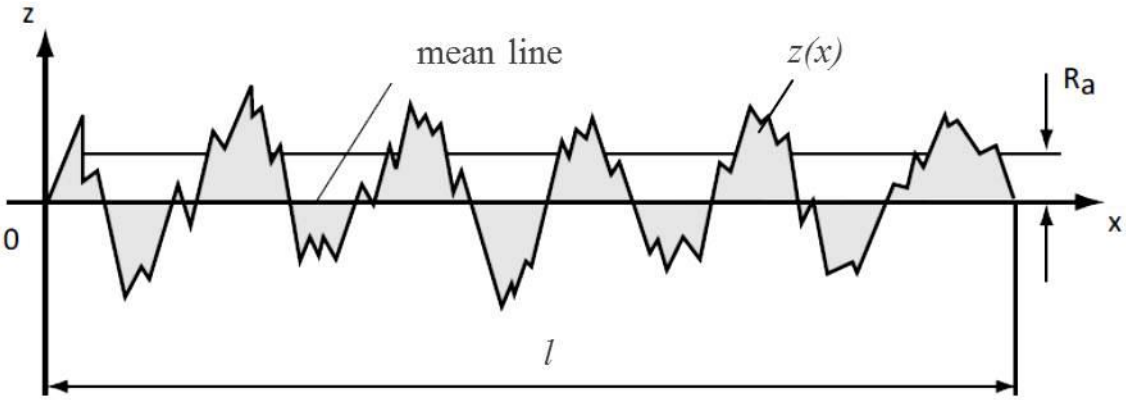

Figure 2.4 *Schematic of average roughness* $\boldsymbol{R_a}$ [42].

Mathematically this parameter is represented by the following equation [42] :

$$\boldsymbol{R_a = \frac{1}{l}\int_0^l |z(x)|dx,} \qquad \textbf{(2.5)}$$

This parameter is easy to define and measure but it only provides a general description of height variations. It is not sensitive enough to detect small changes in the profile nor does it provide any information about the wavelength.

The surface roughness can also be described statistically with the more sensitive standard deviation of the distribution of the surface heights, R_q. The mathematical definition is as follows:

$$\boldsymbol{R_q = \sqrt{\frac{1}{l}\int_0^l \{z(x)\}^2\, dx},} \qquad \textbf{(2.6)}$$

In many studies, these two parameters are used for the characterization of rough substrates. But they do not provide any information about the shape of the surface profile [43] .

The amplitude parameter, which will be used in this thesis, is the distance from the average of the five lowest points to the five highest points of the profile R_z (**Figure 2.5**).

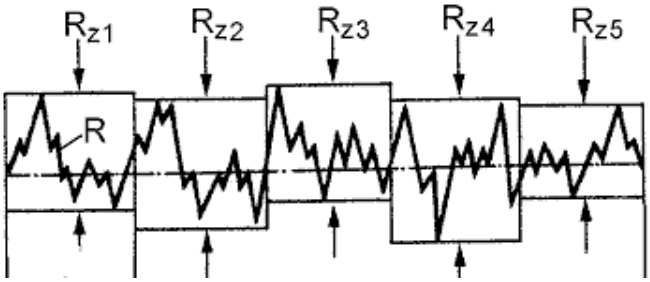

Figure 2.5 *Schematic of the distance from the average of the five lowest points to the five highest points of the profile* $\boldsymbol{R_z}$ [42].

In general, a description of rough or structured surfaces only with vertical parameters is not sufficient for a characterization of the substrates. It is important to describe the roughness also in lateral directions. Therefore, two spacing parameters have been used in this work. The first one is the mean spacing between the profile peaks at mean line, S_m (**Figure 2.6**). S_m can be calculated from the following equation:

$$\boldsymbol{S_m = \frac{1}{N}\sum_{i=1}^{n} S_i,} \qquad \textbf{(2.7)}$$

where N is the number of profile peaks at the mean line and S_i is the distance between the profile peaks.

However, more important in this study is the second spacing parameter S (**Figure 2.6**). It describes the average distance between adjacent local peaks and can be calculated as following:

$$\boldsymbol{S = \frac{1}{N}\sum_{i=1}^{n} S_i,} \qquad \textbf{(2.8)}$$

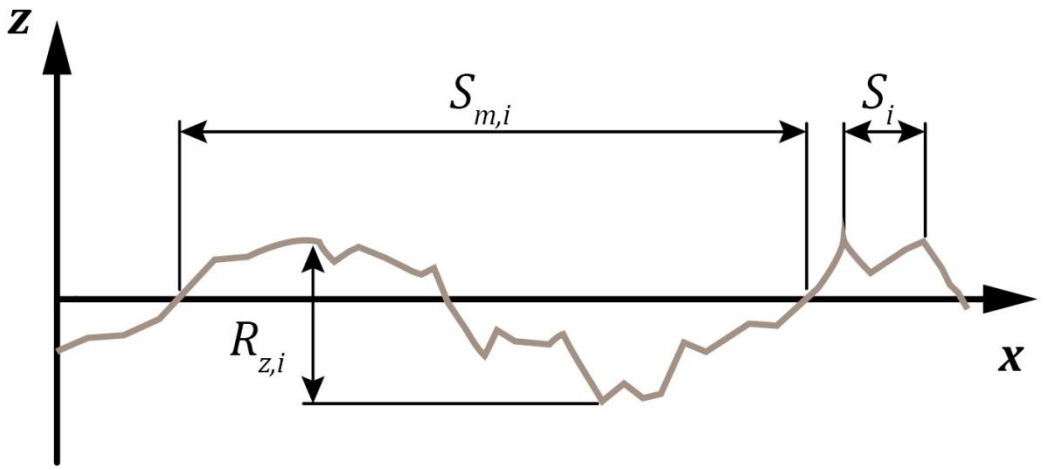

Figure 2.6 *Schematic of the mean spacing between the profile peaks at mean line* $\boldsymbol{S_m}$ *and the average distance between adjacent local peaks S* [44].

The influence of roughness on adhesion can also be described by using the surface roughness power spectrum $C(q)$ (or power spectral density) defined as [45]:

$$\boldsymbol{C(q) = \frac{1}{(2\pi)^2} \int d^2\chi [h(x)h(0)]\, e^{-lqx}} \qquad \textbf{(2.9)}$$

where $\chi = (x, y)$ and $z = h(x)$ is the substrate height and q is the wave vector.

A typical roughness power spectrum for self-affine structures is shown in **Figure 2.7.**

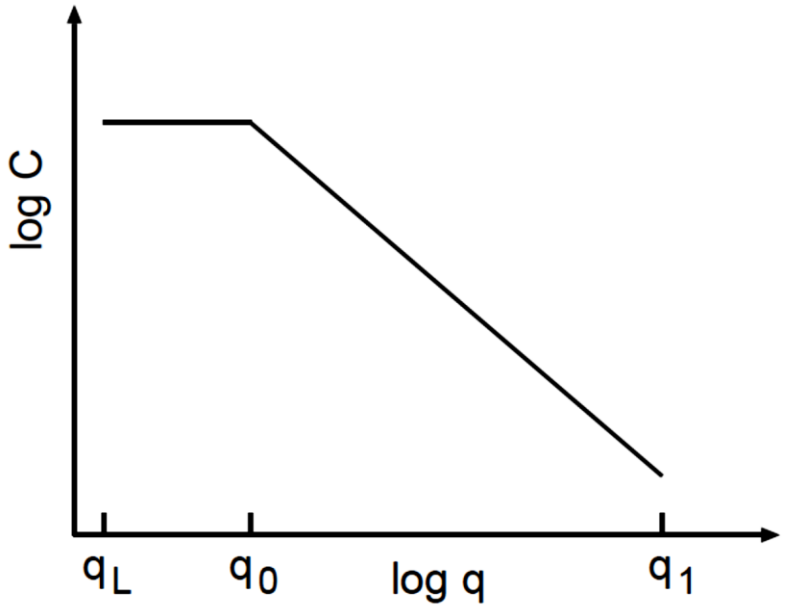

Figure 2.7 *The surface roughness power spectrum of a self-affine fractal surface for* $q_0 < q < q_1$*. The RMS roughness amplitude and the average slope (and the average curvature) are determined mainly by the encircled regions of the power spectrum* [46].

The power spectral density (PSD) of a surface is a mathematical tool that decomposes the measured or mathematically generated topography data into sinusoidal waves using the Fourier transform. The wave vectors q (spatial frequencies) contain all necessary information about the roughness properties of the studied surface. As a result, the roughness power spectrum especially allows describing the distribution of height fluctuations (or the power of the signal) with a frequency or waving vector q and hence provides a more complete description of surface roughness. Furthermore, all parameters characterizing the surface roughness, like amplitude parameter or slope, spacing parameters, can be calculated.

In literature, several methods for computing the PSD from profiling data have been presented and most of them differ in the normalization procedures. Nevertheless, PSD offers the main advantage that it contains statistical information that is indifferent of the chosen scan size and pixel resolution [47]–[49].

2.4 Adhesion at various temperatures

In recent time, the interest for adhesion applications has been directed to polymers due to their surface properties, low cost and mechanical properties. It is well known that the mechanical properties of polymers are strongly temperature dependent [50], especially if the temperature variation passes the glass transition temperature, T_g. At T_g the molecular mobility changes from an immobile so-called glassy state ($T<T_g$), the molecules only experience to a more flexible rubber state ($T>T_g$). Simultaneous to this transition, the elastic modulus strongly decreases. Interestingly, pressure sensitive adhesives (PSAs) present the highest adhesion close to T_g, as has been demonstrated by Zosel et al.[51]. Numerous experimental studies have been carried out on polymers to characterize the mechanical behavior as a function of temperature [52] [53] [54] .

Most of the polymers are amorphous or semi-crystalline, but all can be classified into three different classes: thermoplastics, elastomers or duromers. Each type behaves different when it is subjected to an increasing temperature. Typical Young's moduli – temperature curves are represented in **Figure 2.7**

Below T_g, thermoplastics and elastomers are in a glassy state. Here the macromolecules are immobilized and only thermal vibrations around their mean position are possible. In the range of the glass transition temperature the molecules become mobile due to change of position of entire chain segments. The transition to the rubber state does not occur immediately. In the case of amorphous thermoplastics and elastomers, the Young's modulus decreases strongly in this transition zone. After a further temperature increase and beyond this transition, amorphous thermoplastics enter the quasi-rubbery elastic state, before reaching the processing or yield range. In the case of elastomers, they enter a rubbery elastic state, which is followed by thermal decomposition.

Semicrystalline polymers show a behavior different from amorphous thermoplastics and elastomers. Depending on their fraction of amorphous phase, they present a step in the Young's modulus when reaching the glass transition temperature. Beyond T_g the embedded crystallites have a stiffening effect on the structure. The body maintains its form. If the

temperature is further increased, the material changes into a viscous melt, which is bound to a strong decrease of the Youngs modulus.

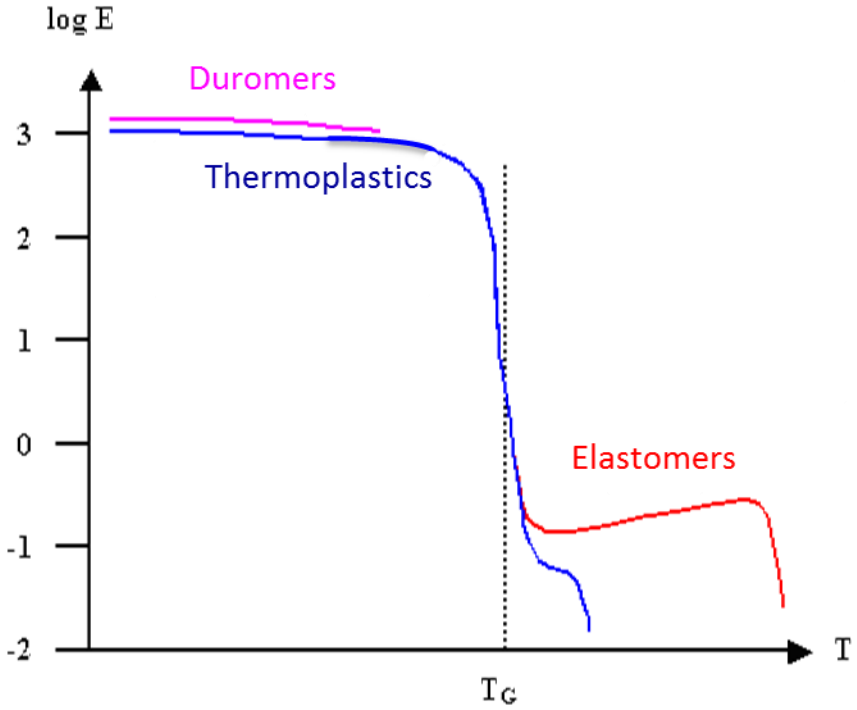

Figure 2.8 *Typical Young's modulus - temperature curves for different polymer groups* [55].

Nevertheless, the adhesion performance is generally not a simple function of temperature: For an ideal contact situation, the higher modulus below T_g can lead to an increase of the adhesion properties of an adhesive film in contact with a rigid flat punch [6]. So the reduction in adhesion with increasing temperature for a rigid contact was reported by Noy et al. [56]. However, Cappella and Stark [57] observed an increase in the adhesion force with increasing temperature during a contact between the AFM tip and a polymer film. They found out that the temperature dependency of the adhesion force results from the mechanical properties modification of the polymers material, when the temperature increases.

A stiffer material, on the other hand, will prevent intimate contact formation, especially on a rough surface, and the diminished contact area can result in reduced adhesion. Above T_g, contact formation may be improved, however the lower modulus can simultaneously lead to a degradation of the adhesion [58]–[60].

Several studies are focused on the viscoelastic behavior of thin polymer films and reported an adhesion increase close to T_g of polymer surfaces [61] [62] [63] [64] [65] [66]. Kim et al. [64] investigated a PMMA film and noticed that the adhesion began to increase rapidly at temperatures close to the T_g. The same effect was observed by Tui et al. [63] while studying poly(*tert*-butyl acrylate) with AFM. Luengo et al. [65] noticed a dramatic increase in pull-off forces on PBMA films around the glass-rubber transition temperature. They suggested a mechanism to describe the enhanced adhesions at T_g, where the enhanced mobility induces molecular rearrangements such as polymer chain entanglements across the interface, similar to the rearrangements obtained in bulk. In addition, inelastic surface deformations or bulk flow might contribute to energy dissipation at higher temperatures and lower rates.

Zeng et al. [66] measured maximal adhesion on the point between solid-like and liquid-like polystyrene films.

Awada et al. [67] studied adhesion between an AFM tip and PDMS and observed a decrease in adhesion at an increase of the temperature in a temperature range of 30 °C to 140 °C. They determined a reduction in adhesion with increasing temperature, which has been explained by higher thermal fluctuations inducing a decrease of intermolecular interactions. Furthermore they demonstrated that the adhesion energy at the nanoscale is directly linked to the thermodynamic work of adhesion, which is related to the surface free energies, and the dissipative energy, which are defined by the molecular mass and a dissipative coefficient.

Shavezipur et al. [68] reported a decrease in the adhesion between polycrystalline silicon surfaces with increasing temperature due to the absence of electrostatic and capillary forces. Li et al. [69] measured the adhesion force in a nitrogen chamber and their results showed that the adhesion force was smaller at ambient conditions. De Crevoisier and Liebler [70] investigated a side-chain liquid crystalline copolymer and detected dramatic changes of the adhesion performance at 35°C due to a transition between a mesomorphic and an isotropic phase.

Tambe and Bhushan [71] focused on hydrophobic and hydrophilic samples (PDMS and PMMA) and found no temperature dependency for highly hydrophobic samples using AFM for adhesion measurements. However, the results for PDMS showed a drop in adhesion at high temperature. This dependency was similar on both micro- and nanoscale.

3 Experimental

Several series of bioinspired structures with different aspect ratios were fabricated. Adhesion measurements were performed with these structures on rough glass and sandpaper substrates. In addition, adhesion was also measured for structures made of three different materials at different temperatures. In order to interpret the results, the thermomechanical properties of the used polymers were also investigated. The individual sample fabrication and substrate preparation steps as well as the measurements will be described in the next subsections.

Three subsections of this chapter are content of publication: Barreau V, Hensel R, Guimard NK, Ghatak A, McMeeking RM, Arzt E. Fibrillar Elastomeric Micropatterns Create Tunable Adhesion Even to Rough Surfaces. Adv Funct Mater. 2016; 26(26):4687-4694. doi:10.1002/adfm.201600652 and are marked with a footnote.

Five subsections of this chapter are content of publication: Barreau V, Yu D, Hensel R, Arzt E. Elevated temperature adhesion of bioinspired polymeric micropatterns to glass. Journal of the Mechanical Behavior of Biomedical Materials. 2017; doi: 10.1016/j.jmbbm.2017.04.007 and are marked with a footnote.

3.1 Fabrication of microstructured surfaces

3.1.1 Photo-lithography

Photo-lithography was performed in the clean room (class 1000/100) of Mitranz, Saarland University, Germany. As substrates for photo-lithography, silicon wafers were used with a <100> orientation in the crystal direction. The resist was spin-coated onto the polished wafers. After thermal evaporation of the solvent of the resist, wafer was exposed by an UV-source (365 nm) through a mask in a Mask Aligner (Carl Süss MicroTec AG, Germany). The mask featured 25 fields with different circle diameters and spacing, as well as a hexagonal packing. The usual area covered by the patterns was 8×8 cm^2. Two different resists were used. The negative-tone SU 8 - 2000 series resist led to the formation of a pillar structure (**Figure 3.1**) and the positive-tone AZ 6632 resist led to a holes (**Figure 3.2**). The depth of the holes (or in case of pillars their heights) were determined by the resist thickness. For getting pillar structures with the SU-8 resist mask, a two-step molding process was needed, which will be described in the following sections.

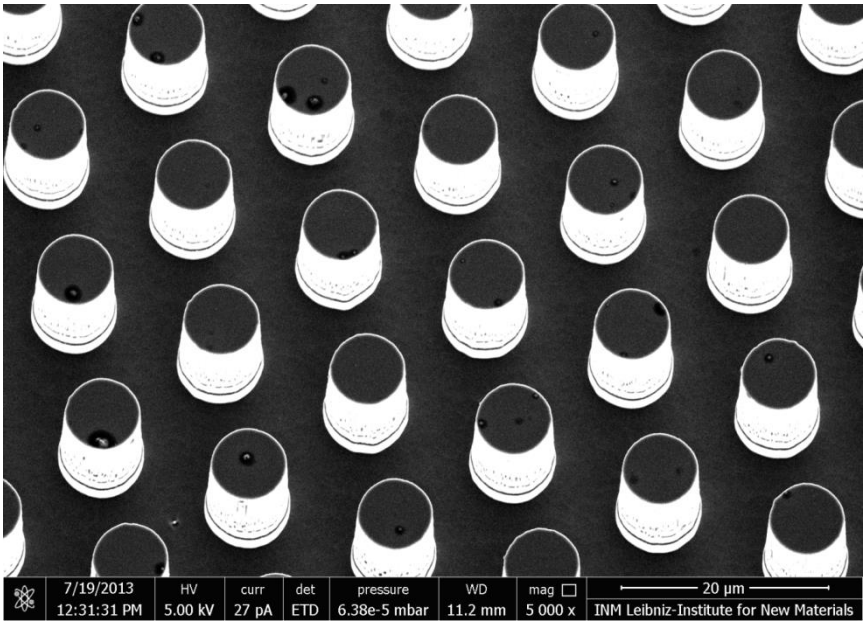

Figure 3.1 *Pillar structure made with negative-tone SU 8 - 2000 series resist.*

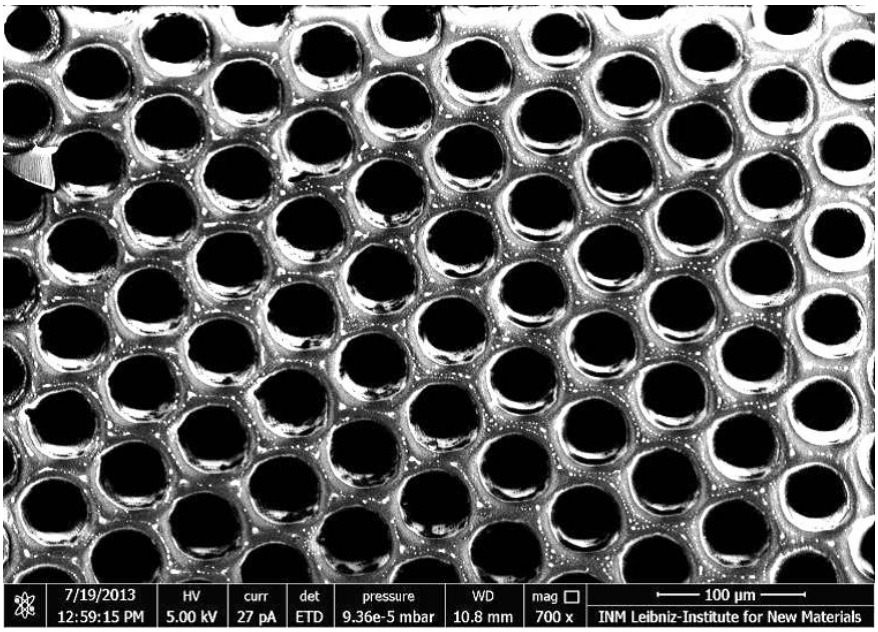

Figure 3.2 *AZ 6632 holes for the replication of PDMS pillars with a diameter of 50 µm and a height of 12 µm.*

3.1.2 PDMS structures by soft molding[1]

Fibrillar gecko-mimetic adhesives were fabricated by soft molding PDMS (Dow Corning, Sylgard 184 kit) from master templates (**Figure 3.3**).

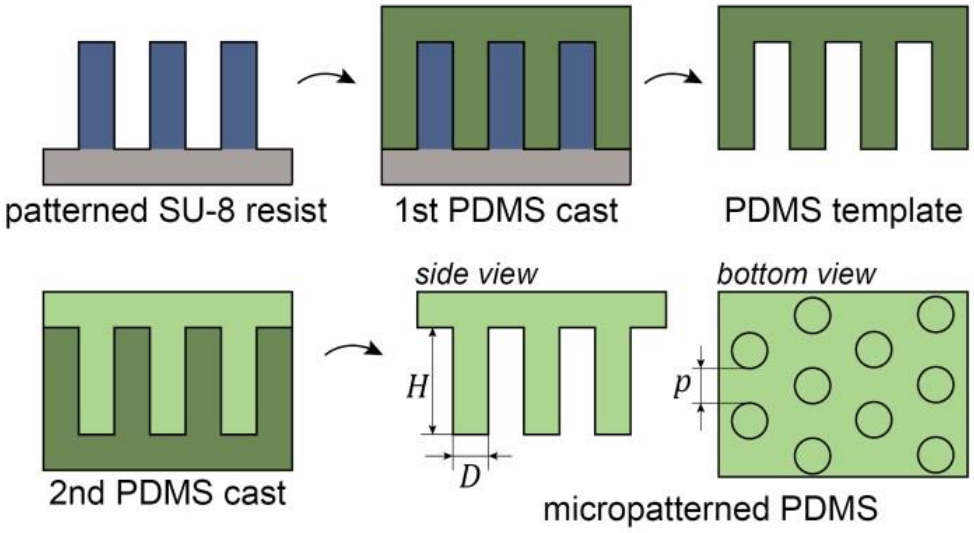

Figure 3.3 *Process scheme for manufacturing micropatterned adhesives. (A) Procedure for the fabrication of polydimethylsiloxane (PDMS) pillar array specimens using pre-patterned SU-8 templates for subsequent two-step replication into PDMS. (B) Scanning electron micrograph of a representative micropatterned PDMS sample.*

The master templates were fabricated from silicon wafers spin coated with a negative photoresist, SU-8 (Micro Resist Technology, Berlin, Germany), using a standard photolithography process. The mask employed during the UV exposure step of the photolithography process consisted of 25 fields of hexagonally packed circles of different diameters and spacings. Prior to soft molding, the templates were silanized by exposing them to approximately 50 µl of hexadecafluoro-1,1,2,2-tetrahydrooctyltrichlorosilane (Alfa Aesar, Germany) under vacuum for 30 minutesю Afterwards, they were placed in an oven at 95°C for 30 minutes. The PDMS base and the crosslinker were mixed (10:1 ratio) and degassed in a desiccator to eliminate bubbles.

[1] This subsection is content of Barreau V, Hensel R, Guimard NK, Ghatak A, McMeeking RM, Arzt E. Fibrillar Elastomeric Micropatterns Create Tunable Adhesion Even to Rough Surfaces. Adv Funct Mater. 2016; 26(26):4687-4694. doi:10.1002/adfm.201600652 but does not contain Figure 3.4.

This mixture was poured onto the templates, degassed again, and cured at 75°C for 24 h to produce the PDMS micropatterned samples. These samples were then carefully peeled off the templates. Each resulting PDMS micropatterned sample consisted of 25 8 x 8 mm^2 regions with different pillar heights (5, 12, 20, 40, or 75 μm) and diameters (5, 7.5, 10, 15, 20, 30, or 50 μm). The PDMS fibrillar arrays of different pillar heights, diameters, and aspect ratios were characterized using a scanning electron microscope (SEM) (FEI Quanta 400 ESEM) operating under high vacuum and with a beam energy of 1-15 kV (**Figure 3.3**) and a white light interferometer (WLI) (**Figure 3.4**).

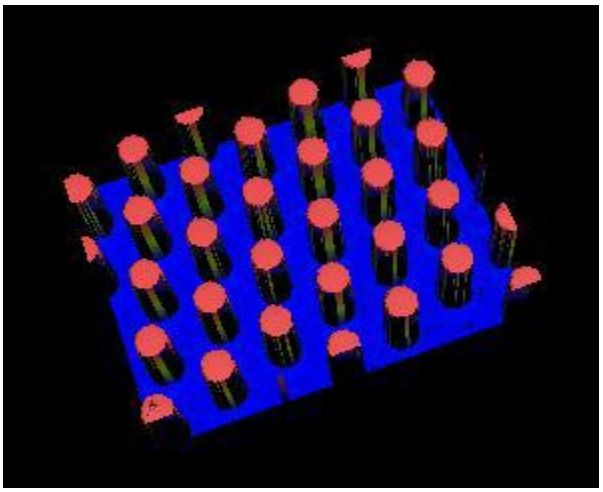

Figure 3.4 *White light interferometer images of patterned PDMS structures. Image shows pillars with a height of 25 μm and a diameter of 12 μm.*

3.1.3 PFPEdma and PU-ht sample fabrication[2]

Micropatterned adhesive surfaces were fabricated from perfluoropolyether dimethacrylate (PFPEdma, Fomblin MD40, Solvay Solexis) and a high-temperature polyurethane, (PU-ht , U-835, Alfa Aesar) using replica molding. Master structures having hexagonal micropillar arrays with aspect ratio 2 and 0.4 (pillar length: 20 µm; pillar diameters: 10 and 50 µm, and a pitch twice the respective pillar diameter) and their corresponding PDMS molds were generated as described previously.[44] For the microstructures, the PDMS prepolymer (10 weight parts of the base to 1 weight part of the curing agent) was degassed under vacuum for 5 min. It was then filled into the mold, degassed for 10 min, and cured at 75 °C for 24 h in an oven. The PFPEdma and PU-ht oligomers were mixed with 0.5 wt-% 2-hydroxy-2 methyl-propiophenone (Sigma Aldrich) as a photoinitiator for UV-curing. The pre-polymer mixtures were poured into the mold and exposed to UV-light (365 nm, Omnicure S1500, Excelitas Technologies) under a nitrogen atmosphere for 5 min. Upon crosslinking, samples were carefully peeled off the molds. For a few analyses, PU-ht was thermally post-baked in addition to a prior UV-crosslinking at 120 °C for 15 min in an oven.

[2] This subsection is content of Barreau V, Yu D, Hensel R, Arzt E. Elevated temperature adhesion of bioinspired polymeric micropatterns to glass. Journal of the Mechanical Behavior of Biomedical Materials. 2017; doi: 10.1016/j.jmbbm.2017.04.007.

3.2 Material characterization

3.2.1 Dynamic mechanical thermal analysis[3]

The mechanical properties of all materials were studied by dynamic mechanical thermal analysis (DMTA, Q800, Waters GmbH). Cuboid polymer samples with dimensions $20 \times 12.5 \times 2.5\ mm^3$ were fabricated and tested in the temperature range between -100 °C and 120 °C at a heating rate of 3 K min^{-1}. The glass transition temperature was determined from the maximum value of the viscoelastic loss factor, $\tan\delta$. All tests were performed under nitrogen atmosphere at an oscillatory frequency of 1.0 Hz in tensile mode.

3.2.2 Differential Scanning Calorimetry

Differential Scanning Calorimetry (DSC) DSC 822 E200 (Mettler Toledo) measurements were performed on PDMS, PFPEdma and PU-ht to determine if endo- or exotherm reactions occurred in the tested temperature range. The samples were first heated from 0 °C to 120 °C and then cooled down back to 0 °C. This heating-cooling cycle was performed three times. As can be seen in **Figures 3.5, 3.6** and **3.7**, the curves are smooth and do not present any peaks. So it can be concluded that the processes are reversible.

[3] This subsection is content of Barreau V, Yu D, Hensel R, Arzt E. Elevated temperature adhesion of bioinspired polymeric micropatterns to glass. Journal of the Mechanical Behavior of Biomedical Materials. 2017; doi: 10.1016/j.jmbbm.2017.04.007.

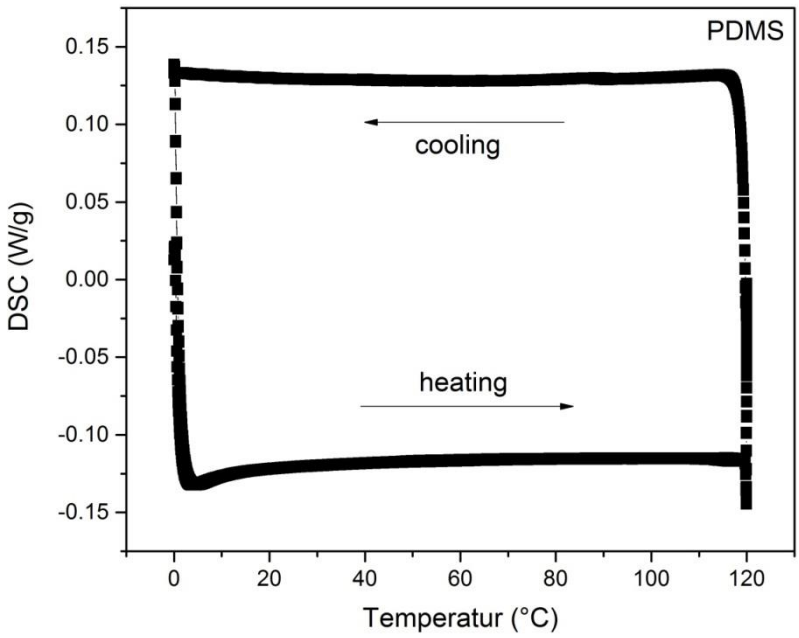

Figure 3.5 *The DSC trace of a PDMS adhesive as a function of the temperature for three heating-cooling cycles.*

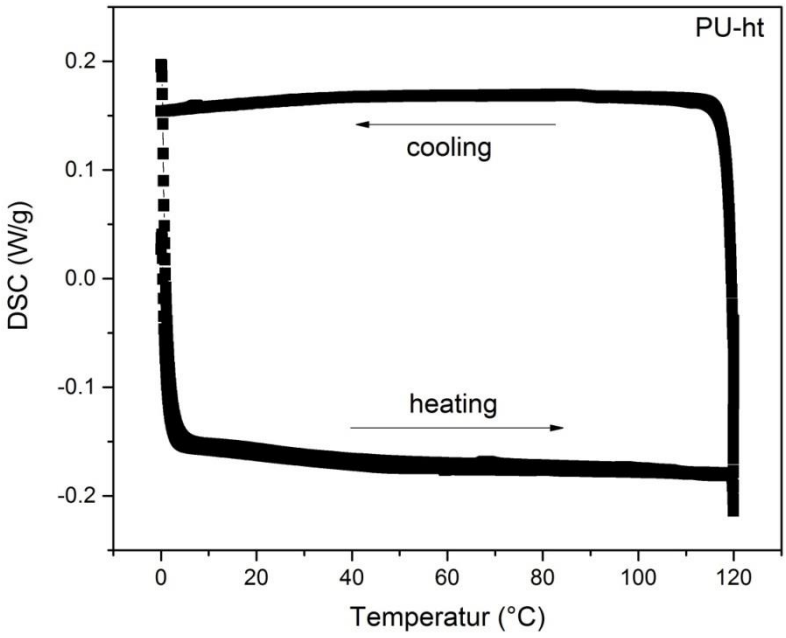

Figure 3.6 *The DSC trace of a PU-ht adhesive as a function of the temperature for three heating-cooling cycles.*

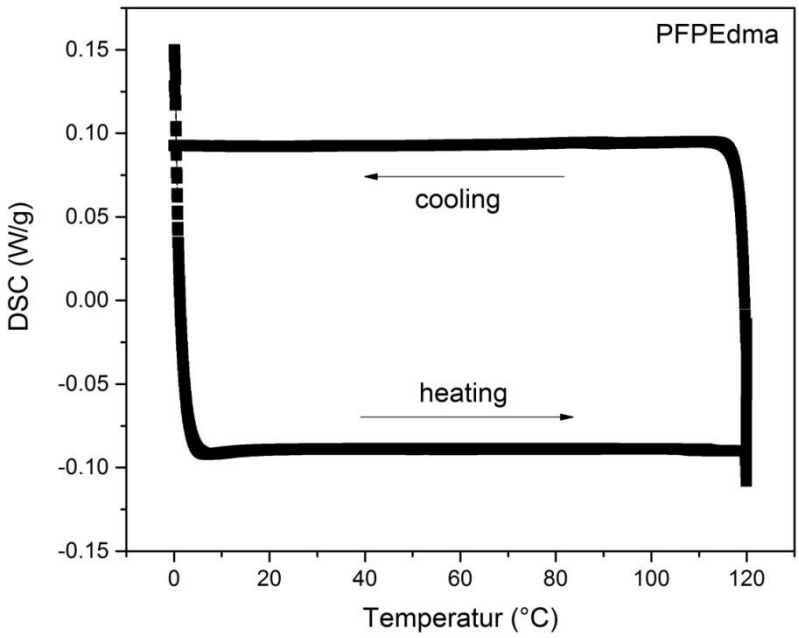

Figure 3.7 *The DSC trace of a PFPEdma adhesive as a function of the temperature for three heating-cooling cycles.*

3.2.3 X-Ray Diffraction Analysis[4]

X-ray diffraction analysis (XRD, X'Pert MRD, PANalytical) was used to characterize the material microstructure of bulk PU-ht upon (a) UV-curing and (b) UV-curing with subsequent post-bake. As a source, Cu K-alpha was used (40 kV, 30 mA). The angle (2*theta) of the incident radiation was varied between 3° and 150° in increments of 0.02°. The Soller slit was set to 2.5° and an aperture of 0.5 was used. The diffraction patterns were analyzed in terms of constructive interference patterns due to crystalline domains in the polymer microstructure.

[4] This subsection is content of Barreau V, Yu D, Hensel R, Arzt E. Elevated temperature adhesion of bioinspired polymeric micropatterns to glass. Journal of the Mechanical Behavior of Biomedical Materials. 2017; doi: 10.1016/j.jmbbm.2017.04.007.

Based on that, variations of the crystallinity before and after post-bake could be qualitatively compared.

3.2.4 Surface free energy measurement[5]

The surface free energy of PU-ht was evaluated using a contact angle goniometer (OCA35, DataPhysics), equipped with analysis software SCA20. A flat film of PU-ht was prepared by coating a 120 µm thick layer of liquid PU-ht resin on PET foil and, subsequently, UV-cross-linking as described above. Contact angles of deionized water with surface tension of 72.3 mN/m and *n*-hexadecane with surface tension of 27.5 mN/m were measured and subsequently used to deduce the surface free energy value by Wu´s Harmonic Mean Method.[72]

[5] This subsection is content of Barreau V, Yu D, Hensel R, Arzt E. Elevated temperature adhesion of bioinspired polymeric micropatterns to glass. Journal of the Mechanical Behavior of Biomedical Materials. 2017; doi: 10.1016/j.jmbbm.2017.04.007.

3.3 Characterization surface roughness

3.3.1 Roughness of the microstructures

For the samples, which are used for adhesion measurement on rough substrates, it is important to identify the surface roughness of the microstructures. For this pur, the AFM 5500 AFM/SPM (Agilent Technologies, Germany) was used. The measurements showed that the surface of the pillars, which have been produced with the resist mask (AZ resist, one step molding), present a lower roughness than the pillars fabricated with the PDMS mask (SU-8 resist, two step molding). The roughness values determined for the samples that have been directly peeled off the resist holes are $R_a = 25.5$ nm and R_z =25.9 nm. In the case of the samples fabricated from the two-step molding process the values of R_a and R_z amount to 12.5 nm and 7.4 nm, respectively (**Figure 3.8**).

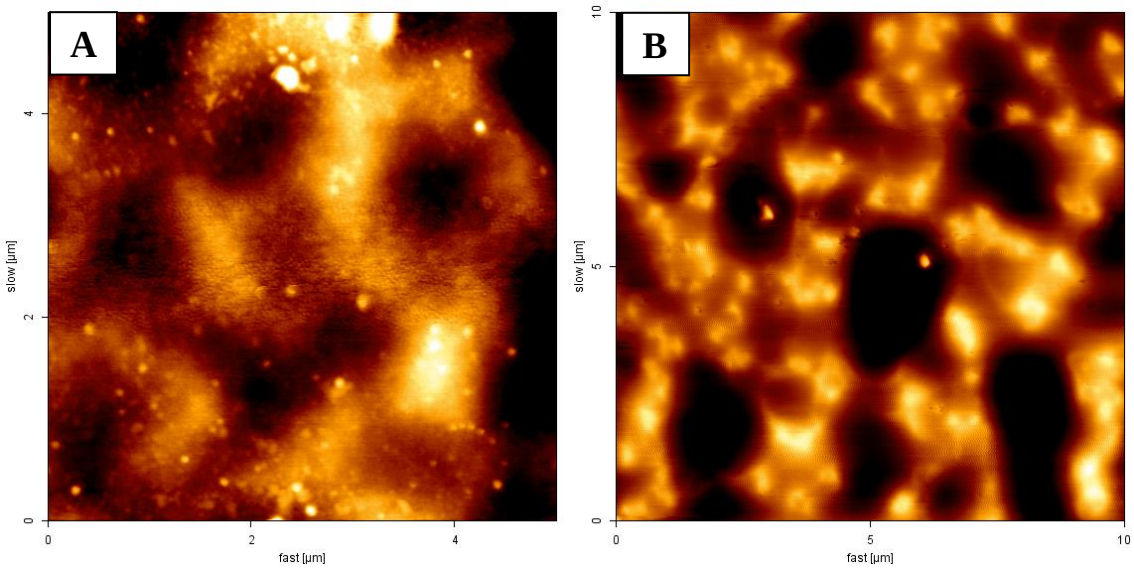

Figure 3.8 *AFM measurements for samples made with (A) resist mask and (B) PDMS mask.*

3.3.2 Preparation and characterization of rough glasses[6]

Flat glass was selected as the substrate to study the adhesion of the PDMS fibrillar samples. Each substrate was roughened with sandpaper (Buehler GmbH, Düsseldorf, Germany) of different asperity sizes. These rough substrates were in turn used as substrates for adhesion measurements. The roughness profile of each substrate was determined using a profilometer (Surform 1500 SD3, Zeiss GmbH)

Measurements were made using a 1 μm radius stylus at $0.3\ \mathrm{mm\ s^{-1}}$ scan speed. Three measurements were taken at different locations on each sample.

The amplitude parameter is the mean peak-to-valley profile roughness that is given by $R_z = \frac{1}{k}\sum_{i=1}^{k} R_{zi}$, where k is the number of cut-off filter lengths and z_i is the peak to valley distance at the i-th location. Two spacing parameters are defined as follows: S_m is the mean distance between successive points as they cross the mean line and is given by $S_m = \frac{1}{n}\sum_{i=1}^{n} S_{mi}$. The mean spacing of adjacent local peaks, *S*, is given by $S = \frac{1}{n}\sum_{i=1}^{n} S_i$. The power spectra of the glass substrates GS1 to GS4 were calculated based on the amplitude of the Fourier transformed data from the line scans using Origin, (*OriginLab, v. 9*).

Normalization of the power spectrum was performed via the mean square amplitude (MSA) method, i.e. $\frac{Re^2+Im^2}{n^2}$ where Re and Im are the real and imaginary parts of the transform data and n is the length of the input sequence

[6] This subsection is content of Barreau V, Hensel R, Guimard NK, Ghatak A, McMeeking RM, Arzt E. Fibrillar Elastomeric Micropatterns Create Tunable Adhesion Even to Rough Surfaces. Adv Funct Mater. 2016; 26(26):4687-4694. doi:10.1002/adfm.201600652.

3.3.3 Preparation and characterization of sandpaper

Commercial sandpaper (Buehler GmbH, Düsseldorf, Germany) with an area of 10 mm² was glued on the glass and used as substrates for adhesion measurements. The roughness and the profile of the substrates were determined with a profilometer (Surform 1500 SD3, Zeiss GmbH) (**Figure 3.9**) and white light interferometry. The average particle diameter and the average roughness R_a are presented in **Table 3.1.**

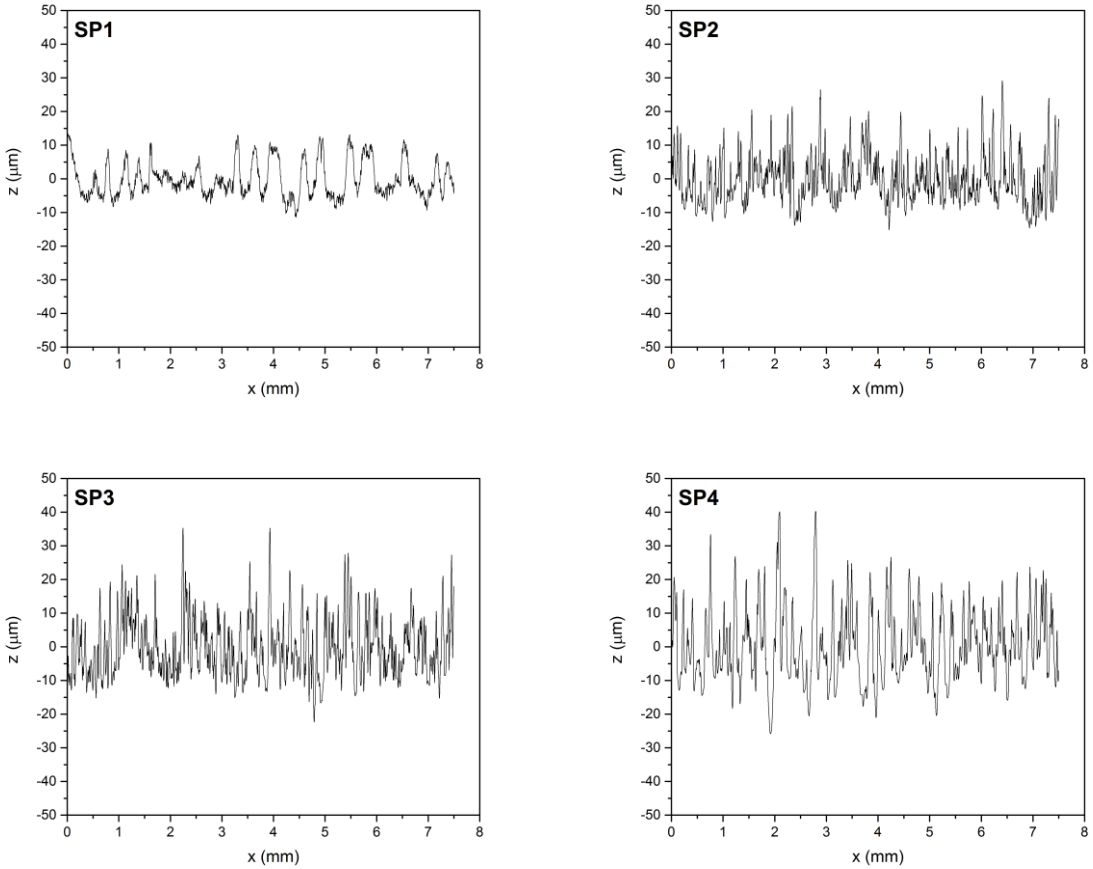

Figure 3.9 *Surface profiles of the sandpaper substrates SP1 to SP4 measured by profilometry.*

Table 3.1 *Average particle diameter and roughness parameters of sandpaper.*

FEPA designation*	Substrate	Average particle diameter (μm)	*Ra* (μm)
P1200	SP1	~14	5.77
P400	SP2	~35	10.61
P240	SP3	~58	13.88
P60	SP4	~269	83.94

**FEPA (Federation of European Producers of Abrasives), ISO 6344 standard.*

3.4 Adhesion measurements

3.4.1 Adhesion measurements to rough substrates with flat probe[7]

Normal adhesion was measured using a custom-built adhesion-measuring device.[73], [74] The base of the device consists of a three-axis piezo stage (Nanocube, physics instruments Karlsruhe, Germany), with nanoscale resolution, sitting on a pivotable six-axis table (Hexapod F.206, physics instruments Karlsruhe, Germany), which is adjustable on the microscale in the x, y and z directions, for sample positioning.

Adhesion to a sample on the stage was measured using a force sensor system comprised of a glass spring (with a spring constant of $2450.7\ \mathrm{N\,m^{-1}}$) and a laser interferometer (**Figure 3.10**). The spring consists of an asymmetrically strained glass slide onto which a mirror is mounted to reflect the light from the laser (SP 100, SIOS Messtechnik, Ilmenau, Germany). The substrate, against which the samples adhesion is tested, was glued onto an adapter with cyanoacrylate glue (Cyanolube, HK Wentworth Ltd., Derbyshire). To allow for further adjustment of the position of the glass spring, the spring is mounted onto a two-axis tilt stage (OWIS GmbH, Stauffenberg, Germany). The whole device sits on an anti-vibration table (TS 150, Technical Manufacturing Corporation, USA) to reduce the noise arising during measurements.

For adhesion measurements, the desired PDMS sample was placed on the pivotable stage and the substrate was immobilized on the spring. The substrate was manually aligned with the sample, such that the surfaces of each were parallel to each other, using two cameras, one located on the y-axis and the other on the x-axis of the sample. Alignment was further optimized by mechanically adjusting the sample stage along the x- and y-axes until a maximum pull-off force was achieved for a constant preload. Once the optimal sample position was identified, the sample was cleaned with ethanol and the pull-off force was measured for each rough surface.

[7] This subsection is content of Barreau V, Hensel R, Guimard NK, Ghatak A, McMeeking RM, Arzt E. Fibrillar Elastomeric Micropatterns Create Tunable Adhesion Even to Rough Surfaces. Adv Funct Mater. 2016; 26(26):4687-4694. doi:10.1002/adfm.201600652.

Each data point represents the mean value of five measurements on four different in-plane positions on each substrate. The error bars indicate the standard deviation. The adhesion of flat, unpatterned PDMS samples, in addition to the micropatterned PDMS samples, was characterized for control purposes. All measurements were performed at an approach/retraction velocity of $5\ \mathrm{m\,s^{-1}}$ at a controlled temperature and relative humidity (RH) of 24°C and 40% RH, respectively. The adhesion results are presented as pull-off stress values, which were derived by dividing the measured force by the apparent contact area.

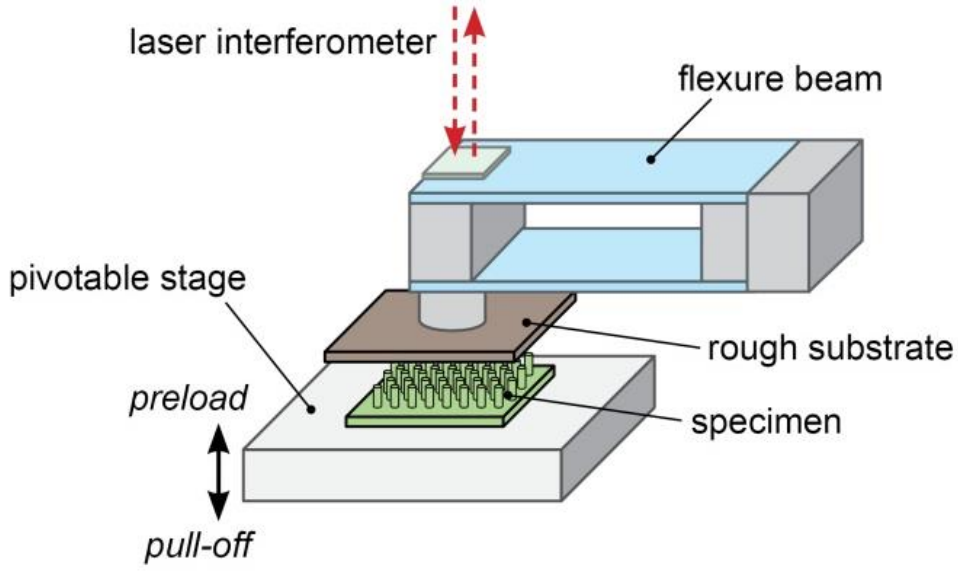

Figure 3.10 *Procedure for the fabrication of polydimethylsiloxane (PDMS) pillar array specimens using pre-patterned SU-8 templates for subsequent two-step replication into PDMS.*

3.4.2 Adhesion measurements at elevated temperatures[8]

In contrast to 3.4.1, the adhesion was measured by a spherical probe.

The adhesion were obtained by using a custom-built adhesion-measuring device, which is schematically shown in **Figure 3.11**. It consists of a pivotable stage, equipped with a heating element (PE120, Linkam), and a spherical glass probe with a curvature radius of 15 mm mounted on a flexible double beam glass spring. Forces were deduced from the beam deflection measured by a laser interferometer multiplied with its spring constant of 2240 N m^{-1}.

Displacements reported correspond to the elongation of the micropatterned adhesives during retraction, i.e., they were calculated from the differential displacement of the stage relative to the deflected beam. The pull-off force (maximum tensile force) was determined from these force-displacement curves. The pull-off stress was calculated by dividing the pull-off force by the apparent contact area. The apparent contact area was calculated according to a geometrical relationship based on the radius of the probe and the indentation depth obtained from the experiments.[75] The work of separation (area under the curve in the tensile regime) was determined from the stress-displacement curves. All measurements were performed at a constant compressive preload of 30 mN, at four different sample positions, at constant displacement velocity of 5 μm s^{-1}, and at a relative humidity of 45 ± 5 %. The adhesion tests were conducted by increasing the temperature of the samples from 20 °C to 120 °C (heating rate: 20 °C min^{-1}) and subsequently decreasing the temperature from 120 °C to 20 °C (cooling rate: 20 °C min^{-1}) in increments of 20 °C. Before the adhesion measurements, the temperature was held constant for more than 15 min. The cooling process was initiated by flowing cold water through the heating stage. Each heating-cooling cycle was traversed three times.

[8] This subsection is content of Barreau V, Yu D, Hensel R, Arzt E. Elevated temperature adhesion of bioinspired polymeric micropatterns to glass. Journal of the Mechanical Behavior of Biomedical Materials. 2017; doi: 10.1016/j.jmbbm.2017.04.007.

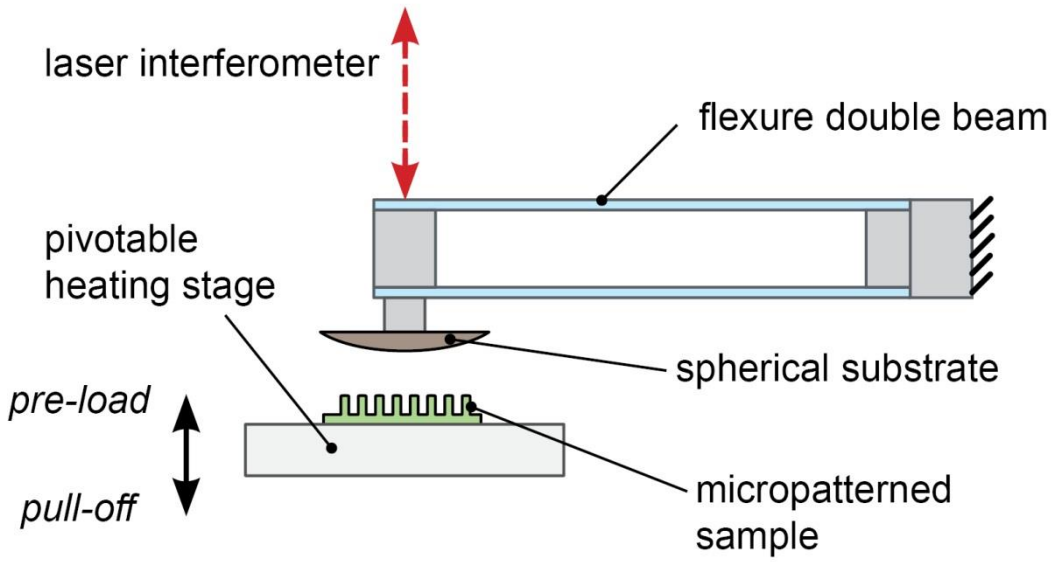

Figure 3.11 *Schematic illustration of the adhesion measurement device that consists of a pivotable and heating stage for sample manipulation and a glass lens mounted on a flexible double beam. The laser interferometer monitors the elastic deflection of the beam, from which the forces are deduced.*

3.4.3 Alignment of the flat, rough substrates

The appearance of an alignment problem during adhesion measurements performed with a flat-ended cylindrical glass probe on a flat and patterned PDMS was already shown by Kroner [76]. For flat PDMS, a 0.2° tilt angle reduced the adhesion value by ~ 10% compared to aligned measurements. For patterned PDMS the impact of the tilt angle 0.2° was more important: for structures with AR = 0.2 pillars, the loss reached 16%, and for AR = 0.4 it even reached 26%.

For rough substrates, such dependencies should be identified. Therefore, force-displacement curves were measured for different tilt angles (**Figure 3.12**). The maximum forces were determined and plotted against the tilt angle.

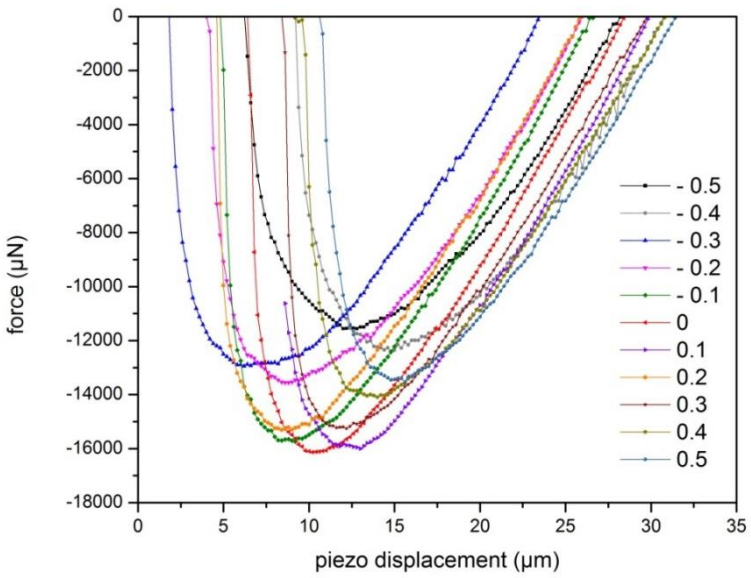

Figure 3.12 *Force-displacement curves measured for different tilt angles for PDMS sample H75, D20 on rough glass with* R_a *= 0.02*

By that, differences for various roughnesses and AR have been identified. For pillars with a height of 75 µm and AR = 3.75 and 1.5 the curves show a clear maximum in the adhesion and a strong dependency on the angle. For a tilt angle of 0.2°, the adhesion dropped about 28% and 12%, respectively. For taller pillars with a height of 5 µm, the curve did not present any defined maximum. Nevertheless, for a tilt angle of 0.2° the adhesion dropped by 26% and 11% for AR = 1.5 and AR = 0.1, respectively (**Figure 3.13**).

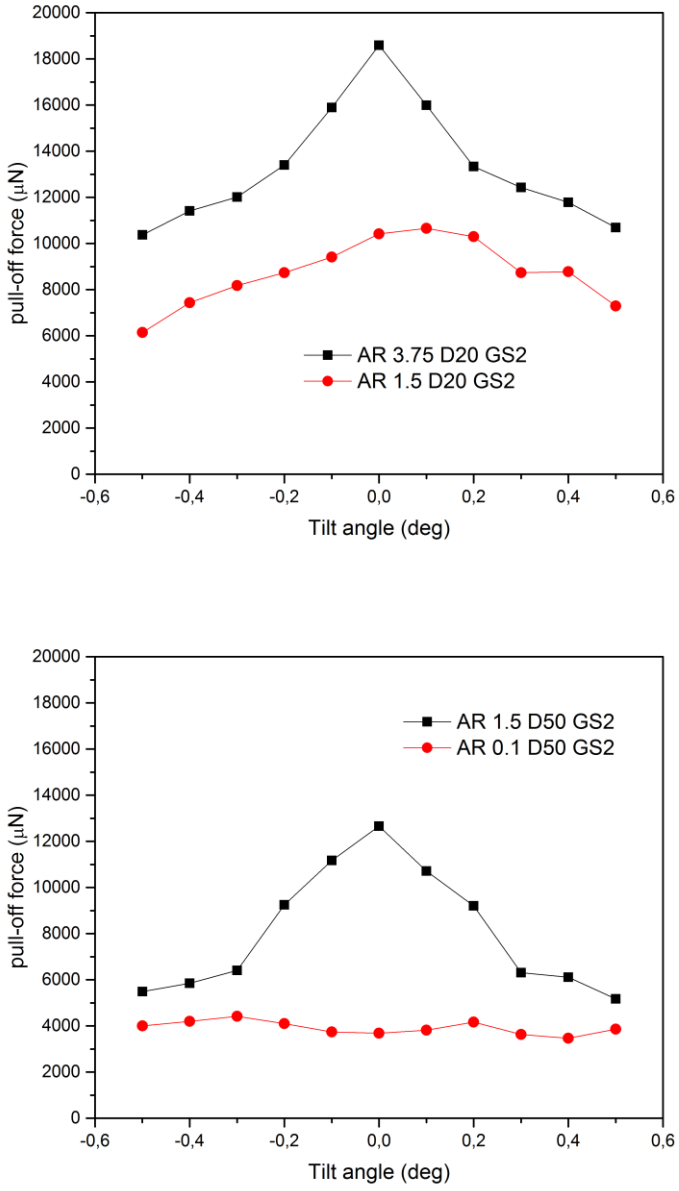

Figure 3.13 *Adhesion of PDMS sample with pillar height of 5 and 75 µm measured on rough glass with R_a = 0.10 µm for different tilt angles.*

Furthermore, it was also observed that different angle dependencies exist on different rough substrates. The dependency of the adhesion values on the tilt angle increased with increasing roughness of the substrates. In such a way, GS2 presents a significantly higher angle dependency than GS1. For pillars with a height of 75 µm, the angle dependency for GS2 amounts to 28% for AR = 3.75 and 26% for AR = 1.5. The angle dependency for GS1 amounts to 12% for AR = 3.75 and 13% for AR = 1.5 (**Figure 3.14**).

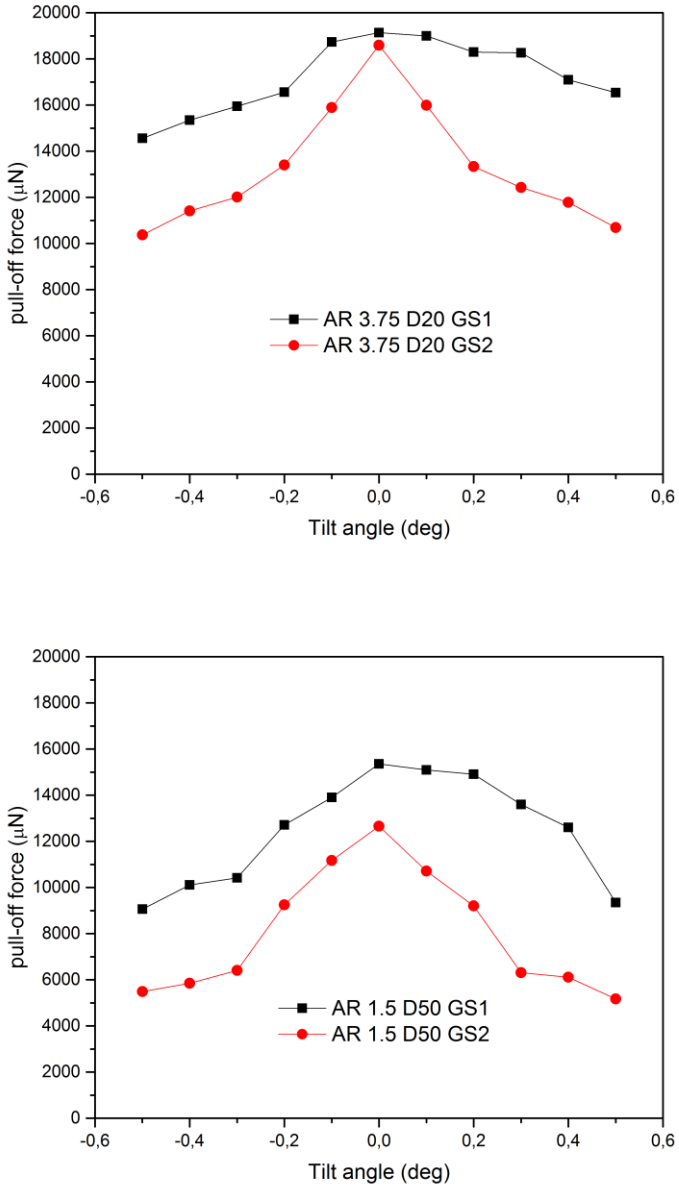

Figure 3.14 *Adhesion of PDMS sample with pillar height of 75 µm measured on rough glass with* R_a *= 0.02 µm* and *Ra = 0.10 µm for different tilt angles.*

The measurements clearly reveal a tendency: The smaller the diameter, the more pillars come into contact and the stronger is the influence of the orientation of the samples on the adhesion. This observation is in agreement with the theoretical results by Bacca et al [77] on the efficiency of load sharing, which decreases with an increasing number of pillars.

3.5 Calculation of contact area

To compare adhesion values for different structures and conditions, the most suitable parameter is the pull-off stress, which can be calculated by dividing the pull-off force by the apparent contact area πa^2. Hereby, the important question is how to calculate the contact radius *a*. Two strategies have been explored in this work. The first is related to a geometrical calculation and the second corresponds to the Hertz theory. Geometrically, the contact radius and thus the contact area can be calculated according to a simple geometrical relationship for each indenter depth (**Figure 3.15**).

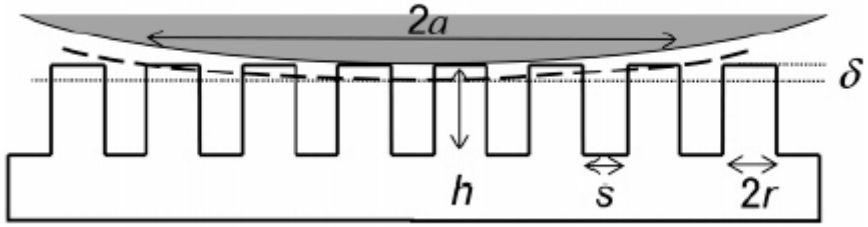

Figure 3.15 *Schematic of the geometric calculation of the contact area: δ is the indentation depth, a the radius of the contact area, h the pillar height, r the pillar radius, s the spacing between the pillars* [75].

The radius of the spherical indenter, R, is a known value and the indentation depth, δ, is determined in the experiments. So, the contact radius can be calculated according to:

$$a = \sqrt{R^2 - (R - \delta)^2}\,. \qquad \textbf{(3.1)}$$

For the calculation of the contact area according to Hertz, it has to reminded that this theory does not consider adhesion and shows a strong dependency on the Young´s modulus, whose values are in the denominator of the equation. As a result, the higher the modulus, the smaller the resulting contact area and thus the greater the pull-off stresses.

The **Figure 3.16** shows the comparison of pull-off force values calculated with the geometrical method and according to the Hertz theory. Hereby, the storage moduli of PDMS

and PFPEdma amount to 2,69 MPa and 9,98 MPa, respectively, while it reaches a value of 49,81 MPa for PU-ht. Furthermore, the results demonstrate that the higher the storage modulus, the more important is the difference in the pull-off stress between both calculation methods. In the case of PDMS with a low storage modulus, a geometric calculation leads to nearly the same result than the Hertz theory. This is, however, quite different for PU-ht, which shows a difference of a factor of two between the pull-off stresses calculated geometrically and according to the Hertz theory.

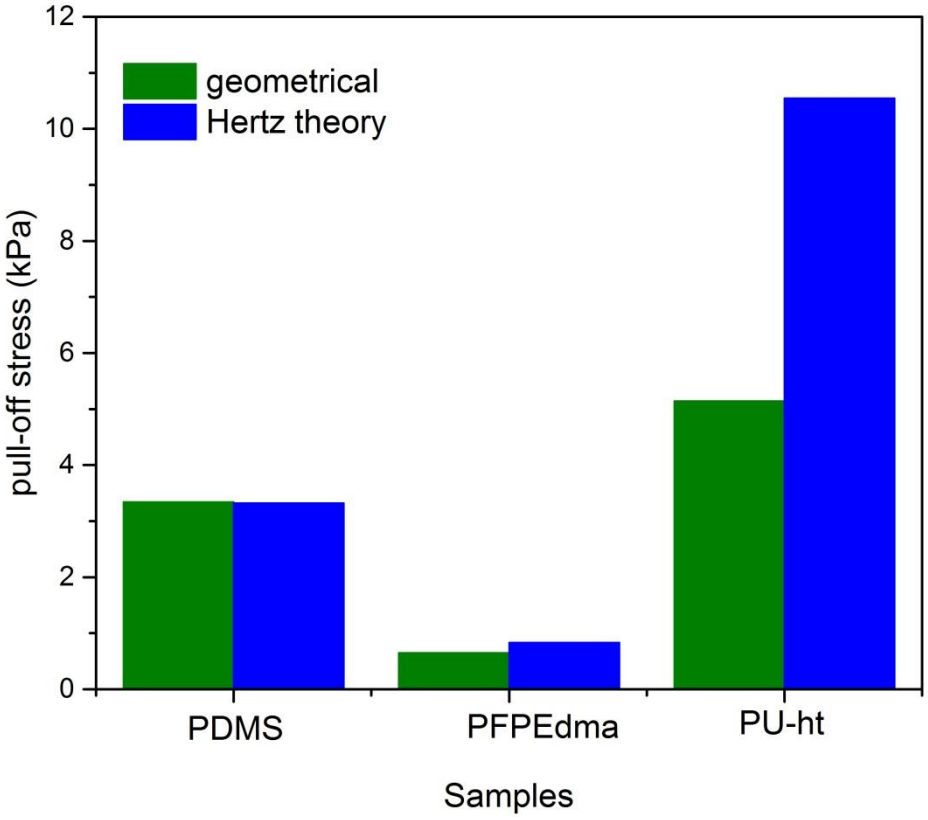

Figure 3.16 *Comparison of pull-off force values calculated with the geometrical method and according to the Hertz theory.*

Another important question is, if these models also work if there is a contact with the backing layer. In any measurements performed in this work, a contact with the backing layer occurred. Deformation of the pillars has been calculated during all the measurements and for all materials. For instance, considering the greatest preload (30 mN) and shortest pillar (10 µm), the deformation amounts to about 70% for PDMS, 30% for PFPEdma and 25% for PU-ht. Crosby [78] et al. showed, that a contact with backing layer is only possible in the case of

low aspect ratio pillars with large separation. The conditions for contact with backing layer were modeled theoretically [79] [80] and calculated by Greiner et al [75]. They found out that for the pillar geometry used in this work a contact with the backing layer can only occur with pillars of a height of 1 nm.

4 Fibrillar elastomeric micropatterns create tunable adhesion even to rough surfaces

4.1 Abstract

Biologically inspired, fibrillar dry adhesives continue to attract much attention as they are instrumental for emerging applications and technologies. To date, the adhesion of micropatterned gecko-inspired surfaces has predominantly been tested on stiff, smooth substrates. However, all natural and almost all artificial surfaces have roughnesses on one or more different length scales. In the present approach, we design and analyze micropillar-patterned PDMS surfaces with superior adhesion to glass substrates with different roughnesses. The results reveal for the first time adhesive and non-adhesive states depending on the micropillar geometry relative to the surface roughness profile. The data obtained further demonstrate that, in the adhesive regime, fibrillar gecko-inspired adhesive structures can be used with advantage on rough surfaces; this finding may open up new applications in the fields of robotics, biomedicine, and space exploration.

[1] This chapter is content of Barreau V, Hensel R, Guimard NK, Ghatak A, McMeeking RM, Arzt E. Fibrillar Elastomeric Micropatterns Create Tunable Adhesion Even to Rough Surfaces. Adv Funct Mater. 2016; 26(26):4687-4694. doi:10.1002/adfm.201600652.

4.2 Introduction

The gecko is considered to be the most interesting animal among those that have the remarkable ability to reversibly adhere to nearly all kinds of surfaces. The growing number of studies published in this field in the last two decades reflects the interest in elucidating the mechanism behind gecko adhesion. Experimental evidence has suggested that the adhesive ability of geckos can be attributed to van der Waals and capillary forces.[12], [81]–[84] These forces are maximized by the structure of the gecko toe pad, which is composed of hundreds of thousands of keratinous hairs (called setae). Each hair is about 110 µm long and branches into hundreds of even finer hairs (called spatula) that are about 20 nm thick and 200 nm long. Thus, the gecko relies on hierarchically organized structures consisting of micro- and nano-sized hairy features to achieve adhesion to almost any surface.[16], [17], [85]–[88]

There are several studies that have demonstrated and characterized the adhesion of gecko-inspired micropatterned surfaces on hard, smooth substrates (for reviews see, for instance, refs.[32], [89]–[95]). However, considering that all natural and almost all artificial surfaces have a roughness on one or more different length scales, little research has been conducted to comprehend and optimize the adhesion of such structures to rough surfaces. Huber *et al.* [23] are among the few that have performed such studies, which include measurements, by atomic force microscopy (AFM), of the normal adhesion of a single gecko spatula to substrates with different roughnesses. They found that a spatula adapts well to a surface with a low root mean square (RMS) roughness (smaller than 200 nm) and also adheres strongly to substrates with an RMS roughness above 200 nm, but shows a distinct minimum in adhesion at RMS roughness of 200 nm, which is a typical spatula dimension. Recently, Gillies *et al*. [27] observed a similar dramatic drop of shear resistance for geckos on wavy substrates that exhibited a length scale of amplitudes and wavelengths similar to the lamella length and inter-lamellar spacing, specifically in the sub-millimeter range. Persson performed the first theoretical studies on adhesion as a function of the setal architecture and surface roughness.[26], [34] He demonstrated that even a relatively small roughness can lead to the disappearance of the adhesion between two surfaces. More recently, studies on the influence of technologically relevant rough surfaces on the adhesion of biomimetic adhesives confirmed that adhesion decreases for rough surfaces when compared to smooth surfaces [36] [38] [39] [96] [97] [98] [99].

Because little is known about the influence of micropillar dimensions on dry adhesion of gecko-mimicking structures on rough substrates, the objective of this study is to systematically and quantitatively characterize this effect. Arrays with different micropillar dimensions were generated from polydimethylsiloxane (PDMS) using soft molding techniques. Then, the influence of pillar diameter and height on adhesion to a number of stiff substrates with different roughness was assessed. The goal was to improve the understanding of the role of surface roughness, in comparison to smooth controls.

4.3 Materials and methods

4.3.1 Sample fabrication

Fibrillar gecko-mimetic adhesives were fabricated by soft molding PDMS (Dow Corning, Sylgard 184 kit) from master templates (**Figure 4.1**). Master templates were fabricated from silicon wafers spin coated with a negative photoresist, SU8 (Micro Resist Technology, Berlin, Germany), using a standard photolithography process.

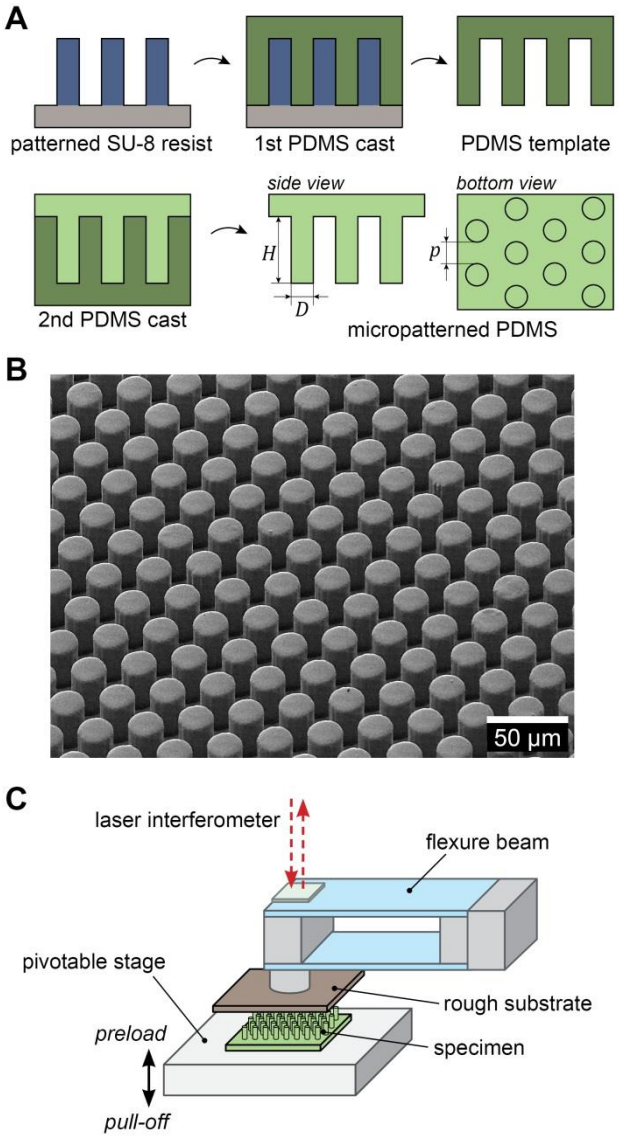

Figure 4.1 *Process scheme for manufacturing micropatterned adhesives and experimental setup for normal adhesion measurements. (A) Procedure for the fabrication of polydimethylsiloxane (PDMS) pillar array specimens using pre-patterned SU-8 templates for subsequent two-step replication into PDMS. (B) Scanning electron micrograph of a representative micropatterned PDMS sample. (C) Schematic illustration of the adhesion measurement device that consists of a pivotable stage for sample manipulation and a rough substrate mounted on a flexible double beam. The laser interferometer monitors the elastic deflection of the beam, from which the forces are deduced, during the measurement.*

The mask employed during the UV exposure step of the photolithography process consisted of 25 fields of hexagonally packed circles of different diameters and spacings. Prior to soft molding, templates were silanized by exposure to approximately 50 µl of hexadecafluoro-1,1,2,2-tetrahydrooctyltrichlorosilane (Alfa Aesar, Germany) under vacuum for 30 minutes. The templates were then placed in an oven at 95°C for 30 minutes. The PDMS base and crosslinker were mixed (10:1 ratio) and degassed in a desiccator to eliminate

bubbles. This mixture was poured onto the templates, degassed again, and cured at 75°C for 24 h to produce the PDMS micropatterned samples. These samples were then carefully peeled off the templates. Each resulting PDMS micropatterned sample consisted of 25 8 x 8 mm^2 regions each with different pillar heights (5, 12, 20, 40, or 75 μm) and diameters (5, 7.5, 10, 15, 20, 30, or 50 μm). The PDMS fibrillar arrays of different pillar heights, diameters, and aspect ratios were characterized using a scanning electron microscope (SEM) (FEI Quanta 400 ESEM) operating under high vacuum and with a beam energy of 1-15 kV.

4.3.2 Preparation and characterization of rough surfaces

Flat glass was selected as the substrate of choice to study the adhesion of the PDMS fibrillar samples. Each substrate was roughened with sandpaper (Buehler GmbH, Düsseldorf, Germany) of different asperity sizes. These rough substrates were in turn used as substrates for adhesion measurements. The roughness profile of each substrate was determined using a profilometer (Surform 1500 SD3, Zeiss GmbH) (**Figure 4.2A**).

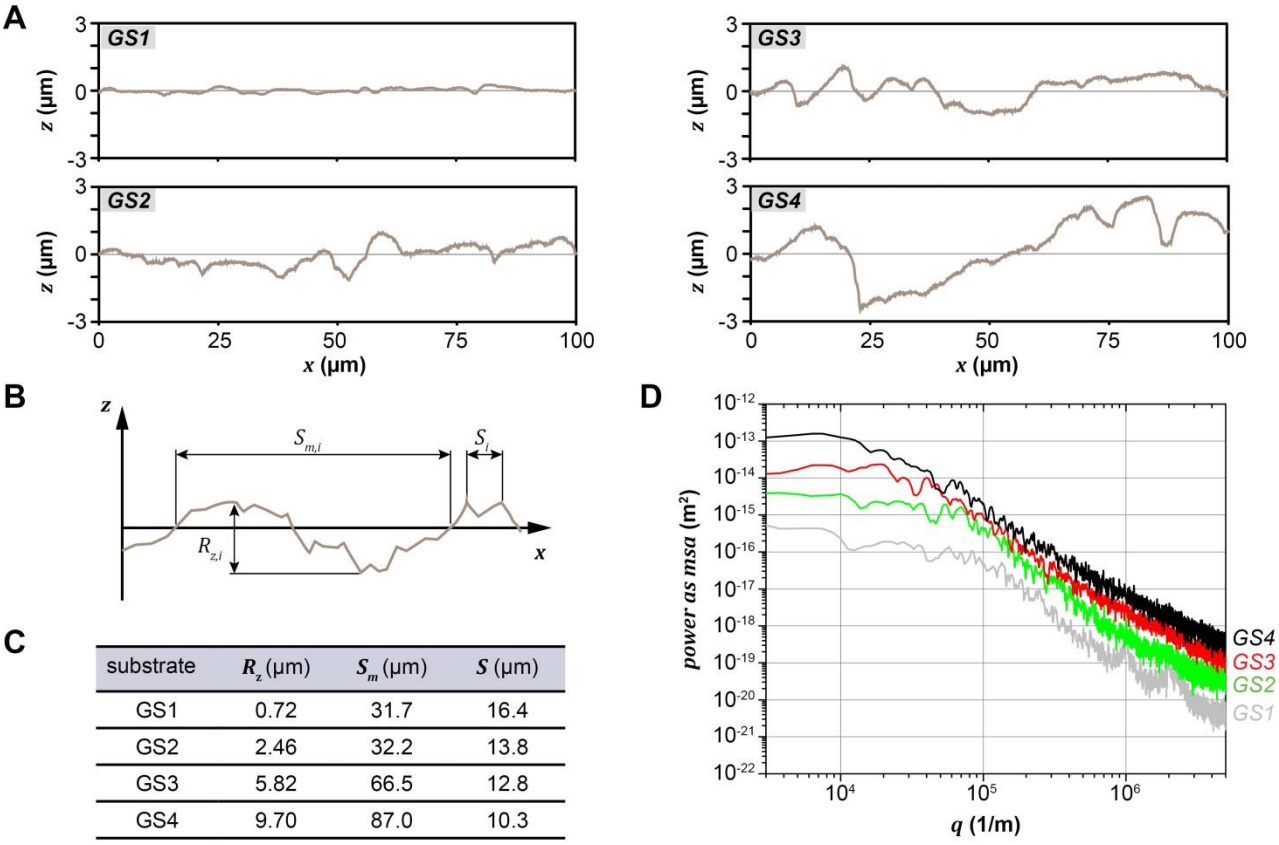

substrate	R_z (µm)	S_m (µm)	S (µm)
GS1	0.72	31.7	16.4
GS2	2.46	32.2	13.8
GS3	5.82	66.5	12.8
GS4	9.70	87.0	10.3

Figure 4.2 *Surface topographies of rough substrates. (A) Surface profiles of the roughened glass substrates GS1 to GS4 measured by profilometry. (B) Schematic representation of the surface roughness parameters. The amplitude parameter of the surface profiles is the mean peak-to-valley profile roughness, given by* $\boldsymbol{R_z = \frac{1}{k}\sum_{i=1}^{k} R_{z,i}}$*. Two spacing parameters are defined:* $\boldsymbol{S_m}$ *is the mean distance between successive points as they cross the mean line and is given by* $\boldsymbol{S_m = \frac{1}{n}\sum_{i=1}^{n} S_{mi}}$*. The mean spacing of adjacent local peaks,* $\boldsymbol{S}$*, is given by* $\boldsymbol{S = \frac{1}{n}\sum_{i=1}^{n} S_i}$*. The subscript* $\boldsymbol{i}$ *refers to the i-th location,* $\boldsymbol{k}$ *is the number of cut-off filter lengths, and* $\boldsymbol{n}$ *is the number of* $\boldsymbol{i}$ *measurements. (C) Results of roughness mean values for the substrates GS1 to GS4 obtained from surface profilometry. (D) Surface roughness power spectra of the glass substrates GS1 to GS4.*

Measurements were made using a 1 µm radius stylus at $0.3\ \mathrm{mm\ s^{-1}}$ scan speed. Three measurements were taken at different locations on each sample.

The amplitude parameter is the mean peak-to-valley profile roughness that is given by $R_z = \frac{1}{k}\sum_{i=1}^{k} R_{zi}$, where k is the number of cut-off filter lengths and z_i is the peak to valley distance at the i-th location. Two spacing parameters are defined as follows: S_m is the mean distance between successive points as they cross the mean line and is given by $S_m = \frac{1}{n}\sum_{i=1}^{n} S_{mi}$. The mean spacing of adjacent local peaks, S, is given by $S = \frac{1}{n}\sum_{i=1}^{n} S_i$. The power spectra of the glass substrates GS1 to GS4 were calculated based on the amplitude of the

Fourier transformed data from the line scans using Origin, (*OriginLab, v. 9*). Normalization of the power spectrum was performed via the mean square amplitude (MSA) method, i.e. $\frac{Re^2+Im^2}{n^2}$ where Re and Im are the real and imaginary parts of the transform data and n is the length of the input sequence.

4.3.3 Adhesion measurements

Normal adhesion was measured using a custom-built adhesion-measuring device (**Figure 4.1C**).[73], [74] The base of the device consists of a three-axis piezo stage (Nanocube, physics instruments Karlsruhe, Germany), with nanoscale resolution, sitting on a pivotable six-axis table (Hexapod F.206, physics instruments Karlsruhe, Germany), which is adjustable on the microscale in the x, y and z directions, for sample positioning. Adhesion to a sample on the stage was measured using a force sensor system comprised of a glass spring (with a spring constant of $2450.7\ \mathrm{N\ m^{-1}}$) and a laser interferometer. The spring consists of an asymmetrically strained glass slide onto which a mirror is mounted to reflect the light from the laser (SP 100, SIOS Messtechnik, Ilmenau, Germany). The substrate, against which the samples adhesion is tested, was glued onto an adapter with cyanoacrylate glue (Cyanolube, HK Wentworth Ltd., Derbyshire). To allow for further adjustment of the position of the glass spring, the spring is mounted onto a two-axis tilt stage (OWIS GmbH, Stauffenberg, Germany). The whole device sits on an anti-vibration table (TS 150, Technical Manufacturing Corporation, USA) to reduce the noise arising during measurements.

For adhesion measurements, the desired PDMS sample was placed on the pivotable stage and the substrate was immobilized on the spring. The substrate was manually aligned with the sample, such that the surfaces of each were parallel to each other, using two cameras, one located on the y-axis and the other on the x-axis of the sample. Alignment was further optimized by mechanically adjusting the sample stage along the x- and y-axes until a maximum pull-off force was achieved for a constant preload. Once the optimal sample position was identified, the sample was cleaned with ethanol and the pull-off force was measured for each rough surface. Each data point represents the mean value of five measurements on four different in-plane positions on each substrate. The error bars indicate

the standard deviation. The adhesion of flat, unpatterned PDMS samples, in addition to the micropatterned PDMS samples, was characterized for control purposes. All measurements were performed at an approach/retraction velocity of $5\ \mathrm{m\ s^{-1}}$ at a controlled temperature and relative humidity (RH) of 24°C and 40% RH, respectively. The adhesion results are presented as pull-off stress values, which were derived by dividing the measured force by the apparent contact area.

4.4 Results

Micropatterned elastomeric PDMS adhesives were produced via a soft molding process from a micropatterned SU-8 photoresist master template (**Figure 4.1A**). To realize the tone inversion, the PDMS replica generated after the first molding process was in turn used as a template for a second replication step, again by soft molding PDMS. By varying the resist thickness and the mask pattern dimensions, specimens with micropillar structures ranging from 5 to 50 µm in pillar diameter, D, and from 5 to 75 µm in pillar height, H, were fabricated. **Figure 4.1B** shows a representative scanning electron micrograph of a micropatterned PDMS specimen. PDMS pillar structures, particularly of small diameters with an aspect ratio, H/D, larger than 4, tended to cluster due to an insufficient bending stiffness. To avoid such artifacts, adhesion measurements were limited to specimens with a maximum aspect ratio of about 3. **Figure 4.1C** schematically illustrates the setup for testing adhesion of the fabricated specimens to several rough substrates. The custom-built device consists of the nominally flat, but micro-rough substrate mounted on the flexure beam and a pivotable stage allowing for specimen manipulation (attachment and detachment) and for the required pre-alignment. A laser interferometer was used to record beam deflection, which was converted into a force through multiplication by the spring constant of the flexure beam.[73]

Figure 4.2 depicts the characteristic height-distance profile, obtained using surface contact profilometry, for glass substrates (GS) roughened with sandpaper. The surface roughness parameters are schematically illustrated in **Figure 4.2B** and the measured surface roughness values for each substrate are tabulated in **Figure 4.2C**. For the substrates GS1 to GS4, the vertical roughness parameter (R_z), which is the mean peak to valley distance,

increases from 0.7 to 9.7 µm and the lateral spacing parameter (S_m), which is the mean distance of the spacing between successive points as they cross the mean line, increases from 31.7 to 87 µm. Additionally, the mean distance between adjacent peaks (S) slightly decreases, from 16.4 to 10.3 µm. The increase of roughness from GS1 to GS4 is also reflected in the Fourier transformed data based on line scans (**Figure 4.2D**). The power spectra indicate a random, self-affine roughness of the substrates upon sandpaper roughening due to the continuous decrease of the square amplitude with increasing wave numbers.[100]

The adhesion measurements were performed by pressing the micropatterned adhesives onto the substrates in the normal direction with various preloads of 10, 25 and 40 mN. The results for the rough substrates GS1 and GS3 and the smooth control are shown as double-logarithmic plots in **Figure 4.3A**. Adhesion is seen to decrease strongly with increasing roughness, which is in agreement with earlier studies with unpatterned elastomeric specimens.[101]–[103] In addition, the pull-off stress for the smooth substrate was found to be preload independent in line with our earlier studies,[104] whereas a strong influence of preload was observed for the rough substrates. This finding is significant and will be discussed in more detail in the next section.

In **Figure 4.3A**, it is further shown that the pull-off stress increases for smaller pillar diameters in the case of the smooth substrate. It is now accepted that for a patterned adhesive surface, like that of the gecko foot, a "contact splitting" mechanism significantly enhances the adhesion strength on a smooth surface.[16], [75] Additional data are shown in **Figure 4.3B**, where the slopes of the (logarithmic) pull-off stress values as a function of the (logarithmic) pillar diameter are indicated (**Figure 4.3B**). Accordingly, the pull-off stress (σ_c) was found to depend on the pillar diameter through a power law $\sigma_c \sim D^n$, where the exponent n is a measure of the "contact splitting efficiency".[17] On the smooth control surface, n was found to be -0.5, in agreement with earlier studies.[14], [17] However, the pillar structures with diameters 30 and 50 µm and low aspect ratios were less adhesive than the fitting curve would predict. An explanation might be an elastic deformation of the backing layer in addition to the pillar deformation under preload that reduces adhesion as reported by Varenberg et al.[13] and, therefore, the smaller adhesion values of the pillars with larger diameters apparently increases the contact splitting efficiency in **Figure 4.3A**.

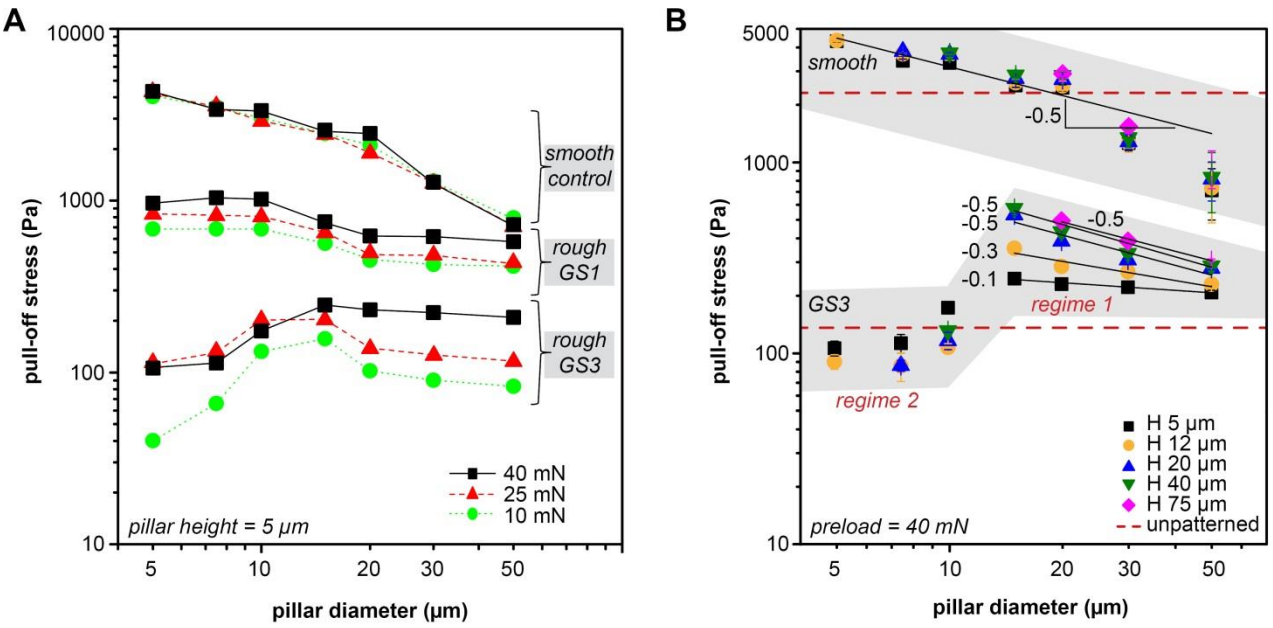

Figure 4.3 *Results of adhesion measurements of PDMS pillar array specimens on smooth and rough substrates. (A) Effects of the preload and pillar diameter on normal adhesion: Pull-off stress as a function of the pillar diameter for certain applied preloads varying from 10 to 40 mN. Measurements were performed on the rough substrates GS1 and GS3 and the smooth control. The height of the pillar structures was 5 µm. (B) The effect of pillar height on pull-off stress as a function of pillar diameter at a constant preload of 40 mN. The black solid lines represent linear fits in the diameter range between 15 to 50 µm (regime 1) on the rough substrate and over the whole range of pillar diameters for the smooth substrate. The numbers -0.5 to -0.1 represent the slopes of the linear fits in the log-log plots and are referred to as the contact splitting efficiency in the text. The dashed line represents the pull-off stress of the unpatterned PDMS specimen measured on the rough substrate GS3. The grey zones are provided to guide the eye.*

On a rough surface, as for example GS3, a new behavior was discovered: First, two adhesive regimes were observed. Regime 1 displays a higher pull-off stress than for unpatterned PDMS (marked by the dashed horizontal line), with adhesion increasing for smaller pillar diameters. A maximum stress is attained at a critical pillar diameter of about 15 µm, below which the pull-off stress abruptly decreases to a value much smaller than for unpatterned PDMS (called regime 2). Second, the contact splitting efficiency in regime 1 is found to be $n = -0.5$ for a pillar height exceeding 20 µm, as for smooth substrates. However, the contact splitting efficiency decreased for shorter pillars, reaching a value of $n = -0.1$ for a pillar height of 5 µm. In regime 2, the contact splitting effect is virtually lost.

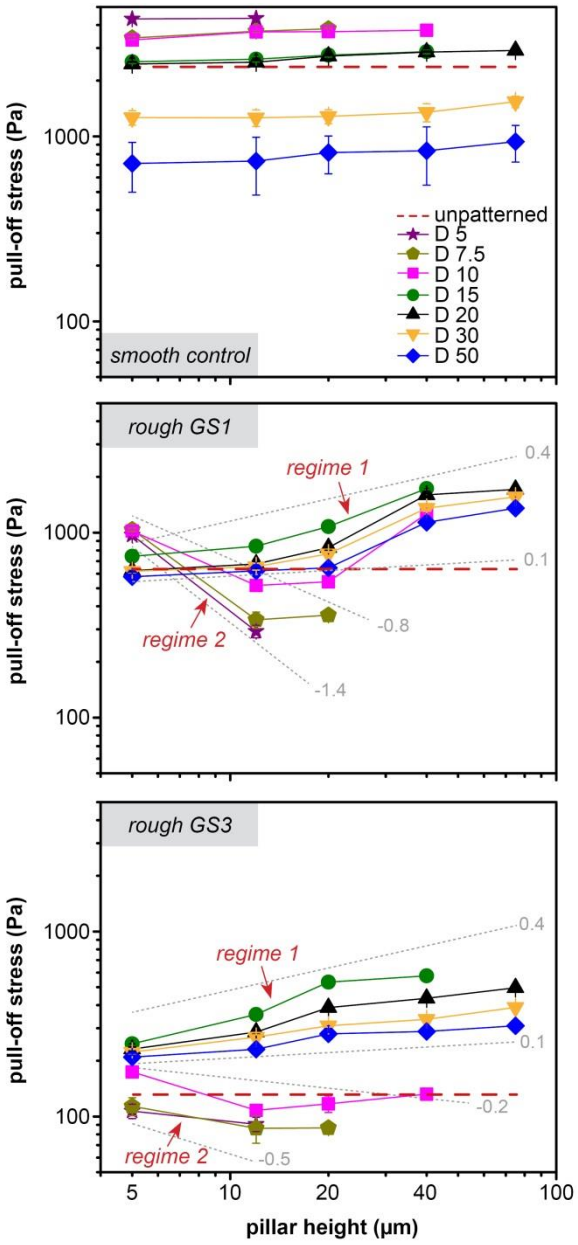

Figure 4.4 *Effect of the pillar height of PDMS pillar array specimens on the results of normal adhesion measurements. The measurements were performed on the rough substrates GS1 and GS3 in reference to the smooth control. The pillar diameters,* ***D****, were varied from 5 to 50 μm and the applied preload was kept constant at about 40 mN. The dashed red lines represent the pull-off stress for an unpatterned PDMS specimen. The grey dotted lines represent the range of positive and negative dependence on pillar height in regime 1 and 2, respectively. The numbers represent the slopes.*

The pull-off stresses as a function of the pillar height are displayed in **Figure 4.4**. For the smooth control substrate, the measured pull-off stress was independent of pillar height (**Figure 4.4A**) and, therefore, the aspect ratio did not affect adhesion. By contrast, the pull-off

stress measured on the rough substrates GS1 (**Figure 4.4B**) and GS3 (**Figure 4.4C**) strongly depended on pillar height. In regime 1 (pillar diameters exceeding 15 µm), adhesion increased with increasing pillar height, until it plateaued at a critical pillar height of about $H = 40$ µm. The pull-off stress was found to vary with H according to a power law, between $H^{0.1}$ and $H^{0.4}$. In contrast, in regime 2 (pillar diameters below 15 µm), the effect of pillar height was reversed: the pull-off stress decreased with an increase in pillar height, eventually attaining a minimum. Before the minimum, the pull-off stress varied as a function of the pillar height from $H^{-0.2}$ to $H^{-1.4}$.

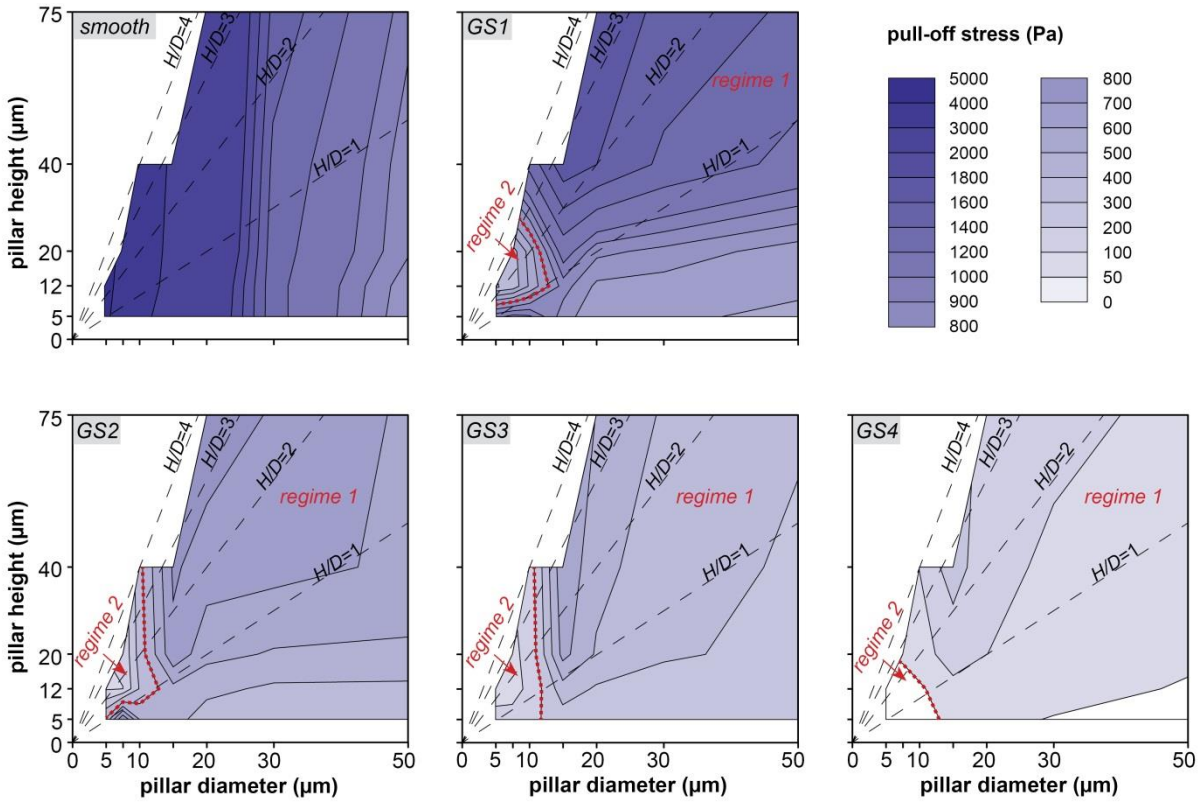

Figure 4.5 *Adhesion as a function of pillar diameter and height: The contour plots represents the pull-off stress values as a function of pillar height and pillar diameter for all rough substrates GS1 to GS4 in reference to the smooth control. The colors correspond to different pull-off stress values. The black dashed lines represent the aspect ratios (**H/D**) of the pillars. The red dashed lines represent the transition from the adhesive regime 1 to the non-adhesive regime 2.*

Both regimes can be illustrated in contour plots (**Figure 4.5**) in which the values of the pull-off stress are represented as functions of pillar diameter and height. Interestingly, the locations of the regimes vary only slightly for all rough substrates (GS1 to GS4) used in this study. Regime 2 is located within the 5 to 15 µm pillar diameter range and within the 12 to 20

µm pillar height range (GS1 and GS2) or the 5 to 20 µm pillar height range (GS3 and GS4). The remaining area displayed in the contour plot represents the adhesive regime 1, in which the adhesion increased for smaller and taller pillar structures, that is for higher aspect ratios. This finding is in line with an earlier analytical study that predicts higher adhesion of fibrillar structures with higher aspect ratio due to enhanced compliance of the micropatterned array and, therefore, better adaptation to rough substrates.[98] Interestingly, high aspect ratios are frequently found in the design of natural dry adhesives as in the case of insects and geckoes.

4.5 Discussion

The results presented above suggest that rough substrates introduce additional effects when they adhere to a micropatterned array of fibrils: in contrast to smooth substrates, adhesion now depends on the preload and the dimensions of the fibrils, in addition to the surface roughness itself. In this study, we have for the first time identified two different interaction regimes: in regime 1, adhesive values exceed those of the unpatterned PDMS adherent, whereas typically lower adhesive values compared to the unpatterned adherent are found in regime 2. We therefore propose to name regime 1 the “adhesive regime” and regime 2 the “non-adhesive regime”.

Our observations can be qualitatively rationalized by considering the mechanisms of contact formation between an elastic pillar structure and a rigid, rough substrate. Initial contact will occur only at the local peaks on the substrate. The contact area will be immediately increased due to free surface energy minimization in accordance with the Johnson, Kendall and Roberts (JKR) theory.[4] As compressive pre-load is applied, the pillar structure will be forced to adapt to the surface topography of the substrate. Two mechanisms can come into play: elastic deformation predominantly in the axial direction and off-axis pillar bending or buckling. Which of these mechanisms is predominant will depend on the pillar dimensions in relation to the roughness values in the following way:

i) In the **adhesive regime** 1, the pillar diameter of the fibrils is always larger than the mean spacing, S, of adjacent local peaks on all rough substrates (*i.e.*, $D > S$). In this case, the pillars will rest on several local roughness peaks; hence contact area will be increased mostly by local elastic deformation of the pillars without significant bending or buckling (**Figure 4.6A**). The energy stored in the required local elastic deformation will increase with the peak-to-valley distance, R_z, of the rough substrate; this strain energy penalty will, however, decrease for taller pillars. This can explain why larger R_z values lead to lower adhesion (as is known from the literature [98], [100], [101], [103] and shown in **Figures 3A, 4** and **5**) while taller pillars show better adhesion (see **Figures 3B** and **4**). In this regime, the adhesion force of fibrillar surfaces was increased by a factor between 2.7 (for GS1) and 4.2 (for GS3) over that of the unpatterned control surface.

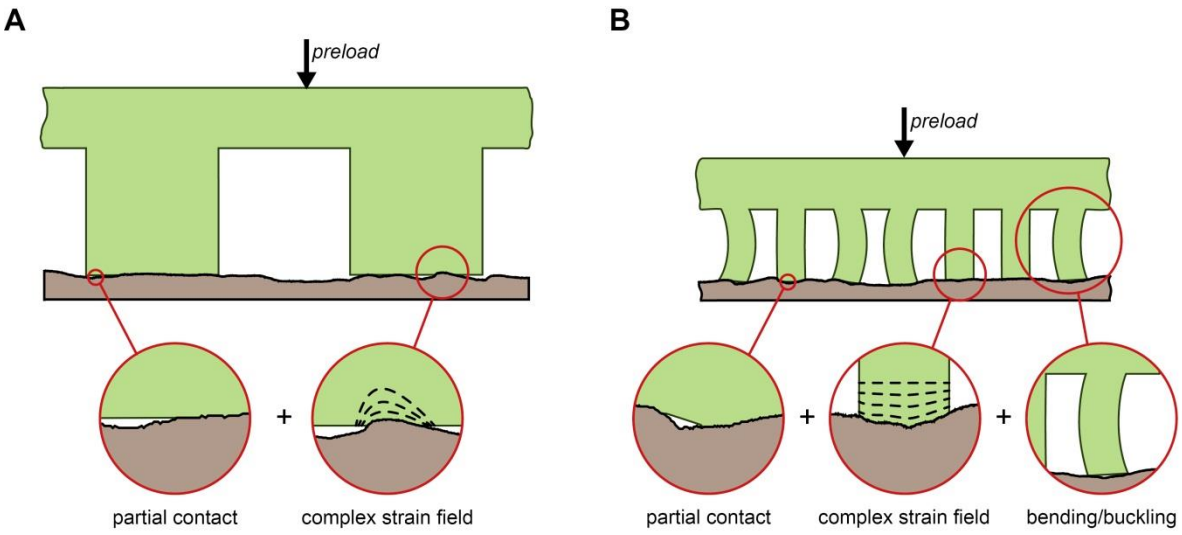

Figure 4.6 *Contact mechanisms for regimes 1 and 2: Schematic illustration of a micropatterned array of pillars pressed onto a rough substrate in (A) regime 1 and (B) regime 2. Insets represent the partial contact and a complex strain field at the pillar faces found to occur in both regimes. Additionally, bending and buckling of pillars can occur in regime 2 as shown in the inset.*

ii) In the **non-adhesive regime** 2, the pillar diameter is smaller than the mean spacing of adjacent local peaks (*i.e.*, $D < S$). Therefore, the pillar faces will now predominantly meet the substrate in the sidewalls of grooves and peaks to accommodate the local misorientation. Now, bending of the pillars will be more efficient for achieving a larger contact area as demonstrated in **Figure 4.6B**. The off-axial bending of the pillars results in elastic bending

energy that in addition to the elastic strain energy by local elastic deformation at the pillar faces (see regime 1) works against the adhesive energy. We argue that the higher elastic energy resulting from this process can explain the lower adhesion forces measured in this regime. The bending energy shows a strong size dependence: a pillar diameter dependence of $\sim D^4$ and a pillar height dependence of $\sim H^{-2}$. For arbitrarily small pillar structures, the bending energy of the total array is, therefore, expected to vanish. Hence, we cannot exclude the possibility that adhesion values will increase again for much smaller pillars (< 5 µm in diameter) than studied in this paper. Such small dimensions would be reminiscent of the length scale of adhesion organs of large animals such as geckoes, which exhibit terminal elements on the nanoscale.

Another phenomenon that will reduce adhesion to rough surfaces is the increased propensity for buckling on rough surfaces with a resulting loss of contact between pillar and substrate.[105] When a perfectly aligned array of micropillars comes into contact with a smooth surface, all pillars contact the substrate fully in one step, without buckling (provided that the preload is smaller than the critical buckling load). On the other hand, the same array will only gradually come into contact with a rough substrate due to the height irregularities. The pillars that do come into contact with the surface will carry the entire load and will be more likely to buckle. As the critical load for buckling varies with the number of pillars in contact with the substrate, the pillars that formed contact early on will also tend to buckle first and will not be able to contribute much to adhesion under tension. Note that buckling will more likely occur for aspect ratios larger than 1. However, the propensity for buckling is enhanced by the axial non-eccentric loading due to local misorientation of the pillar faces to the surface asperities. We argue that this explains the lowest adhesion values in regime 2 obtained for pillar heights of 12 and 20 µm, in contrast to slightly better adhesion for only 5 µm tall pillar structures (see **Figure 4.4**).

Overall, our results suggest a new strategy for optimizing fibrillar surfaces in contact with rough surfaces. The most relevant finding in light of possible applications is that fibrillar adhesive microstructures do not increase adhesion only to smooth surfaces, according to the principle of contact splitting, as has been reported frequently. Also for rough substrates, fibrillar structures demonstrated increased adhesion, provided that the fibril diameter is chosen judiciously with regard to the substrate roughness: D must lie close to, but above the lateral roughness parameter S of the substrate (to avoid bending and buckling). In addition, a large pillar height should be chosen (to minimize elastic strain energy). In any case, the

transition region between the adhesive regime 1 and the non-adhesive regime 2 as defined in our paper must be avoided.

4.6 Conclusions

We present a detailed study of normal adhesion for micropatterned adhesives on rough, rigid substrates. For the first time, a systematic variation of pillar diameters and heights was performed and the adhesion force values were analyzed in connection with the roughness parameters of the substrate. The following conclusions were drawn:

- Fibrillar adhesive surfaces can improve the adhesion to rough substrates by a factor between 2 and 4 compared to unpatterned surfaces. The principle of "contact splitting", advocated first for smooth substrates, has thus been shown to apply also to rough substrates.
- To take advantage of this effect, the dimensions of the fibrils must be chosen in relation to the roughness parameters of the substrate. The fibril diameter should be small, but not smaller than the mean spacing between local peaks on the substrate. The pillar height should be as large as possible without jeopardizing stability.
- Two new regimes of adhesion were identified: regime 1, in which the diameter of pillars exceeds the spacing between the local peaks of the substrate, and regime 2 where the converse relationship applies. The superior adhesion in regime 1 was attributed to only small elastic deformations required in forming contact; by contrast, the non-adhesive regime 2 is ascribed to frequent pillar bending and buckling events, which store much energy and reduce the contact area.
- Contour plots were developed which depict the coexistence of both regimes as a function of both pillar diameter and height. This makes the adhesion of micropillar arrays on rough substrates distinct from that on a smooth substrate. We believe that these results are particularly relevant for designing micropatterned adhesives suitable for both adhesive and non-adhesive phenomena and applications connected to surface roughness.

5 Adhesion on sandpaper

5.1 Introduction

The adhesion of fibrillar polydimethylsiloxane (PDMS) pillar arrays with flat tips was studied on sandpaper surfaces and compared to unpatterned samples.
In comparison to the previous chapter, the current chapter deals with the investigation of adhesion on far rougher surfaces namely sandpaper. Canas et al. [38] already showed that adhesion of micro-rough surfaces presents a maximum at a certain intermediate roughness, which has been explained by the inability of micropatterned surfaces to conform to surface asperities. This study was only considering a few samples and aspect ratios. In this chapter, however, the influence of the roughness of sandpaper is systematically analyzed on a large spectrum of aspect ratios.

5.2 Results

Micropatterned PDMS adhesives with different pillar lengths (12 μm, 40 μm and 75 μm) and aspect ratios (from 0.4 to 3.75) were tested on sandpaper with increasing average roughness (from SP1 to SP4). Figure 5.1, 5.2 and 5.3 show the pull-off strength of patterned PDMS samples with pillar heights of 12 μm, 40 μm and 75 μm, respectively, on different sandpaper substrates. It is interesting to observe that the pull-off stress ranges in tens of Pa, which represents a more important decrease in adhesion compared to the adhesion measured to rough glass and is comparable to the non-adhesive regime, reported in chapter 4. When looking at the smaller pillars, with a height of 12 μm, no significant differences between the various roughnesses and pillar diameters could be observed (**Figure 5.1**).

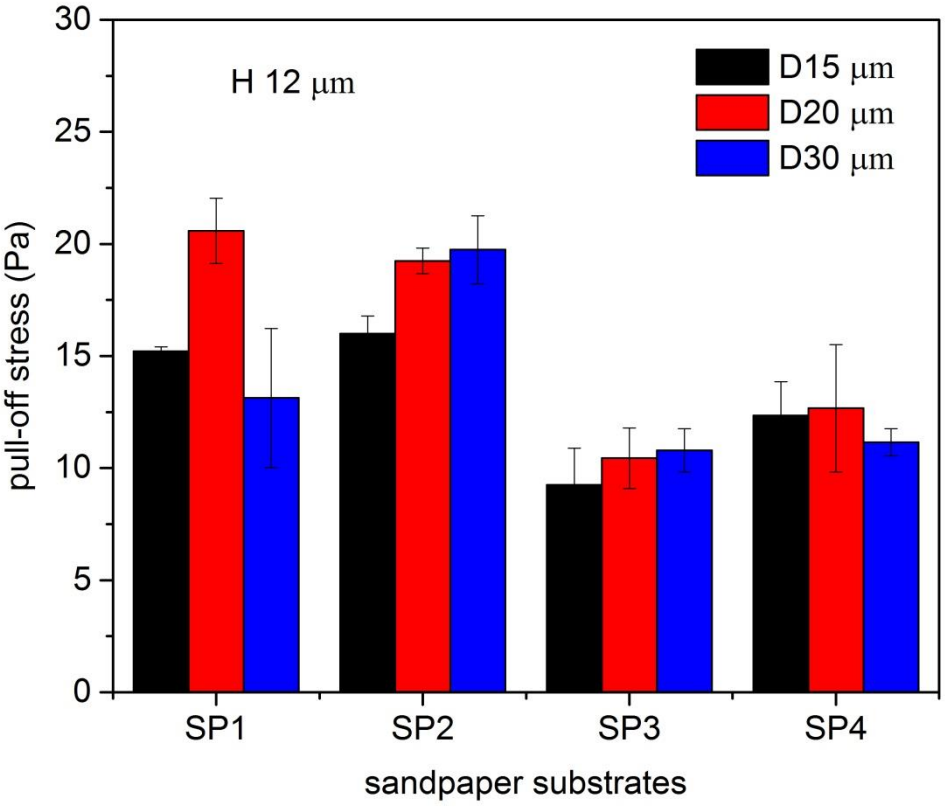

Figure 5.1 *Comparison of pull-off stress of micropatterned PDMS with different pillar diameters (D from 15 µm to 30 µm) and height 12 µm against sandpaper SP1 to SP4.*

In the case of pillars with a height of 40 µm, the structures adhere better to the substrate with lowest roughness. Nevertheless, there is still no clear trend observable for the different pillar diameters. However, it is interesting that for higher roughness (substrates SP3 und SP4) samples with a larger pillars diameter led to a better adhesion (**Figure 5.2**).

.

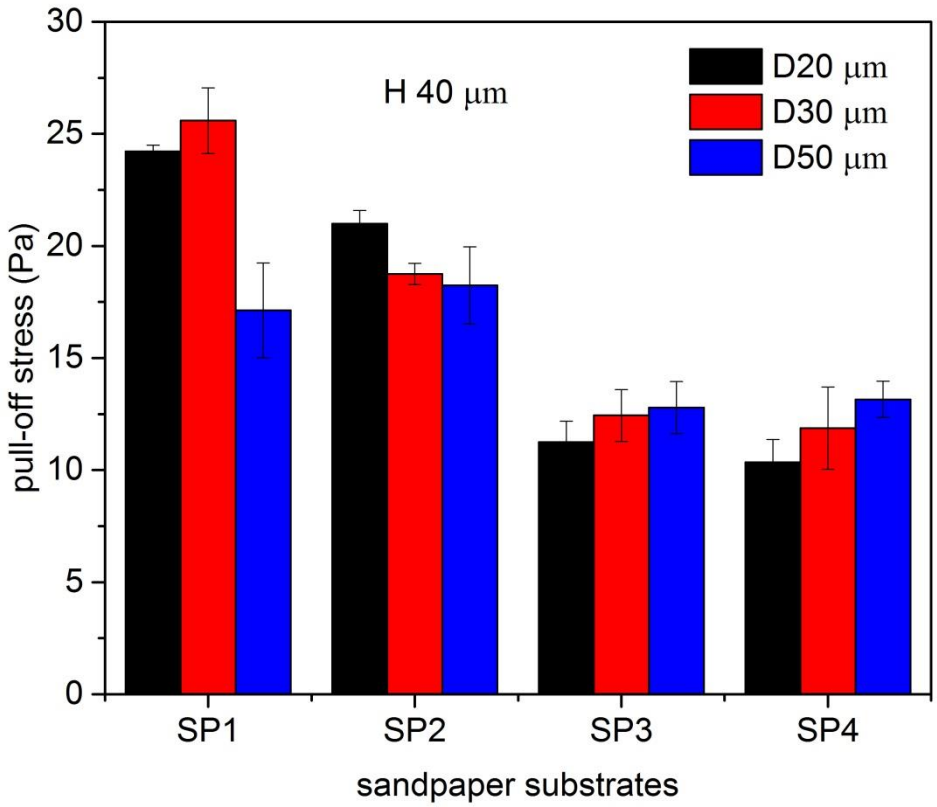

Figure 5.2 *Comparison of pull-off stress of micropatterned PDMS with different pillar diameters (D from 15 µm to 30 µm) and height 40 µm against sandpaper SP1 to SP4.*

In contrast, the pillars with a height of 75 µm showed a clear trend: with increasing roughness, the adhesion diminishes (**Figure 5.3**). In addition, the influence of different diameters on the adhesion for the different substrates could be observed. The adhesion values are increasing with decreasing diameter and hence higher aspect ratios.

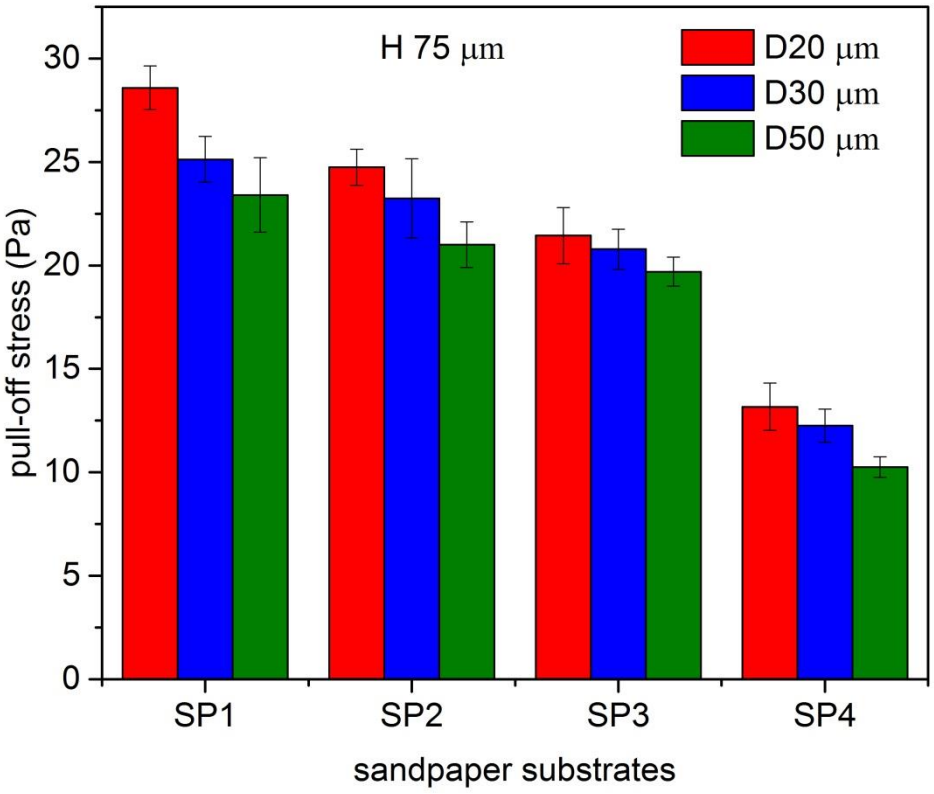

Figure 5.3 *Comparison of pull-off stress of micropatterned PDMS with different pillar diameters (D from 15 μm to 30 μm) and height 75 μm against sandpaper SP1 to SP4.*

By inspecting **Figure 5.4**, which summarizes the pull-off stresses obtained from all samples, the same trend could be observed: with increasing roughness, the adhesion decreases. The only exception is the unpatterned PDMS film, which did not show any measurable adhesion.

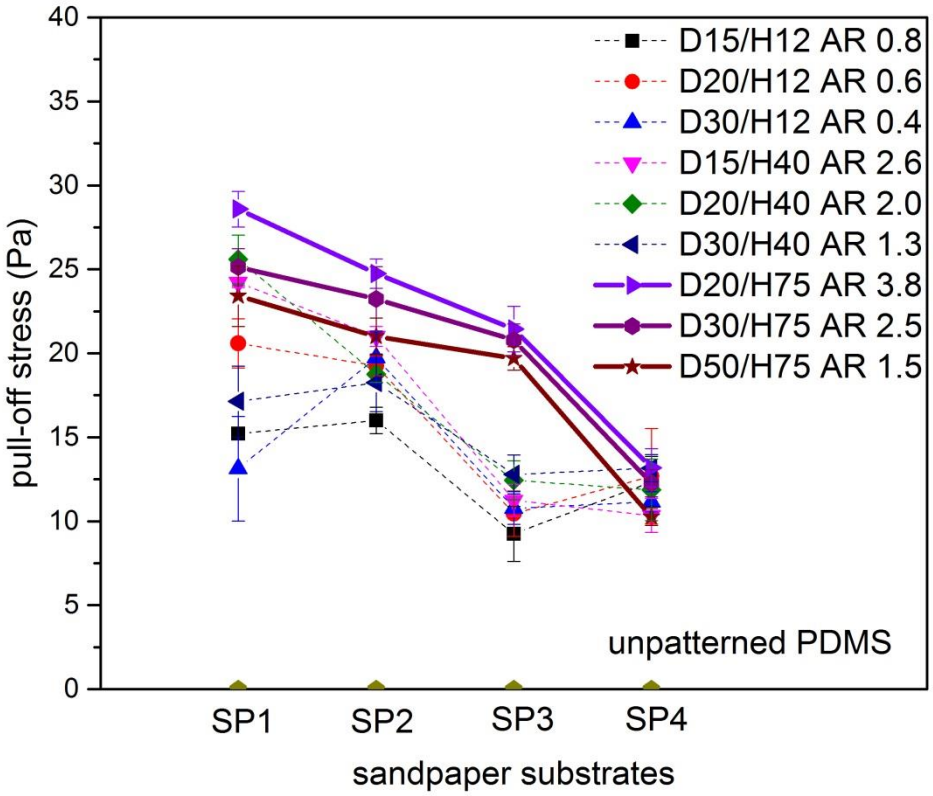

Figure 5.4 *Comparison of the pull-off stress for patterned and flat PDMS samples on sandpaper substrates SP1 to SP4.*

5.3 Discussion

The low pull-off stress values proved that micropatterned structures used in this study showed low adhesion to sandpaper. PDMS structures have smaller effective elastic moduli and could buckle to perform better contact with rough profile, but the stored elastic energy is too high. In addition, the small height of the pillars and the big lateral roughness of sandpaper lead to a small contact area and low adhesion values. So the pillars with a height of 12 µm are not capable to fit into the valleys and hence present the lowest adhesion.

Nevertheless, clear trends can be observed. The adhesion decreases with increasing roughness. Furthermore, for pillars with enough height to establish a sufficient contact area, the contactsplitting principle works on sandpaper.

5.4 Conclusions

In contrast to unpatterned PDMS, structured samples showed no adhesion to sandpaper, microstructures showed adhesion. Fibrillar adhesives exhibit much lower adhesion to sandpaper then on rough glass due to the higher roughness. Hereby, relationships between the pillar height and the pillar diameter of the sample and the roughness of the sandpaper substrate have been identified. It has been demonstrated that the adhesion of samples with pillar heights of 40 μm and 75 μm decreases with increasing roughness of the substrate. The only exception to this trend is made by the samples with pillar diameters of 50 μm and a height of 40 μm. Furthermore, for pillar heights of 75 μm, the adhesion decreases not only with increasing roughness, but also with increasing pillar diameter. This relationship has not been clearly observed on smaller pillar heights, although it started to manifest itself on samples presenting a pillar height of 40 μm. In addition, it has been shown that the contact splitting principle works on sandpaper if the pillars present a sufficient height to develop enough contact with the roughness.

6 Elevated temperature adhesion of bioinspired polymeric micropatterns to glass

6.1 Abstract

Micropatterned polymer surfaces that operate at various temperatures are required for emerging technical applications such as handling of objects or space debris. As the mechanical properties of polymers can vary significantly with temperature, adhesion performance can exhibit large variability. In the present paper, we experimentally study temperature effects on the adhesion of micropatterned adhesives (pillar length 20 µm, aspect ratios 0.4 and 2) made from three different polymers, i.e., polydimethylsiloxane (PDMS), perfluoropolyether dimethacrylate (PFPEdma), and polyurethane (PU-ht). PU specimens showed the highest pull-off stresses of about 57 kPa at 60 °C, i.e., more than twice the value of unpatterned control samples. The work of separation similarly showed a maximum at that temperature, which was identified as the glass transition temperature, T_g. PDMS and PFPEdma specimens were tested above their T_g. As a result, the adhesion properties decreased monotonically (about 50 % for both materials) for temperature elevation from 20 to 120 °C. Overall, the results obtained in our study indicate that the operating temperature related to the glass transition temperature should be considered as a significant parameter for assessing the adhesion performance of micropatterned adhesives and in the technical design of adhesion devices.

[1] This subsection is content of Barreau V, Yu D, Hensel R, Arzt E. Elevated temperature adhesion of bioinspired polymeric micropatterns to glass. Journal of the Mechanical Behavior of Biomedical Materials. 2017; doi: 10.1016/j.jmbbm.2017.04.007

6.2 Introduction

Synthetic fibrillar dry adhesives are currently of great interest for enabling novel pick-and-place systems and other emerging applications. Particularly, their applicability even to rough substrate materials[44] and the possible handling of fragile objects[106] even in vacuum[107] may pave the way for a new generation of handling and gripping systems. Over the last decade, several design parameters of fibrillar dry adhesives have been systematically studied.[14], [75], [108], [109] In general, splitting of an adhesive contact leads to better properties compared to an unpatterned, smooth adhesive contact because of a strong reduction of the elastic strain energy penalty for smaller contacts (size effect).[16] Furthermore, contact splitting leads to an extrinsic contribution to the work of separation due to the interrupted crack propagation along the single contacts, an enhanced adaptability to rough substrates related to the higher compliance of the patterned surface, and a reduced sensitivity to defects compared to a single unpatterned contact.[93] For the rational design of fibrillar adhesives, Spolenak *et al*. and Greiner *et al*. proposed maps that predict the optimal pillar geometry as function of the elastic properties and the tip shapes including limits such as cohesive strength, agglomeration of the fibrils, and the upper limit for the adhesion strength.[110], [111] Many additional parameters such as the stiffness of the substrate,[112], [113] elastic gradients inside the structures[109], [114] or material viscoelasticity[58]–[60] have been studied experimentally and theoretically.

A critical issue that was neglected for micropatterned adhesives is the adverse effects of higher than ambient temperatures on adhesive properties. The mechanical properties of polymers drastically change with temperature, particularly if the temperature variation exceeds the glass transition temperature, T_g. At T_g, the molecular mobility changes from a glassy state ($T < T_g$) to a more flexible rubber state ($T > T_g$) with a simultaneous strong decrease of the elastic modulus. However, the adhesion performance is generally not a simple function of temperature: For an ideal contact situation, the higher modulus below T_g can enhance the adhesion properties of an adhesive film in contact with a rigid flat punch.[6], [113] By contrast, a stiffer material will prevent intimate contact formation, particularly on a rough surface, and the diminished contact area can result in reduced adhesion. Above T_g, contact formation may be improved but the lower modulus can at the same time reduce the adhesion.[58]–[60] For viscoelastic materials, viscoelastic losses additionally contribute to stiffness variations. Hence, the work of separation will increase when energy is dissipated in

the system. At the glass transition temperature, the viscoelastic loss factor exhibits a maximum.[115] Accordingly, Zosel measured the highest adhesion for pressure sensitive adhesives (PSAs) close to T_g.[116], [117] Theoretically, energy dissipation due to viscoelastic losses at the crack tip will enhance the critical energy release rate necessary for crack propagation.[118]–[120] In addition to interfacial dissipative processes, energy dissipation due to bulk deformation can contribute to enhanced adhesion, which occurs particularly in case of strong interfacial attraction.[121], [122]

Detailed studies of bulk and interfacial contributions to the adhesion energy were performed by atomic force microscopy (AFM). For polydimethylsiloxane (PDMS), Awada *et al*.[67] found, with increasing temperature (from 30 to 140 °C), a reduction in adhesion which they attributed to the decrease of intermolecular interactions due to higher thermal fluctuations.[56] They further demonstrated that the adhesion energy at the nanoscale was a function of the thermodynamic work of adhesion (related to the surface free energies) and the dissipative energy, expressed by molecular mass and a dissipative coefficient, which depends on temperature and separation rate. Similar relationships were further established by experiments and so-called master curves showing the correlation between adhesion strength, temperature, and separation rate.[57], [63] Luengo *et al*.[65] suggested a mechanism to describe the enhanced adhesion at T_g, where the enhanced mobility induces molecular rearrangements such as polymer chain entanglements across the interface, like molecular rearrangements occurring in bulk. In addition, inelastic surface deformations or bulk flow might contribute to energy dissipation at higher temperatures and lower rates.[66]

The materials used in the present study were polydimethylsiloxane (PDMS), polyurethane (PU-ht), and perfluoropolyether dimethacrylates (PFPEdma). All materials are highly cross-linked elastomers that exhibit a certain stability at elevated temperatures, which makes them interesting candidates for applications at elevated temperatures. PDMS, which has been widely used as a ‘standard’ material for micropatterned adhesives, decomposes thermally above 300 °C.[123] PFPEdma exhibits considerable high temperature resistance due to the fluorine content of about 54 at-% and can be applied at temperatures ranging from -50 °C to 290 °C. However, the material inherently exhibits a very low surface free energy and hydrophobicity;[124], [125] hence, its application for adhesives needs to be critically evaluated. In contrast, polyurethanes can exhibit very strong adhesion,[126], [127] but show lower thermal stability (up to 150 °C) than the silicones and fluorinated polymers.

In the present chapter, the adhesion of micropatterned polymer adhesives to a spherical glass probe was investigated at elevated temperatures up to 120 °C. The adhesion characteristics were evaluated in terms of pull-off stress and work of separation. The results obtained will be discussed in relation to thermally induced variations of the viscoelastic material properties.

6.3 Materials and methods

6.3.1 Sample Fabrication

Micropatterned adhesive surfaces were fabricated from polydimethylsiloxane (PDMS, Sylgard 184 kit, Dow Corning), perfluoropolyether dimethacrylate (PFPEdma, Fomblin MD40, Solvay Solexis) and a high-temperature polyurethane, (PU-ht , U-835, Alfa Aesar) using replica molding. Master structures having hexagonal micropillar arrays with aspect ratio 2 and 0.4 (pillar length: 20 µm; pillar diameters: 10 and 50 µm, and a pitch twice the respective pillar diameter) and their corresponding PDMS molds were generated as described previously.[44] For the microstructures, the PDMS prepolymer (10 weight parts of the base to 1 weight part of the curing agent) was degassed under vacuum for 5 min. It was then filled into the mold, degassed for 10 min, and cured at 75 °C for 24 h in an oven. The PFPEdma and PU-ht oligomers were mixed with 0.5 wt-% 2-hydroxy-2 methyl-propiophenone (Sigma Aldrich) as a photoinitiator for UV-curing. The pre-polymer mixtures were poured into the mold and exposed to UV-light (365 nm, Omnicure S1500, Excelitas Technologies) under a nitrogen atmosphere for 5 min. Upon crosslinking, samples were carefully peeled off the molds. For a few analyses, PU-ht was thermally post-baked in addition to a prior UV-crosslinking at 120 °C for 15 min in an oven.

6.3.2 Adhesion measurements

The adhesion data presented in this paper were obtained by using a custom-built adhesion-measuring device, which is schematically shown in **Figure 6.1a**. It consists of a pivotable stage, equipped with a heating element (PE120, Linkam), and a spherical glass probe with a curvature radius of 15 mm mounted on a flexible double beam glass spring. Forces were deduced from the beam deflection measured by a laser interferometer multiplied with its spring constant of 2240 N m^{-1}. Displacements reported correspond to the elongation of the micropatterned adhesives during retraction, i.e., they were calculated from the differential displacement of the stage relative to the deflected beam. The pull-off force (maximum tensile force) was determined from these force-displacement curves. The pull-off stress was calculated by dividing the pull-off force by the apparent contact area. The apparent contact area was calculated according to a geometrical relationship based on the radius of the probe and the indentation depth obtained from the experiments.[75] The work of separation (area under the curve in the tensile regime) was determined from the stress-displacement curves. All measurements were performed at a constant compressive preload of 30 mN, at four different sample positions, at constant displacement velocity of 5 μm s^{-1}, and at a relative humidity of 45 ± 5 %. The adhesion tests were conducted by increasing the temperature of the samples from 20 °C to 120 °C (heating rate: 20 °C min^{-1}) and subsequently decreasing the temperature from 120 °C to 20 °C (cooling rate: 20 °C min^{-1}) in increments of 20 °C. Before the adhesion measurements, the temperature was held constant for more than 15 min. The cooling process was initiated by flowing cold water through the heating stage. Each heating-cooling cycle was traversed three times.

6.3.3 Material analysis

The mechanical properties of all materials were studied by dynamic mechanical thermal analysis (DMTA, Q800, Waters GmbH). Cuboid polymer samples with dimensions $20 \times 12.5 \times 2.5\ \mathrm{mm}^3$ were fabricated and tested in the temperature range between -100 °C and 120 °C at a heating rate of $3\ \mathrm{K\ min}^{-1}$. The glass transition temperature was determined from the maximum value of the viscoelastic loss factor, $\tan\delta$. All tests were performed under nitrogen atmosphere at an oscillatory frequency of 1.0 Hz in tensile mode. X-ray diffraction analysis (XRD, X'Pert MRD, PANalytical) was used to characterize the material microstructure of bulk PU-ht upon (a) UV-curing and (b) UV-curing with subsequent post-bake. As a source, Cu K-alpha was used (40 kV, 30 mA). The angle (2*theta) of the incident radiation was varied between 3° and 150° in increments of 0.02°. The Soller slit was set to 2.5° and an aperture of 0.5 was used. The diffraction patterns were analyzed in terms of constructive interference patterns due to crystalline domains in the polymer microstructure. Based on that, variations of the crystallinity before and after post-bake could be qualitatively compared.

6.3.4 Surface free energy measurement

The surface free energy of PU-ht was evaluated using a contact angle goniometer (OCA35, DataPhysics), equipped with analysis software SCA20. A flat film of PU-ht was prepared by coating a 120 µm thick layer of liquid PU-ht resin on PET foil and, subsequently, UV-cross-linking as described above. Contact angles of deionized water with surface tension of 72.3 mN/m and *n*-hexadecane with surface tension of 27.5 mN/m were measured and subsequently used to deduce the surface free energy value by Wu´s Harmonic Mean Method.[72]

6.4 Results

6.4.1 Adhesion measurements

Micropillar arrays generated from PDMS, PFPEdma and PU-ht are exemplarily shown in **Figure 6.1b**. **Figure 6.2** shows the results obtained from adhesion measurements at different temperatures for the PDMS specimens. Typical force–displacement curves (tensile forces in retraction mode) of microstructures with a diameter of 10 µm at different temperatures are displayed in **Figure 6.2a**. While the shapes of the curves were similar, the pull-off forces (maximum forces) and the displacements at pull-off decreased with increasing temperature by a factor of almost 2. **Figure 6.2b** represents the decrease of the pull-off stress with increasing temperature for the patterned and unpatterned PDMS samples in three consecutive heating cycles. The highest pull-off stress of 3.4 kPa was obtained at 20 °C for the pillar diameter of 10 µm (aspect ratio 2). The values of the unpatterned control were slightly higher than the values for the pillar diameter of 50 µm (aspect ratio 0.4). This result is in line with our earlier study, where we detached similar PDMS microstructures from smooth and rough substrates.[44] **Figure 6.2c** shows how the work of separation decreased with increasing temperature. Interestingly, this behavior is more strongly pronounced in the unpatterned control (from 3.4 to 0.3 mJ/mm^2; i.e. a decrease by factor of 11) than for the micropatterned surface with pillar diameter 10 µm (from 12.8 to 3.6 mJ/mm^2; i.e. a decrease by factor of 3.5). Thus, the reduction of the work to separate the adherents at higher temperatures could be decreased by surface patterning. **Figure 6.2d** depicts the monotonic decrease of the pull-off stress and the maximum strain at detachment with increasing temperature; however, the apparent stiffness of the system (that is the slope of the secants; dotted lines) remained almost constant for the whole temperature range.

Figure 6.3 shows the results of the adhesion measurements for the microstructures made from PFPEdma. The force-displacement curves for temperatures ranging from 20 to 60 °C exhibit almost identical profiles (**Figure 6.3a**).

At 80 °C, however, the pull-off force drops by factor 2 compared to the lower temperatures. At temperatures above 80 °C, the curves are again almost identical. The force-displacement curves were again similar for all heating cycles.

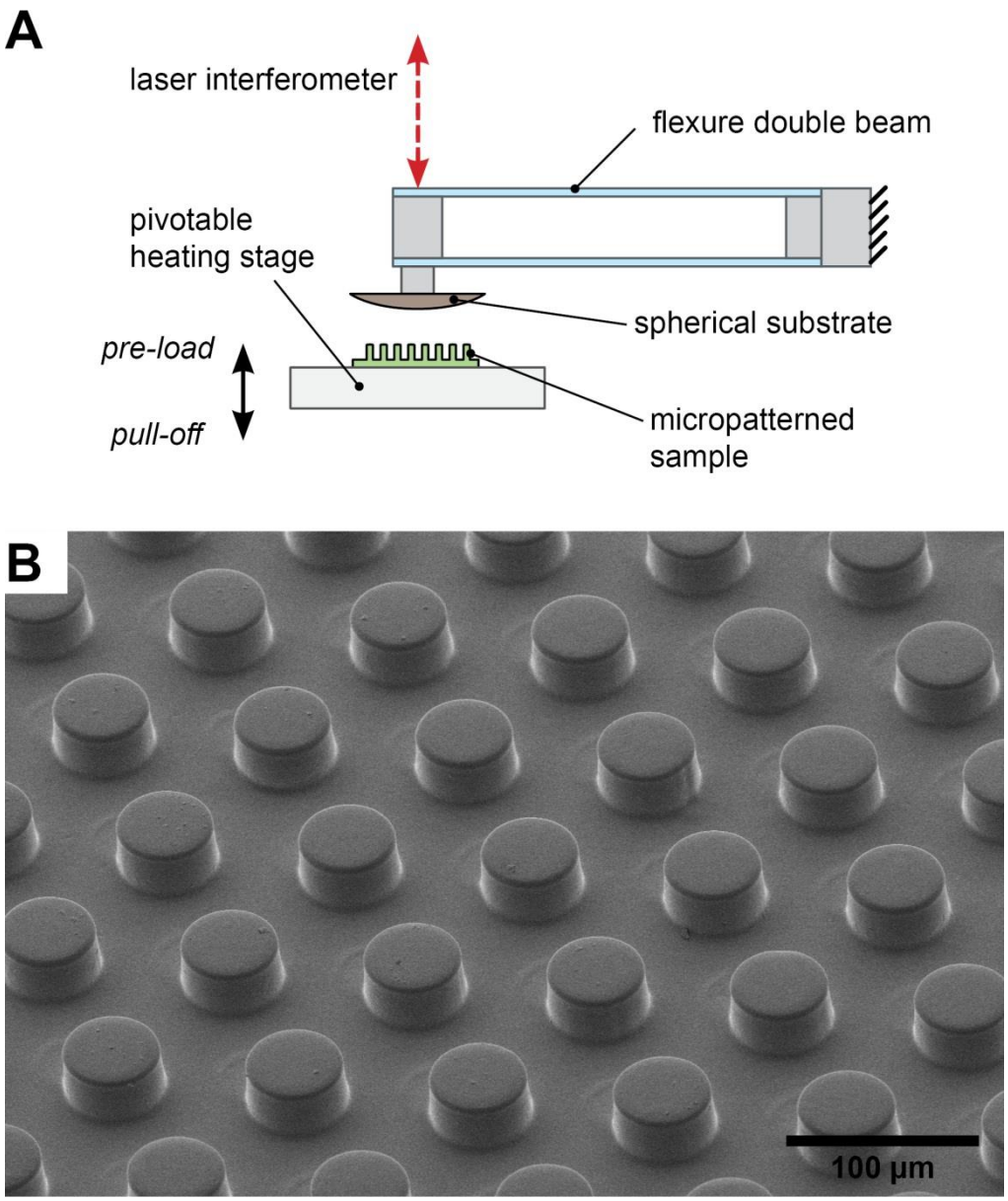

Figure 6.1 *(A) Schematic illustration of the adhesion measurement device that consists of a pivotable and heating stage for sample manipulation and a glass lens mounted on a flexible double beam. The laser interferometer monitors the elastic deflection of the beam, from which the forces are deduced. (B) Scanning electron micrograph of a representative micropatterned PDMS sample with pillars of length 20 µm and diameter 50 µm.*

The pull-off stresses of the PFPEdma specimens decreased only slightly from 20 to 60 °C but dropped to the half of the value (for pillar structures with 10 µm diameter) at temperatures of 80 °C and higher (**Figure 6.3b**). Overall, the pull-off stress of the micropatterned PFPEdma specimens was almost one order of magnitude smaller than for the PDMS specimens.

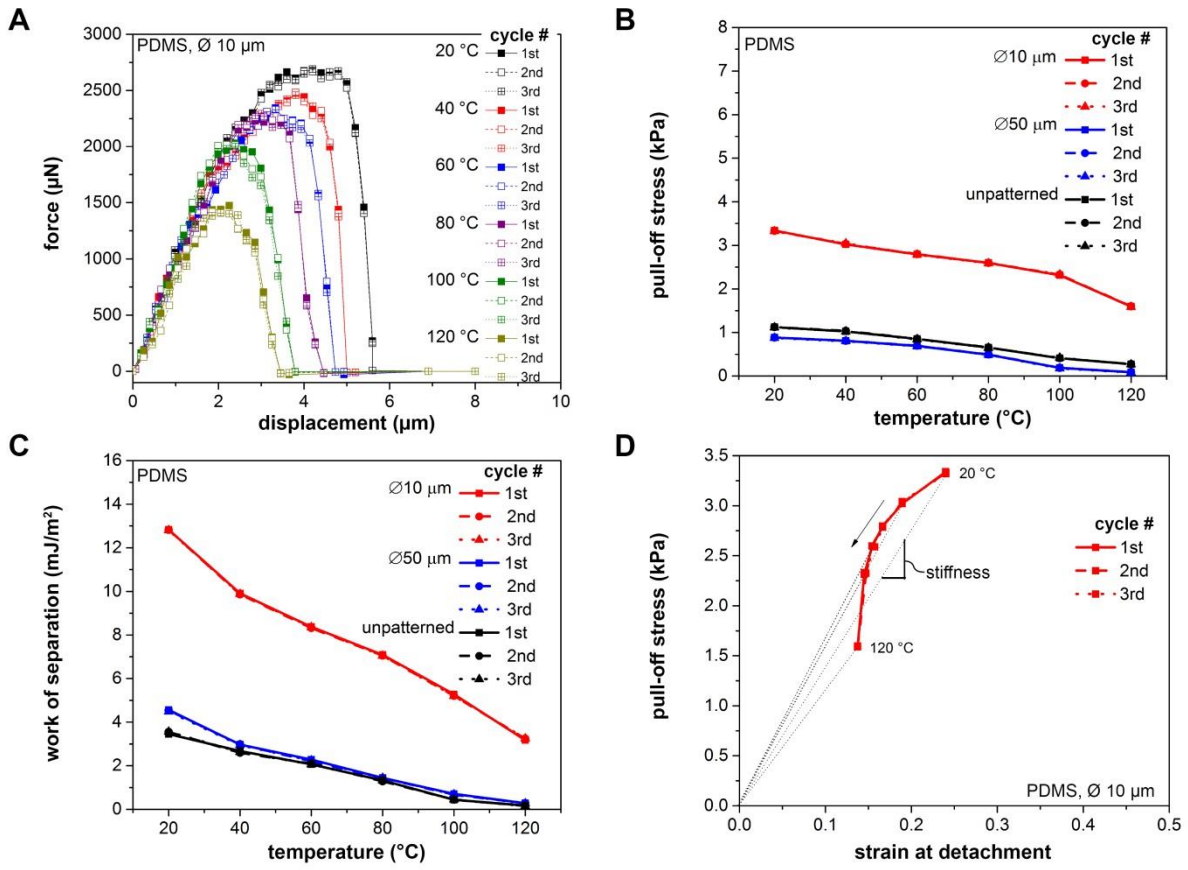

Figure 6.2 *Results of adhesion measurements of PDMS micropatterned specimens obtained from three heating-cooling cycles. (A) Force-displacement curves as a function of temperature for pillar structures with diameter 10 µm and aspect ratio 2. (B) Pull-off stresses and (C) work of separation as a function of temperatures, for the different micropatterned specimens (red: 10 µm pillar diameter, blue 50 µm pillar diameter) and an unpatterned control (black). (D) Pull-off stress in terms of the strain at detachment for pillar structures with diameter 10 µm at various temperatures. The slope of the secants (dotted lines) represents the apparent stiffness of the adhesives.*

Figure 6.3c shows a similar trend for the work of separation as a function of temperature. Interestingly, the pull-off stress and the work of separation obtained for the unpatterned PFPEdma control were almost equal to zero whereas the patterned specimens showed measurable adhesion. Hence, the highly-fluorinated polymer was intrinsically non-adhesive, but became slightly adhesive if patterned. The apparent stiffness of the adhesive dropped by a factor 2 for a temperature increase from 60 to 80 °C (**Figure 6.3d**), while below and above this transition the stiffnesses were similar.

Figure 6.4 shows the substantially different results for PU-ht. In the first heating cycle, the force-displacement curves reveal that the adhesion *increased* up to 60 °C, where the pull-off force and the displacement exhibited a maximum of about 5.5 mN and 3.8 µm, respectively (**Figure 6.4a**). Above 60 °C, the adhesive forces dropped and reached 700 µN at 120 °C. In the second heating cycle, the specimens behaved much stiffer at temperatures below 80 °C; the stiffness (i.e. the slope of the force-displacement curve) increased by a factor 3 from about 1800 N m^{-1} to 5000 N m^{-1} for all samples measured from 20 to 60 °C. Interestingly, the maximum pull-off forces in that temperature range were similar in all heating cycles, whereas the displacements at pull-off were significantly reduced. The differences of the pull-off stress, strain at detachment, and the apparent stiffness between the first and the second heating cycle are further displayed in **Figure 6.4d**. Hence, the overall stiffer structures in the second cycle are more adhesive. The results obtained in third heating cycle were almost identical to those obtained in the second cycle. At 100 and 120 °C, the force-displacement curves and stiffness of the specimens were similar for all three cycles. **Figure 6.4b** shows the pull-off stresses of the PU-ht specimens, which exhibited values of roughly one order of magnitude higher than PDMS and two orders of magnitude higher than PFPEdma. PU-ht was the only material that showed an *increase* in adhesion up to 60 °C, where a maximum pull-off stress value was obtained for all cycles. Unlike the pull-off force in **Figure 6.4a**, the pull-off stress was further enhanced by factor 6 in the second and third cycle; this is the result of the higher material stiffness in conjunction with a reduced contact area. The work of separation similarly exhibited a maximum value at 60 °C (**Figure 6.4c**); however, in contrast to the pull-off stress, it was reduced by a factor of 2.5 (for microstructures with a diameter of 10 µm) upon the first heating cycle, which is most likely due to the enhanced stiffness and reduced strain of the specimens (**Figure 6.4d**). At low (20 °C) and high (100 and 120 °C) temperatures, in turn, the work of separation was fairly small with similar values for all samples in all cycles.

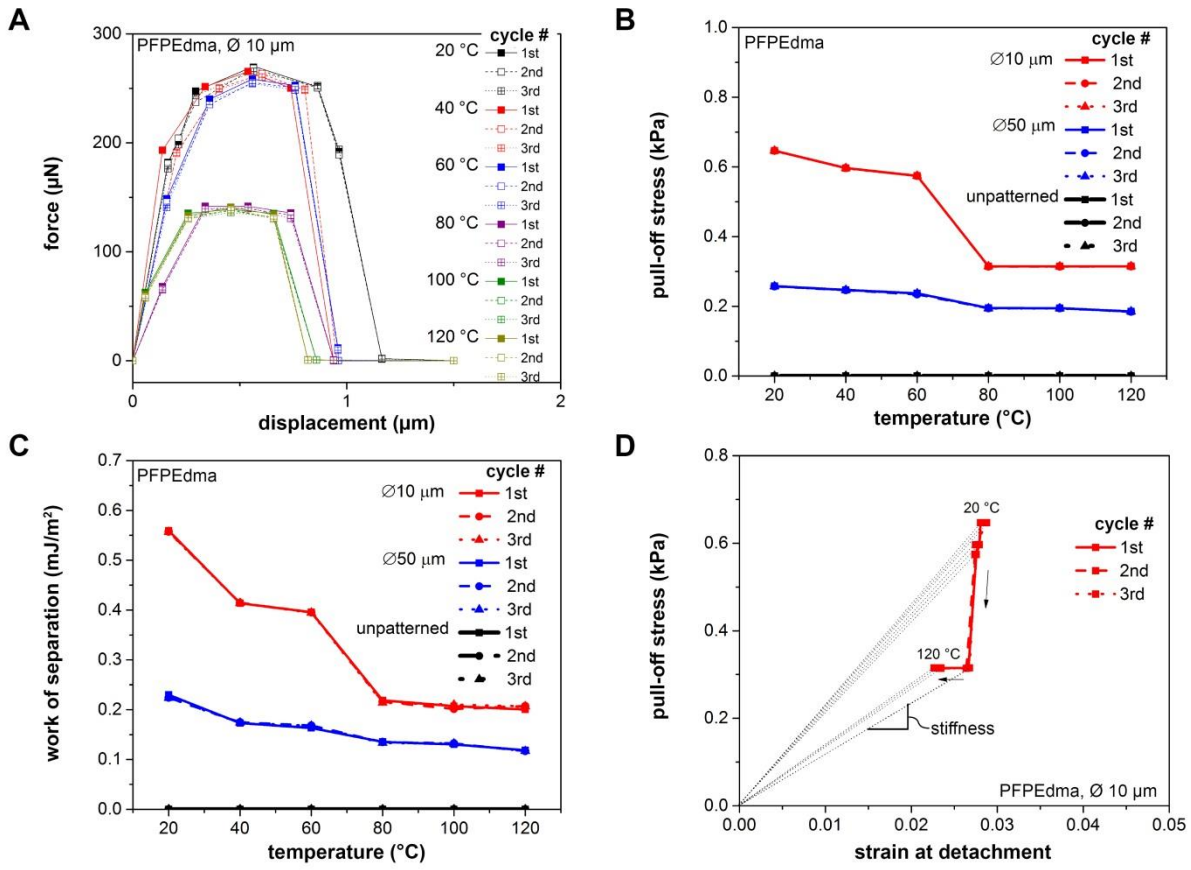

Figure 6.3 *Results of adhesion measurements of PFPEdma micropatterned specimens obtained from three heating-cooling cycles. (A) Force-displacement curves as a function of temperature for pillar structures with diameter 10 µm and aspect ratio 2. (B) Pull-off stresses and (C) work of separation as a function of temperatures, for the different micropatterned specimens (red: 10 µm pillar diameter, blue 50 µm pillar diameter) and an unpatterned control (black). (D) Pull-off stress in terms of the strain at detachment for pillar structures with diameter 10 µm at various temperatures. The slope of the secants (dotted lines) represents the apparent stiffness of the adhesives.*

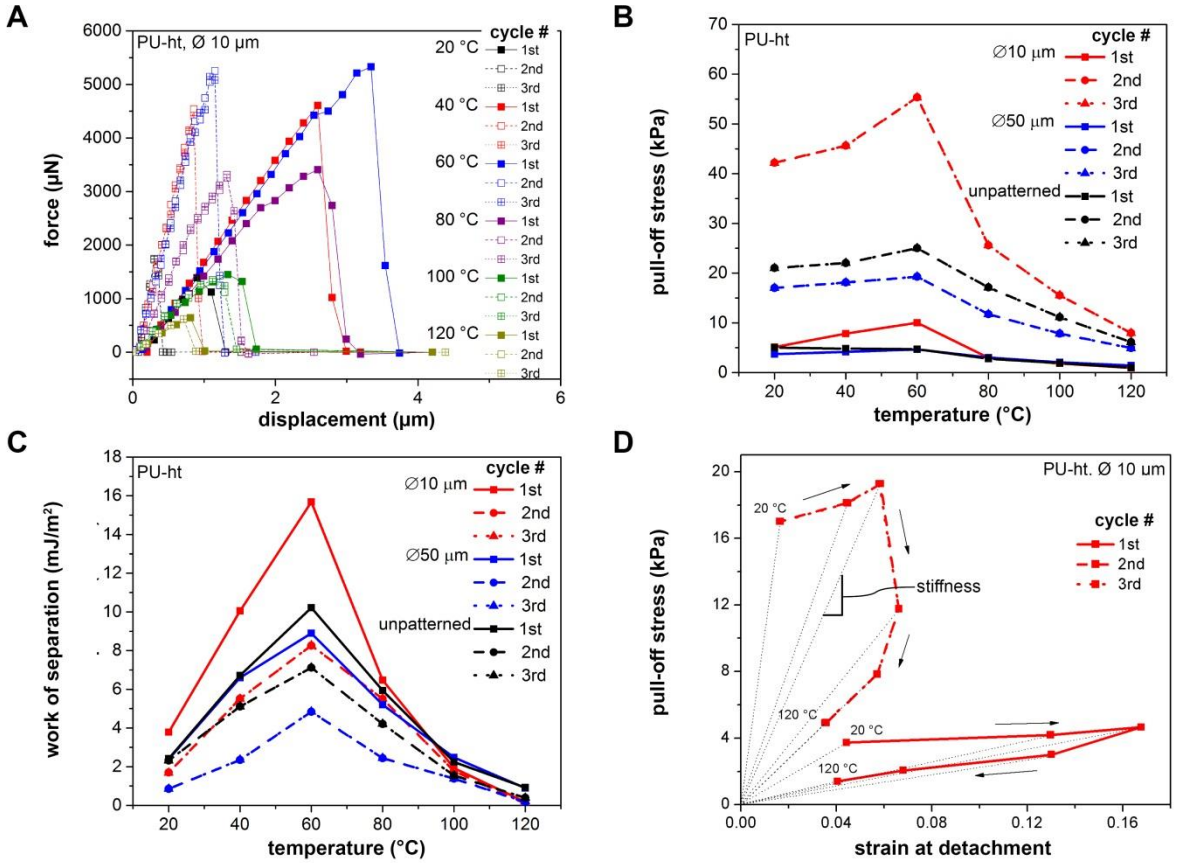

Figure 6.4 *Results of adhesion measurements of PU-ht micropatterned specimens obtained from three heating-cooling cycles. (A) Force-displacement curves as a function of temperature for pillar structures with diameter 10 µm and aspect ratio 2. (B) Pull-off stresses and (C) work of separation as a function of temperatures, for the different micropatterned specimens (red: 10 µm pillar diameter, blue 50 µm pillar diameter) and an unpatterned control (black). (D) Pull-off stress in terms of the strain at detachment for pillar structures with diameter 10 µm at various temperatures. The slope of the secants (dotted lines) represents the apparent stiffness of the adhesives.*

6.4.2 Dynamic mechanical tests

To separate materials from structure effects, dynamic mechanical tests of the materials within the relevant temperature range were performed. The storage and loss modulus and the viscoelastic loss factor, $tan\,\delta$, for all materials are presented in the **Figures 6.5, 6.6 and 6.7** as a function of temperature. The material glass transition temperatures, T_g, *obtained from the maxima in the* $tan\,\delta$ curves are summarized in **Table 6.1**. PDMS has the lowest glass transition temperature of -28 °C and PU-ht the highest T_g of 59 °C. For PFPEdma, two glass transition temperatures were identified at -20 °C and 27 °C (**Figure 6.6a**). The viscoelastic loss factor, $tan\,\delta$, *was found to lie below 0.15* for PDMS and PFPEdma at temperatures above 20 °C (**Figures 6.5b and 6.6b**).

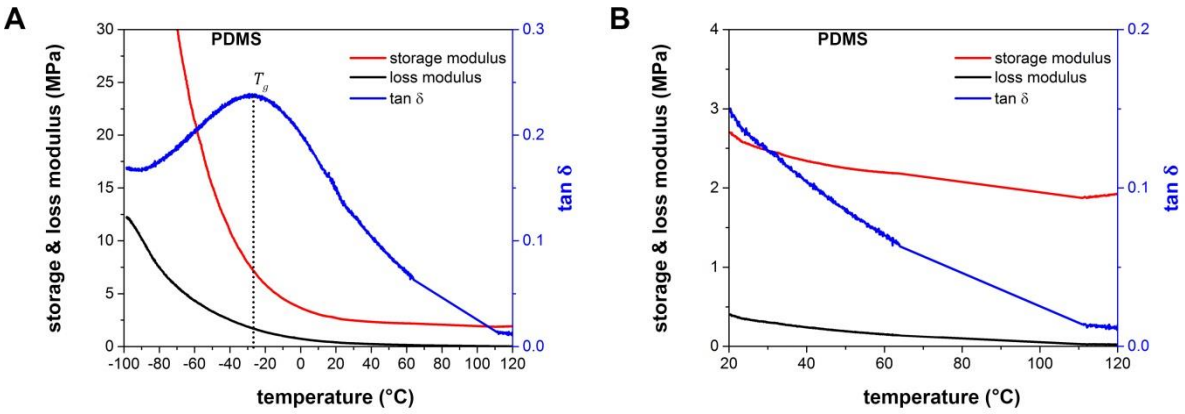

Figure 6.5 *Results of dynamic mechanical tests of bulk PDMS. The storage modulus (red), loss modulus (black), and the viscoelastic loss factor,* **tan δ** (blue)*, are plotted as a function of temperature. The glass transition temperature is determined from the maximum value of* **tan δ** *as highlighted with the dotted line.* (A) *Temperature range of the DMTA from -100 °C to 120 °C. (B) Temperature range of the adhesion measurements from 20 °C to 120 °C.*

Hence, these materials can be considered as largely elastic, particularly at higher temperatures, where $tan\,\delta$ was further reduced. The storage modulus of PDMS and PFPEdma decreased slightly with increasing temperature: For PDMS, it decreased from 2.7 MPa at 20 °C to 1.9 MPa at 120 °C (**Figure 6.5b**); for PFPEdma, the storage modulus decreased from

10 MPa at 20 °C to 8.5 MPa at 60 °C and then remained almost constant at higher temperatures (**Figure 6.6b**).

Table 6.1 *The material glass transition temperatures (T_g) and surface free energies (γ).*

Polymer	T_g **(°C)**	γ **(mJ m^{-2})**
PDMS	-28	22 ([128])
PFPEdma	-20 & 27	16 ([124])
PU-ht	59	42

In contrast to PDMS and PFPEdma, the UV-cured polyurethane PU-ht is more viscoelastic exhibiting a viscoelastic loss factor of up to 3.3 at 59 °C (**Figures 6.7a and 6.7b**). In addition, the storage modulus varied strongly from 50 MPa at 20 °C down to 2.5 MPa at 80 °C. Interestingly, the thermo-mechanical properties varied during the first heating cycle (**Figures 6.7a and 6.7b**).

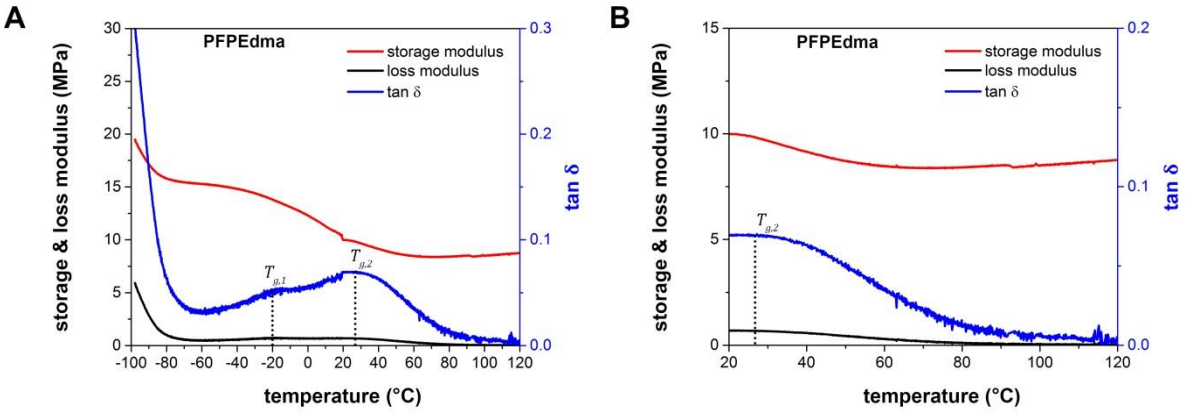

Figure 6.6 ***Results of dynamic mechanical tests of bulk PFPEdma****. The storage modulus (red), loss modulus (black), and the viscoelastic loss factor,* tan δ (blue), *are plotted as a function of temperature. The glass transition temperatures are determined from the maximum value of* tan δ as *highlighted with the dotted line.* ***(A)*** *Temperature range of the DMTA from -100 °C to 120 °C.* ***(B)*** *Temperature range of the adhesion measurements from 20 °C to 120 °C.*

Hereby, the material further stiffened as the storage modulus increased almost 10 times compared to the first cycle, most probably due to a secondary thermally induced cross-linking (referred to as post-bake, see **Figures 6.7c and 6.7d**). In the same way, the material became less viscoelastic with a maximum $tan\,\delta$ of about 0.3, i.e. one order of magnitude less compared to the initial viscoelasticity upon UV-curing *(***Figure 6.7d***)*. To exclude effects of morphological variations such as crystallization, XRD analysis was performed for PU-ht directly upon UV-curing and a subsequent post-bake at 120 °C. Upon both treatments, the diffraction patterns were found to be similar without any characteristic patterns due to crystalline domains (**Figure 6.8**). The broad impulses at $2\Theta = 19.8^{\circ}$ demonstrate the amorphous microstructure of the polymers that did not vary by further cross-linking of the material. Thus, the results obtained indicate an amorphous morphology for both PU-ht samples without significant variations upon additional thermal cross-linking.

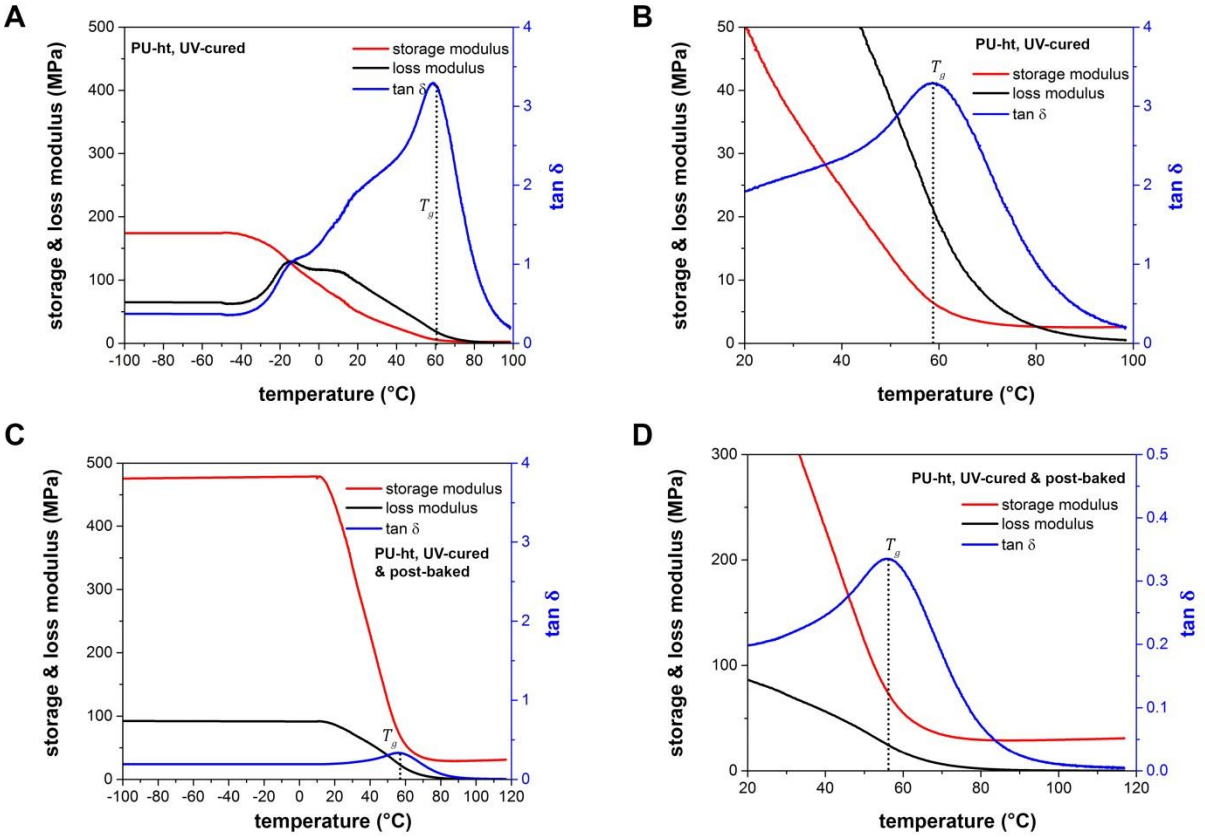

Figure 6.7 *Results of dynamic mechanical tests of bulk PU-ht. The storage modulus (red), loss modulus (black), and the viscoelastic loss factor,* $\boldsymbol{\tan\delta}$ (blue), *are plotted as a function of temperature. The glass transition temperature is determined from the maximum value of* $\boldsymbol{\tan\delta}$ as highlighted with the dotted line. *(A,B) DMTA trace of PU-ht upon UV-curing*: (A) Temperature range of the DMTA from *-100 °C to 100 °C. (B) Temperature range of the adhesion measurements from 20 °C to 100 °C. (C,D) DMTA trace of PU-ht upon UV-curing and subsequent post-bake at 120 °C:* (C) Temperature range of the DMTA from *-100 °C to 120 °C. (D) Temperature range of the adhesion measurements from 20 °C to 120 °C.*

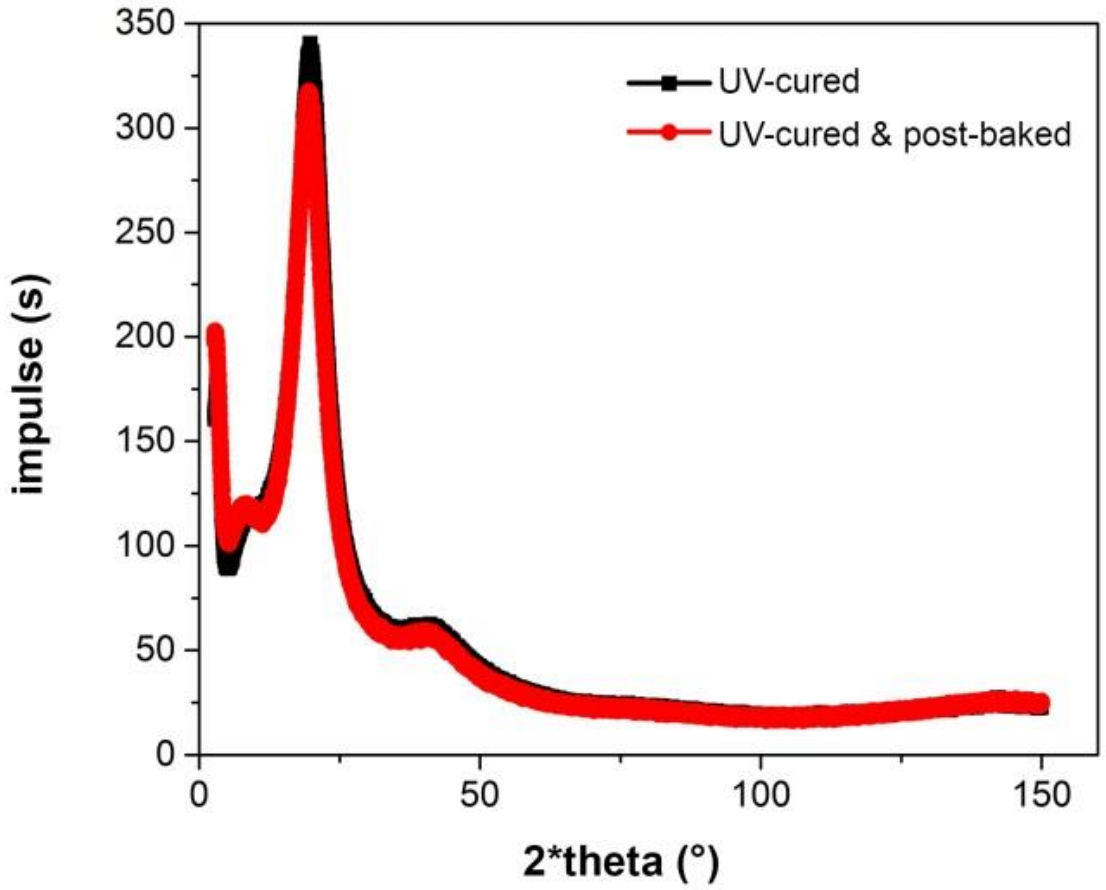

Figure 6.8 *XRD analysis of PU-ht immediately upon UV-curing (black squares) and after subsequent post-bake at 120 °C (red circles).*

6.5 Discussion

The results presented in this paper showed that the adhesion properties of micropatterned polymer surfaces can depend significantly on temperature. The specimens made from PDMS and PFPEdma were operated at temperatures higher than their glass transition temperature. For both materials, the pull-off stress dropped in the order of about 50 % for a temperature elevation from 20 °C to 120 °C and completely recovered when cooled down to 20 °C again. In the same temperature regime, the viscoelastic loss factor, $tan\,\delta$, decreased with increasing temperature for both materials. For PU-ht, the maximum pull-off stress was obtained at the temperature close to the glass transition, where the viscoelasticity of cross-linked elastomers is most pronounced. Viscoelasticity involves dissipative processes during detachment, which enhance the work of separation. This most likely explains the maximum at 60 °C for the patterned and unpatterned PU-ht specimens (**Figure 6.4c**). Upon post-bake at 120 °C, however, the work of separation decreased due to an additional thermal cross-linking (only observed for PU-ht), resulting in a stiffer polymer network and a reduced viscoelastic loss factor (**Figure 6.7b**).[117] In contrast to the decrease in work of separation, the pull-off stress drastically increased with the stiffened structures. The reason lies in the fact that pull-off stress reflects the smaller contact area in the stiffer material. Thus, the stiffer structures led to higher adhesion, which is in line with earlier studies.[60], [129]

In addition to various degrees of viscoelasticity, the different surface free energies of the three tested polymers result in distinctive levels of adhesion. The highest pull-off stresses (of several ten kPa) were obtained with polyurethane (PU-ht); it has the highest surface energy of 42 mJ m^{-2} due to nonpolar and polar groups originating from diisocyanates and polyols. PDMS and PFPEdma are hydrophobic polymers with surface energies of 22 and 16 mJ m^{-2}, respectively.[124], [128] Particularly for PFPEdma, the high fluorine content (about 54 at%) and its high electron negativity make the material much less polarizable and, thus, reduce the probability for van der Waals interactions. This explains most probably the reduction of pull-off stress and the work of separation over two orders of magnitude compared to PU-ht.[116]

Of particular interest for adhesive devices is the effect of surface micropatterning on adhesive performance. Our study confirms earlier results that surface micropatterning can

significantly enhance adhesion over unpatterned controls, which were much less adhesive or even non-adhesive (see results for PFPEdma). However, micropatterning *per se* does not always lead to higher adhesion. For PDMS and PU-ht, only the smallest pillar structures (diameter 10 µm, aspect ratio 2) were more adhesive than the unpatterned control (in terms of pull-off stresses). By contrast, the coarser pillar structures with aspect ratio 0.4 were always inferior to the finer pillar structures with aspect ratio 2 and, for PDMS and PU-ht, even to the unpatterned samples. The explanation lies in the fact that micropatterning, at first, creates adhesive structures with a trivial geometric disadvantage: it invariably reduces the nominal contact area compared to an ideal unpatterned contact; this penalty needs to be overcome by the adhesion-enhancing contact splitting effects, which require good contact formation and small elastic strain energy build-up. It stands to reason that, all other things being equal, the pillar aspect ratio will decide whether a micropatterned surface is anti-adhesive (inferior to an unpatterned control) or adhesive (superior to an unpatterned contact). A higher aspect ratio results in a lower effective stiffness of a patterned structure, which typically results in better contact formation and reduced elastic strain energy for a given strain value.[110] At a critical value of the aspect ratio (in our study between 0.4 and 2), the geometric disadvantage is overruled, rendering an adhesive micropattern. The actual contact area further correlates with the flexibility to bend and to adapt to the spherical probe, which increases with the length of the pillars.[60] In addition to that, the amount of dissipated energy during pull-off scales linearly with the length of the pillar.[130] Therefore, pillar structures with higher aspect ratio are more adhesive as demonstrated in our results for all tested materials in accordance to literature.[75], [110]

6.6 Conclusions

In this paper, we presented a detailed study on the impact of temperatures on three different polymeric, micropatterned adhesives. We demonstrated that the adhesion is enhanced by the viscoelastic characteristics of the materials and the surface micropatterning. The glass transition temperature was identified as the temperature of maximum adhesion due to the peak in the viscoelastic loss factor. The following conclusions were drawn:

- The pull-off stress and the work of separation critically depend on the temperature as found for three different materials, namely, PDMS, PFPEdma, and PU-ht. For PDMS and PFPEdma, both quantities monotonically decreased with increasing temperature; whereas for PU-ht, the pull-off stress and the work of separation exhibit maxima at 60 °C.
- Viscoelastic contributions alter adhesion in terms of the work of separation. To take advantage of this effect, the operating temperature of an adhesive should be chosen close to the material glass transition temperature for maximum performance.
- The adhesion performance strongly varies close to the glass transition temperature. Hence, for a reliable, predictable adhesion performance over a certain temperature range, the glass transition temperature should be avoided.
- The adhesion is higher for materials with higher surface free energy. To enhance the intrinsic adhesion by micropatterning, pillars with an adequate length to adapt to curved substrates are necessarily required.
- It must be noticed that cross-linking of PU-ht by UV-exposure was not sufficient to generate the complete polymer network. Only upon post-bake at 120 °C were the structures completely cross-linked. Such a two-step cross-linking procedure might open ways to create tunable or even switchable adhesives.

Taken together, the temperature-dependent viscoelasticity of elastomers has a strong impact on adhesion and is different for varying temperatures. Hence, the temperature needs to be considered carefully in the material selection and the technical design of micropatterned adhesive devices.

7 Summary and Outlook

The fabrication of gecko-inspired dry adhesives is a continuously developing field of research, which has seen great success over the last years, due to its potential industrial applications. Although there have been many attempts in the fabrication of bioinspired adhesives, they mostly have been tested on smooth surfaces. In this thesis, adhesion on rough substrates was for the first time investigated systematically. Adhesion on rough substrates is of major importance for industrial applications. Many processes are not running at room temperature, but at elevated temperatures. For this reason, adhesion was investigated at different temperatures.

The first part of this works deals with the design and analysis of micropillar-patterned PDMS surfaces and the investigation of their adhesion behavior on glass substrates with different roughnesses. The structures, which were studied in this part of the thesis, were made of PDMS, since it is a common material in the field of bioinspired structures. Hereby, the pillar height and diameter were systematically varied. It was demonstrated that fibrillar adhesive surfaces can improve the adhesion to rough substrates. The principle of contact splitting was shown to apply to rough surfaces. Both are, however, strongly dependent on the pillar diameter and height. For the first time two regimes of adhesion were identified, which are delimited by a critical value of pillar diameter. Regime 1 refers to the case when the pillar diameter exceeds the spacing between local peaks of the substrates, leading to a superior adhesion compared to regime 2 where the converse relationship applies. However, the development of contour plots revealed the coexistence of both regimes as function of pillar diameter as well as pillar height.

So, with these new results it was possible to distinguish adhesive and non-adhesive states depending on the micropillar geometry relative to the surface roughness profile. The data obtained further demonstrate that, in the adhesive regime, fibrillar gecko-inspired adhesive structures can be used with advantage on rough surfaces. The results allow us to tune the adhesion perfomance through the structure dimensions and roughness profile.

These investigations were extended by performing adhesion measurements on much rougher surface than the previously prepared glass substrates. Fibrillar adhesives of PDMS and unpatterned PDMS were tested on sandpaper. Hereby, unpatterned PDMS did not show

any measurable adhesion on very rough surfaces. The micropillar patterned PDMS surfaces, on the other hand, exhibited adhesion for sufficiently large pillar heights. Nevertheless, the contact splitting principle mechanism has also been documented on sandpaper.

After focusing mainly on the pillar geometry of micropatterned PDMS surfaces and the substrate roughness, the third part of this work deals with the study of the influence of the temperature on the adhesion behavior of three different materials: PDMS, perfluoropolyether (PFPEdma) and polyurethane methacrylate (PU-ht). Therefore, beside PDMS, two additional materials were also investigated, which may be interesting for industrial application, due to their thermal stability. Again, several samples with various pillar geometries were fabricated and subjected to up to three heating-cooling cycles covering a temperature range from 20° C to 120° C. In a first step, the viscoelastic properties of these polymers were characterized as function of the temperature, which is essential for the understanding of the adhesion phenoma. It has been demonstrated that each material presents a unique temperature dependent adhesion behavior, which was determined by measuring the pull-off forces at temperatures from 20° C to 120° C in 20° C increments.

For PDMS, the adhesion force decreases when the temperature increases.

During heating, no changes occur in the structure of PDMS, so the loss modulus remains stable even after undergoing several heating and cooling processes. In the case of the cross-linked PDMS used in this study, the polymer remains in a rubbery state in the investigated range of temperatures.

PFPEdma remains mostly stable in the temperature range covered, hence no significant changes in the pull-off stress were observed. It has to be noticed that the PFPEdma samples showed the lowest pull-of stresses compared to the PDMS and PU-ht samples.

PU-ht exhibited changes of the viscoelastic properties at increasing temperatures, which coincides with a significant change of the adhesion behavior. The adhesion increases until the sample reaches a temperature of 60° C. This can be explained by the material becoming softer, so the deformation of the pillars increases, which leads to a larger contact area and hence an increase of pull-off force stress. DMA measurements show that the loss factor curve indicates the maximum of viscoelastic properties at 60° C, which supports this explanation. However, after passing this critical temperature, the adhesion decreases notably.

The presented results clearly demonstrate that the adhesion behavior is linked to the viscoelastic properties of the polymers. Especially, the glass transition temperature is an important parameter, since the adhesion behavior is significantly different below and above T_g. Furthermore, it can be used to control the adhesion behavior of a polymer at elevated temperatures.

Outlook – For the analysis of the results a specific pillar behavior was assumed. The apparent contact area, which is not the real contact area on rough substrates, was used to calculate the adhesion stresses. In this framework, in situ visualization could open a new way of data interpretation. It could allow observing exact changes of the contact area on different rough substrates. As a result, it should be possible to calculate the real contact area. Pillars fabricated from materials stiffer than PDMS are expected to have lower propensity of buckling and bending. In addition, it would be useful to measure the shear forces of the pillar structures and to determine the shear adhesion and friction. The characterization of rough substrates could be complemented by using the power spectrum, which could provide a means to very accurately calculate several roughness parameters.

When considering adhesion at different temperatures, it would be useful to extend the temperature range, since some industrial machines work at temperatures above 120 °C. It would also be interesting to investigate the adhesion behavior below room temperature. In this thesis, only the structured samples were heated. Performing measurements with a heated substrate on both unheated and heated structures could also be the subject of further investigations.

List of Figures

List of Tables

Bibliography

[1] C. Poisson, V. Hervais, M. F. Lacrampe, and P. Krawczak, "Optimization of PE/binder/PA extrusion blow-molded films. II. Adhesion properties improvement using binder/EVA blends," *J. Appl. Polym. Sci.*, vol. 101, no. 1, pp. 118–127, 2006.

[2] C. J. Van Oss, *Interfacial forces in aqueous media*. Taylor & Francis, 2006.

[3] H. Hertz, "Ueber die Berührung fester elastischer Körper.," *J. für die reine und Angew. Math.*, vol. 92, pp. 156–171.

[4] K. L. Johnson, K. Kendall, and A. D. Roberts, "Surface Energy and the Contact of Elastic Solids," *Proc. R. Soc. A Math. Phys. Eng. Sci.*, vol. 324, no. 1558, pp. 301–313, Sep. 1971.

[5] B. . Derjaguin, V. . Muller, and Y. . Toporov, "Effect of contact deformations on the adhesion of particles," *J. Colloid Interface Sci.*, vol. 53, no. 2, pp. 314–326, Nov. 1975.

[6] K. Kendall, "1_0962_The adhesion and surface energy of elastic solids," *J. Phys. D. Appl. Phys.*, vol. 4, pp. 1186–1195, 1971.

[7] K. Autumn, A. Dittmore, D. Santos, M. Spenko, and M. Cutkosky, "Frictional adhesion: A new angle on gecko attachment.," *J. Exp. Biol.*, vol. 209, pp. 3569–3579, 2006.

[8] J. N. Israelachvili, *Intermolecular and Surface Forces*. Intermolecular and Surface Forces, 2011.

[9] K. M. Ainslie, R. D. Lowe, T. T. Beaudette, L. Petty, E. M. Bachelder, and T. A. Desai, "Microfabricated devices for enhanced bioadhesive drug delivery: Attachment to and small-molecule release through a cell monolayer under flow," *Small*, vol. 5, pp. 2857–2863, 2009.

[10] B. Aksak, M. P. Murphy, and M. Sitti, "Adhesion of biologically inspired vertical and angled polymer microfiber arrays," *Langmuir*, vol. 23, pp. 3322–3332, 2007.

[11] E. Arzt, "Biological and artificial attachment devices: Lessons for materials scientists from flies and geckos," *Mater. Sci. Eng. C*, vol. 26, pp. 1245–1250, 2006.

[12] K. Autumn, M. Sitti, Y. A. Liang, A. M. Peattie, W. R. Hansen, S. Sponberg, T. W. Kenny, R. Fearing, J. N. Israelachvili, and R. J. Full, "Evidence for van der Waals adhesion in gecko setae.," *Proc. Natl. Acad. Sci. U. S. A.*, vol. 99, pp. 12252–12256, 2002.

[13] M. Varenberg, B. Murarash, Y. Kligerman, and S. N. Gorb, “Geometry-controlled adhesion: Revisiting the contact splitting hypothesis,” *Appl. Phys. A Mater. Sci. Process.*, vol. 103, no. 4, pp. 933–938, 2011.

[14] A. Del Campo, C. Greiner, and E. Arzt, “Contact shape controls adhesion of bioinspired fibrillar surfaces,” *Langmuir*, vol. 23, no. 20, pp. 10235–10243, 2007.

[15] C. Greiner, A. del Campo, and E. Arzt, “Adhesion of Bioinspired Micropatterned Surfaces: Effects of Pillar Radius, Aspect Ratio, and Preload,” *Langmuir*, vol. 23, no. 7, pp. 3495–3502, Mar. 2007.

[16] E. Arzt, S. Gorb, and R. Spolenak, “From micro to nano contacts in biological attachment devices.,” *Proc. Natl. Acad. Sci. U. S. A.*, vol. 100, pp. 10603–10606, 2003.

[17] R. Spolenak, S. Gorb, H. Gao, and E. Arzt, “Effects of contact shape on the scaling of biological attachments,” *Proceedings of the Royal Society A: Mathematical, Physical and Engineering Sciences*, vol. 461, no. 2054. pp. 305–319, 2005.

[18] H. E. Jeong, J.-K. Lee, H. N. Kim, S. H. Moon, and K. Y. Suh, “A nontransferring dry adhesive with hierarchical polymer nanohairs.,” *Proc. Natl. Acad. Sci. U. S. A.*, vol. 106, no. 14, pp. 5639–44, 2009.

[19] M. T. Northen, C. Greiner, E. Arzt, and K. L. Turner, “A Gecko-Inspired Reversible Adhesive,” *Adv. Mater.*, vol. 20, no. 20, pp. 3905–3909, Oct. 2008.

[20] S. Gorb, M. Varenberg, A. Peressadko “Biomimetic mushroom-shaped fibrillar adhesive microstructure.,” *J. R. Soc. Interface*, vol. 4, no. 13, pp. 271–5, 2007.

[21] J. M. R. Bullock and W. Federle, “The effect of surface roughness on claw and adhesive hair performance in the dock beetle Gastrophysa viridula,” *Insect Sci.*, vol. 18, no. 3, pp. 298–304, 2011.

[22] A. P. Russell and M. K. Johnson, “Real-world challenges to, and capabilities of, the gekkotan adhesive system: contrasting the rough and the smooth,” *Can. J. Zool.*, vol. 85, no. 12, pp. 1228–1238, Dec. 2007.

[23] G. Huber, S. N. Gorb, N. Hosoda, R. Spolenak, and E. Arzt, “Influence of surface roughness on gecko adhesion,” *Acta Biomater.*, vol. 3, pp. 607–610, 2007.

[24] N. M. Pugno and E. Lepore, “Observation of optimal gecko’s adhesion on nanorough surfaces,” *BioSystems*, vol. 94, no. 3, pp. 218–222, 2008.

[25] D. J. Irschick, C. C. Austin, K. Petren, R. N. Fisher, J. B. Losos, and O. Ellers, “A comparative analysis of clinging ability among pad-bearing lizards,” *Biol. J. Linn. Soc.*, vol. 59, no. 1, pp. 21–35, 1996.

[26] B. N. J. Persson, “On the mechanism of adhesion in biological systems,” *J. Chem. Phys.*, vol. 118, no. 16, pp. 7614–7621, 2003.

[27] A. G. Gillies, A. Henry, H. Lin, A. Ren, K. Shiuan, R. S. Fearing, and R. J. Full, "Gecko toe and lamellar shear adhesion on macroscopic, engineered rough surfaces," *J. Exp. Biol.*, vol. 217, no. 2, 2014.

[28] B. N. J. Persson, "Relation between interfacial separation and load: A general theory of contact mechanics," *Phys. Rev. Lett.*, vol. 99, no. 12, 2007.

[29] B. Q. Luan, S. Hyun, J. F. Molinari, N. Bernstein, and M. O. Robbins, "Multiscale modeling of two-dimensional contacts," *Phys. Rev. E*, vol. 74, no. 4, p. 046710, Oct. 2006.

[30] A. Peressadko, N. Hosoda, and B. N. J. Persson, "Influence of Surface Roughness on Adhesion between Elastic Bodies," *Phys. Rev. Lett.*, vol. 95, no. 12, pp. 1–4, 2005.

[31] B. N. J. Persson, "Wet adhesion with application to tree frog adhesive toe pads and tires," *J. Phys. Condens. Matter*, vol. 19, p. 376110, 2007.

[32] A. Jagota and C. Y. Hui, "Adhesion, friction, and compliance of bio-mimetic and bio-inspired structured interfaces," *Mater. Sci. Eng. R Reports*, vol. 72, no. 12, pp. 253–292, 2011.

[33] R. Spolenak, S. Gorb, and E. Arzt, "Adhesion design maps for bio-inspired attachment systems," *Acta Biomater.*, vol. 1, no. 1, pp. 5–13, 2005.

[34] B. N. J. Persson, "Biological Adhesion for Locomotion on Rough Surfaces: Basic Principles and A Theorist's View," *MRS Bulletin*, vol. 32. pp. 486–490, 2007.

[35] P. R. Guduru, "Detachment of a rigid solid from an elastic wavy surface: Theory," *J. Mech. Phys. Solids*, vol. 55, no. 3, pp. 445–472, 2007.

[36] J. Davies, S. Haq, T. Hawke, and J. P. Sargent, "A practical approach to the development of a synthetic Gecko tape," *Int. J. Adhes. Adhes.*, vol. 29, pp. 380–390, 2009.

[37] R. Roshan, D. G. Jayne, T. Liskiewicz, G. W. Taylor, P. H. Gaskell, L. Chen, A. Montellano-Lopez, A. Morina, and A. Neville, "Effect of tribological factors on wet adhesion of a microstructured surface to peritoneal tissue," *Acta Biomater.*, vol. 7, no. 11, pp. 4007–4017, 2011.

[38] N. Cañas, M. Kamperman, B. Völker, E. Kroner, R. M. McMeeking, and E. Arzt, "Effect of nano- and micro-roughness on adhesion of bioinspired micropatterned surfaces," *Acta Biomater.*, vol. 8, pp. 282–288, 2012.

[39] C. T. Bauer, E. Kroner, N. A. Fleck, E. Arzt "Hierarchical macroscopic fibrillar adhesives: *in situ* study of buckling and adhesion mechanisms on wavy substrates," *Bioinspir. Biomim.*, vol. 10, no. 6, p. 066002, Oct. 2015.

[40] J. Yu, S. Chary, S. Das, J. Tamelier, K. L. Turner, and J. N. Israelachvili, "Friction and Adhesion of Gecko-Inspired PDMS Flaps on Rough Surfaces," *Langmuir*, vol. 28, no. 31, pp. 11527–11534, Aug. 2012.

[41] J. F. Archard, “Elastic Deformation and the Laws of Friction,” *Proc. R. Soc. A Math. Phys. Eng. Sci.*, vol. 243, no. 1233, pp. 190–205, 1957.

[42] E. S. Gadelmawla, M. M. Koura, T. M. A. Maksoud, I. M. Elewa, and H. H. Soliman, “Roughness parameters,” *J. Mater. Process. Technol.*, vol. 123, no. 1, pp. 133–145, 2002.

[43] K. L. Johnson, “Contact Mechanics,” *Journal of the American Chemical Society*, vol. 37. pp. 1–17, 1985.

[44] V. Barreau, R. Hensel, N. K. Guimard, A. Ghatak, R. M. McMeeking, and E. Arzt, “Fibrillar Elastomeric Micropatterns Create Tunable Adhesion Even to Rough Surfaces,” *Adv. Funct. Mater.*, vol. 26, no. 26, pp. 4687–4694, Jul. 2016.

[45] P. R. Nayak, “Random Process Model of Rough Surfaces,” *J. Lubr. Technol.*, vol. 93, no. 3, p. 398, 1971.

[46] B. N. J. Persson, O. Albohr, U. Tartaglino, A. I. Volokitin, and E. Tosatti, “On the nature of surface roughness with application to contact mechanics, sealing, rubber friction and adhesion.,” *J. Phys. Condens. Matter*, vol. 17, no. 1, pp. R1–R62, Jan. 2005.

[47] A. Duparré, J. Ferre-Borrull, S. Gliech, G. Notni, J. Steinert, and J. M. Bennett, “Surface characterization techniques for determining the root-mean-square roughness and power spectral densities of optical components,” *Appl. Opt.*, vol. 41, no. 1, p. 154, Jan. 2002.

[48] R. K. Leach, “Introduction to metrology for micro- and nanotechnology,” in *Fundamental Principles of Engineering Nanometrology*, Elsevier, 2010, pp. 1–4.

[49] J. C. Stover, *Optical Scattering Measurement and Analysis*. Society of Photo Optical, 2016.

[50] J. G. Swadener, K. M. Liechti, and A. l. d. Lozanne, “The intrinsic toughness and adhesion mechanisms of a glass/epoxy interface,” *J. Mech. Phys. Solids*, vol. 47, no. 2, pp. 223–258, 1999.

[51] A. Zosel, “MOLECULAR STRUCTURE, MECHANICAL BEHAVIOUR AND ADHESION PERFORMANCE OF PRESSURE SENSITIVE ADHESIVES,” *Adhes Sealants Ind Mag* , pp. 193–203, 2001.

[52] J. D. Ferry, “Viscoelastic Properties of Polymers,” *Polymer (Guildf).*, p. 641, 1980.

[53] N. Lagakos, J. Jarzynski, J. H. Cole, and J. A. Bucaro, “Frequency and temperature dependence of elastic moduli of polymers,” *J. Appl. Phys.*, vol. 59, no. 12, pp. 4017–4031, 1986.

[54] J. Richeton, S. Ahzi, K. S. Vecchio, F. C. Jiang, and R. R. Adharapurapu, “Influence of temperature and strain rate on the mechanical behavior of three amorphous polymers: Characterization and modeling of the compressive yield stress,” *Int. J. Solids Struct.*, vol. 43, no. 7–8, pp. 2318–2335, 2006.

[55] H. Domininghaus, *Kunststoffe : Eigenschaften und Anwendungen*. Springer Berlin, 2011.

[56] A. Noy, S. Zepeda, C. A. Orme, Y. Yeh, and J. J. De Yoreo, "Entropic barriers in nanoscale adhesion studied by variable temperature chemical force microscopy," *J. Am. Chem. Soc.*, vol. 125, no. 5, pp. 1356–1362, 2003.

[57] B. Cappella and W. Stark, "Adhesion of amorphous polymers as a function of temperature probed with AFM force-distance curves," *J. Colloid Interface Sci.*, vol. 296, no. 2, pp. 507–514, 2006.

[58] N. Lakhera, A. Graucob, A. S. Schneider, E. Kroner, M. Micciché, E. Arzt, and C. P. Frick, "Adhesion behavior of polymer networks with tailored mechanical properties using spherical and flat contacts," *MRS Commun.*, vol. 3, no. 01, pp. 73–77, Mar. 2013.

[59] H. Yu, Z. Li, and Q. Jane Wang, "Viscoelastic-adhesive contact modeling: Application to the characterization of the viscoelastic behavior of materials," *Mech. Mater.*, vol. 60, pp. 55–65, 2013.

[60] G. Castellanos, E. Arzt, and M. Kamperman, "Effect of viscoelasticity on adhesion of bioinspired micropatterned epoxy surfaces," *Langmuir*, vol. 27, no. 12, pp. 7752–7759, 2011.

[61] X. P. Wang, O. K. C. Tsui, and X. Xiao, "Dynamic Study of Polymer Films by Friction Force Microscopy with Continuously Varying Load," *Langmuir*, vol. 18, no. 18, pp. 7066–7072, Sep. 2002.

[62] G. H. Jon A. Hammerschmidt , Wayne L. Gladfelter, "Probing Polymer Viscoelastic Relaxations with Temperature-Controlled Friction Force Microscopy," *Macromolecules*, vol. 32, pp. 3360 – 3367, 1999.

[63] O. K. C. Tsui, X. P. Wang, J. Y. L. Ho, T. K. Ng, and X. Xiao, "Studying Surface Glass-to-Rubber Transition Using Atomic Force Microscopic Adhesion Measurements," *Macromolecules*, vol. 33, no. 11, pp. 4198–4204, May 2000.

[64] K. S. Kim, J. C. Heo, and K. W. Kim, "Effects of temperature on the microscale adhesion behavior of thermoplastic polymer film," *Tribol. Lett.*, vol. 38, no. 2, pp. 97–106, 2010.

[65] G. Luengo, J. Pan, M. Heuberger, and J. N. Israelachvili, "Temperature and Time Effects on the 'Adhesion Dynamics' of Poly(butyl methacrylate) (PBMA) Surfaces," *Langmuir*, vol. 14, no. 1, pp. 3873–3881, 1998.

[66] H. B. Zeng, N. Maeda, N. H. Chen, M. Tirrell, and J. Israelachvili, "Adhesion and friction of polystyrene surfaces around T(g)," *Macromolecules*, vol. 39, no. 6, pp. 2350–2363, 2006.

[67] H. Awada, O. Noel, T. Hamieh, Y. Kazzi, and M. Brogly, "Contributions of chemical and mechanical surface properties and temperature effect on the adhesion at the nanoscale," *Thin Solid Films*, vol. 519, no. 11, pp. 3690–3694, 2011.

[68] M. Shavezipur, W. Gou, C. Carraro, and R. Maboudian, “Characterization of adhesion force in MEMS at high temperature using thermally actuated microstructures,” *J. Microelectromechanical Syst.*, vol. 21, no. 3, pp. 541–548, 2012.

[69] G. H. Li, I. Laboriante, F. Liu, M. Shavezipur, B. Bush, C. Carraro, and R. Maboudian, “Measurement of adhesion forces between polycrystalline silicon surfaces via a MEMS double-clamped beam test structure,” *J. Micromechanics Microengineering*, vol. 20, no. 9, p. 095015, 2010.

[70] G. De Crevoisier, P. Fabre, J. M. Corpart, and L. Leibler, “Switchable tackiness and wettability of a liquid crystalline polymer,” *Science (80-.).*, vol. 285, no. 5431, pp. 1246–1249, 1999.

[71] N. S. Tambe and B. Bhushan, “Scale dependence of micro/nano-friction and adhesion of MEMS/NEMS materials, coatings and lubricants,” *Nanotechnology*, vol. 15, no. 11, pp. 1561–1570, 2004.

[72] S. Wu, “Polar and Nonpolar Interactions in Adhesion,” *J. Adhes.*, vol. 5, no. 1, pp. 39–55, 1973.

[73] E. Kroner, R. Maboudian, and E. Arzt, “Adhesion characteristics of pdms surfaces during repeated pull-off force measurements,” *Adv. Eng. Mater.*, vol. 12, no. 5, pp. 398–404, 2010.

[74] E. Kroner, J. Blau, and E. Arzt, “Note: An adhesion measurement setup for bioinspired fibrillar surfaces using flat probes,” *Review of Scientific Instruments*, vol. 83, no. 1. 2012.

[75] C. Greiner, A. Del Campo, and E. Arzt, “Adhesion of bioinspired micropatterned surfaces: Effects of pillar radius, aspect ratio, and preload,” *Langmuir*, vol. 23, no. 7, pp. 3495–3502, 2007.

[76] E. K. Kroner, “Adhesion Measurements on Patterned Elastomeric Surfaces,” 2011.

[77] M. Bacca, J. A. Booth, K. L. Turner, and R. M. McMeeking, “Load sharing in bioinspired fibrillar adhesives with backing layer interactions and interfacial misalignment,” *J. Mech. Phys. Solids*, vol. 96, pp. 428–444, 2016.

[78] A. J. Crosby, M. Hageman, and A. Duncan, “Controlling Polymer Adhesion with ‘Pancakes,’” *Langmuir*, vol. 21, no. 25, pp. 11738–11743, Dec. 2005.

[79] K. G. Sharp, G. S. Blackman, N. J. Glassmaker, A. Jagota, and C. Y. Hui, “Effect of stamp deformation on the quality of microcontact printing: Theory and experiment,” *Langmuir*, vol. 20, pp. 6430–6438, 2004.

[80] C. Y. Hui, A. Jagota, Y. Y. Lin, and E. J. Kramer, “Constraints on microcontact printing imposed by stamp deformation,” *Langmuir*, vol. 18, no. 4, pp. 1394–1407, 2002.

[81] K. Autumn and A. M. Peattie, “Mechanisms of adhesion in geckos.,” *Integr. Comp. Biol.*, vol. 42, pp. 1081–1090, 2002.

[82] E. Kroner and C. S. Davis, “A Study of the Adhesive Foot of the Gecko: Translation of a Publication by Franz Weitlaner,” *J. Adhes.*, vol. 91, no. 6, pp. 481–487, 2015.

[83] G. Huber, H. Mantz, R. Spolenak, K. Mecke, K. Jacobs, S. N. Gorb, and E. Arzt, “Evidence for capillarity contributions to gecko adhesion from single spatula nanomechanical measurements.,” *Proc. Natl. Acad. Sci. U. S. A.*, vol. 102, pp. 16293–16296, 2005.

[84] T. W. Kim and B. Bhushan, “The adhesion model considering capillarity for gecko attachment system,” *J. R. Soc. Interface*, vol. 5, no. 20, pp. 319–327, 2008.

[85] K. Autumn, Y. A. Liang, S. T. Hsieh, W. Zesch, W. P. Chan, T. W. Kenny, R. Fearing, and R. J. Full, “Adhesive force of a single gecko foot-hair.,” *Nature*, vol. 405, pp. 681–685, 2000.

[86] Y. Tian, N. Pesika, H. Zeng, K. Rosenberg, B. Zhao, P. McGuiggan, K. Autumn, and J. Israelachvili, “Adhesion and friction in gecko toe attachment and detachment.,” *Proc. Natl. Acad. Sci. U. S. A.*, vol. 103, pp. 19320–19325, 2006.

[87] S. N. Gorb, *Functional surfaces in biology*, vol. 2. Springer, 2009.

[88] H. Gao, X. Wang, H. Yao, S. Gorb, and E. Arzt, “Mechanics of hierarchical adhesion structures of geckos,” in *Mechanics of Materials*, 2005, vol. 37, pp. 275–285.

[89] Y. Mengüç and M. Sitti, “Gecko-Inspired Polymer Adhesives,” in *Polymer Adhesion, Friction, and Lubrication*, Hoboken, NJ, USA: John Wiley & Sons, Inc., 2013, pp. 351–389.

[90] L. Heepe and S. N. Gorb, “Biologically Inspired Mushroom-Shaped Adhesive Microstructures,” *Annu. Rev. Mater. Res.*, vol. 44, no. 1, pp. 173–203, 2014.

[91] A. Pattantyus-Abraham, J. Krahn, and C. Menon, “Recent Advances in Nanostructured Biomimetic Dry Adhesives,” *Front. Bioeng. Biotechnol.*, vol. 1, pp. 1–10, 2013.

[92] M. Zhou, N. Pesika, H. Zeng, Y. Tian, and J. Israelachvili, “Recent advances in gecko adhesion and friction mechanisms and development of gecko-inspired dry adhesive surfaces,” *Friction*, vol. 1, no. 2, pp. 114–129, 2013.

[93] M. Kamperman, E. Kroner, A. Del Campo, R. M. McMeeking, and E. Arzt, “Functional adhesive surfaces with ‘Gecko’ effect: The concept of contact splitting,” *Adv. Eng. Mater.*, vol. 12, pp. 335–348, 2010.

[94] C. Greiner, “Gecko-Inspired Nanomaterials,” in *Biomimetic and Bioinspired Nanomaterials*, vol. 7, Wiley-VCH, 2010, pp. 1–39.

[95] L. F. Boesel, C. Cremer, E. Arzt, A. Del Campo, C. Greiner, E. Arzt, A. del Campo, C. Cremer, E. Arzt, and A. Del Campo, “Gecko-Inspired Surfaces: A Path to Strong and Reversible Dry Adhesives,” *Adv. Mater.*, vol. 22, no. 19, pp. 2125–2137, Jun. 2010.

[96] A. Asbeck, S. Dastoor, A. Parness, L. Fullerton, N. Esparza, D. Soto, B. Heyneman, and M. Cutkosky, “Climbing rough vertical surfaces with hierarchical directional

adhesion," in *Proceedings - IEEE International Conference on Robotics and Automation*, 2009, pp. 2675–2680.

[97] S. Vajpayee, A. Jagota, and C.-Y. Hui, "Adhesion of a Fibrillar Interface on Wet and Rough Surfaces," *The Journal of Adhesion*, vol. 86. pp. 39–61, 2010.

[98] C.-Y. Hui, N. J. Glassmaker, and A. Jagota, "How Compliance Compensates for Surface Roughness in Fibrillar Adhesion," *J. Adhes.*, vol. 81, pp. 699–721, 2005.

[99] H. Kasem and M. Varenberg, "Effect of counterface roughness on adhesion of mushroom-shaped microstructure.," *J. R. Soc. Interface*, vol. 10, no. 87, p. 20130620, 2013.

[100] B. N. J. Persson, O. Albohr, U. Tartaglino, a I. Volokitin, and E. Tosatti, "On the nature of surface roughness with application to contact mechanics, sealing, rubber friction and adhesion.," *J. Phys. Condens. Matter*, vol. 17, no. 1, pp. R1–R62, 2005.

[101] K. N. G. Fuller and D. Tabor, "The effect of surface roughness on the adhesion of elastic solids," *Proc. R. Soc. Lond. A. Math. Phys. Sci.*, vol. 345, no. 1642, pp. 327–342, 1975.

[102] G. A. D. Briggs and B. J. Briscoe, "The effect of surface topography on the adhesion of elastic solids," *J. Phys. D. Appl. Phys.*, vol. 10, no. 18, pp. 2453–2466, 1977.

[103] B. N. J. Persson and E. Tosatti, "The effect of surface roughness on the adhesion of elastic solids," *J. Chem. Phys.*, vol. 115, no. 12, p. 5597, 2001.

[104] E. Kroner, D. R. Paretkar, R. M. McMeeking, and E. Arzt, "Adhesion of Flat and Structured PDMS Samples to Spherical and Flat Probes: A Comparative Study," *J. Adhes.*, vol. 87, no. 5, pp. 447–465, 2011.

[105] D. R. Paretkar, M. D. Bartlett, R. McMeeking, A. J. Crosby, and E. Arzt, "Buckling of an Adhesive Polymeric Micropillar," *J. Adhes.*, vol. 89, no. 2, pp. 140–158, Feb. 2013.

[106] M. Zhou, Y. Tian, D. Sameoto, X. Zhang, Y. Meng, and S. Wen, "Controllable interfacial adhesion applied to transfer light and fragile objects by using gecko inspired mushroom-shaped pillar surface," *ACS Appl. Mater. Interfaces*, vol. 5, no. 20, pp. 10137–10144, 2013.

[107] J. Purtov, M. Frensemeier, and E. Kroner, "Switchable Adhesion in Vacuum Using Bio-Inspired Dry Adhesives," *ACS Appl. Mater. Interfaces*, vol. 7, no. 43, pp. 24127–24135, 2015.

[108] E. Kroner and E. Arzt, "Single macropillars as model systems for tilt angle dependent adhesion measurements," *Int. J. Adhes. Adhes.*, vol. 36, pp. 32–38, 2012.

[109] S. C. L. Fischer, E. Arzt, and R. Hensel, "Composite pillars with tuneable interface for adhesion to rough substrates.," *ACS Appl. Mater. Interfaces*, vol. 9, pp. 1036–1044, 2017.

[110] R. Spolenak, S. Gorb, and E. Arzt, “Adhesion design maps for bio-inspired attachment systems,” *Acta Biomater.*, vol. 1, pp. 5–13, 2005.

[111] C. Greiner, R. Spolenak, and E. Arzt, “Adhesion design maps for fibrillar adhesives: The effect of shape,” *Acta Biomater.*, vol. 5, pp. 597–606, 2009.

[112] E. Cheung and M. Sitti, “Adhesion of biologically inspired polymer microfibers on soft surfaces,” *Langmuir*, vol. 25, pp. 6613–6616, 2009.

[113] S. N. Khaderi, N. A. Fleck, E. Arzt, and R. M. McMeeking, “Detachment of an adhered micropillar from a dissimilar substrate,” *J. Mech. Phys. Solids*, vol. 75, pp. 159–183, Feb. 2015.

[114] R. G. Balijepalli, S. C. L. Fischer, R. Hensel, R. M. McMeeking, and E. Arzt, “Numerical study of adhesion enhancement by composite fibrils with soft tip layers,” *J. Mech. Phys. Solids*, vol. 99, pp. 357–378, Dec. 2017.

[115] E. Turi, *Thermal characterization of polymeric materials*. Elsevier, 2012.

[116] A. Zosel, “Adhesion and tack of polymers: Influence of mechanical properties and surface tensions,” *Colloid Polym. Sci.*, vol. 263, no. 7, pp. 541–553, 1985.

[117] A. Zosel, “Effect Of Cross-Linking On Tack And Peel Strength Of Polymers,” *J. Adhes.*, vol. 34, pp. 201–209, 1991.

[118] E. H. Andrews and A. J. Kinloch, “Mechanics of Adhesive Failure. II,” *Proc. R. Soc. London. A. Math. Phys. Sci.*, vol. 332, no. 1590, pp. 401–414, 1973.

[119] M. Barquins and D. Maugis, “Tackiness of Elastomers,” *J. Adhes.*, vol. 13, no. 1, pp. 53–65, Dec. 1981.

[120] J. A. Greenwood and K. L. Johnson, “The mechanics of adhesion of viscoelastic solids,” *Philosophical Magazine A*, vol. 43. pp. 697–711, 1981.

[121] A. J. Crosby and K. R. Shull, “Adhesive failure analysis of pressure-sensitive adhesives,” *J. Polym. Sci. Part B Polym. Phys.*, vol. 37, no. 24, pp. 3455–3472, Dec. 1999.

[122] K. R. Shull, “Contact mechanics and the adhesion of soft solids,” *Materials Science and Engineering: R: Reports*, vol. 36, no. 1. pp. 1–45, 2002.

[123] C. Camino, S. M. Lomakin, and M. Lazzari, “Polydimethylsiloxane thermal degradation part 1. Kinetic aspects,” *Polymer (Guildf).*, vol. 42, no. 6, pp. 2395–2402, 2001.

[124] R. Hensel, H.-G. Braun, H. Jin, M. Kettunen “Free-floating hydrogel-based rafts supporting a microarray of functional entities at fluid interfaces,” *Soft Matter*, vol. 8, no. 19, p. 5293, 2012.

[125] R. Hensel, A. Finn, R. Helbig, S. Killge, H.-G. Braun, and C. Werner, “In situ experiments to reveal the role of surface feature sidewalls in the Cassie-Wenzel transition,” *Langmuir*, vol. 30, no. 50, pp. 15162–15170, 2014.

[126] S. Kim, B. Aksak, and M. Sitti, “Enhanced friction of elastomer microfiber adhesives with spatulate tips,” *Appl. Phys. Lett.*, vol. 91, no. 22, 2007.

[127] M. P. Murphy, B. Aksak, and M. Sitti, “Adhesion and anisotropic friction enhancements of angled heterogeneous micro-fiber arrays with spherical and spatula tips,” *J. Adhes. Sci. Technol.*, vol. 21, no. 12–13, pp. 1281–1296, Jan. 2007.

[128] J. P. Rolland, E. C. Hagberg, G. M. Denison, K. R. Carter, and J. M. De Simone, “High-Resolution Soft Lithography: Enabling Materials for Nanotechnologies,” *Angew. Chemie Int. Ed.*, vol. 43, no. 43, pp. 5796–5799, Nov. 2004.

[129] T. Tang, C.-Y. Hui, and N. J. Glassmaker, “Can a fibrillar interface be stronger and tougher than a non-fibrillar one?,” *J. R. Soc. Interface*, vol. 2, no. 5, pp. 505–516, 2005.

[130] A. Jagota and S. J. Bennison, “Mechanics of adhesion through a fibrillar microstructure.,” *Integr. Comp. Biol.*, vol. 42, pp. 1140–1145, 2002.